STUDY ON RESPONSIVE RELATIONSHIP BETWEEN CLIMATE DRY-WET CYCLE AND REGIONAL DEBRIS FLOW SUSCEPTIBILITY

JIERUI LI

PhD

The Hong Kong Polytechnic University

This programme is jointly offered by The Hong Kong Polytechnic University and Sichuan University

2025

The Hong Kong Polytechnic University

Department of Land Surveying and Geo-Informatics

Sichuan University

Institute for Disaster Management and Reconstruction

Study on Responsive Relationship between Climate Dry-wet Cycle and Regional Debris Flow Susceptibility

Jierui LI

A thesis submitted in partial fulfilment of the requirements for the degree of Doctor of Philosophy

September 2024

CERTIFICATE OF ORIGINALITY

I hereby declare that this thesis is my own work and that, to the best of my knowledge and belief, it reproduces no material previously published or written, nor material that has been accepted for the award of any other degree or diploma, except where due acknowledgement has been made in the text.

_____ (Signed)

Jierui LI (Name of student)

ABSTRACT

Debris flow is a type of gravity flow involving significant solid material movement, commonly occurring in mountainous areas. However, due to the threat debris flows pose to lives, properties, and infrastructures, preventing unexpected events is crucial. Challenges in quantitatively characterizing the formation and initiation mechanism of debris flows often lead to inaccurate warnings, either missing alarms or causing false ones. The frequency and scale of debris flows have increased due to recent extreme weather events. Though current warning techniques have considered extreme weather influences by extreme rainstorms or tropical cyclones, the impacts of extreme droughts and climate dry-wet cycles have been overlooked. Thus, preventing and mitigating debris flows regionally under extreme dry-wet events is a new scientific challenge. Urgent research is needed to explain the formation and initiation mechanisms of debris flows related to extreme weather.

This study focuses on the typical rainfall-induced debris flows in subtropical monsoon climates. Sichuan Province and the Hong Kong Special Administrative Region, both in mountainous areas of China, are selected as study areas. Historical debris flow inventories and geo-environmental databases, including geological, terrain, meteorological, soil, and land use, are compiled. Dry-wet cycle characteristics are derived from long-term historical dry-wet indices based on the geo-environmental databases using autocorrelation function, wavelet

analysis, and multifractal spectrum analysis, while debris flow average recurrence intervals are estimated using historical debris flow inventories. Statistically based on dry-wet indices, in the two study areas of this study, debris flows occur when suffering extreme wet, while extreme drought generally exists 6-8 years before debris flow occurrences. The responsive relationship between climatic dry-wet cycles and debris flow susceptibility is explored by analyzing the debris flow average recurrence intervals and the dry-wet cycle characteristics in the study areas. Stronger correlations have been observed between debris flow recurrence interval and dry-wet cycles compared to that between debris flow recurrence interval and maximum rainfall, which is one of the most used factors for debris flow early warning. Soil sampling and testing in typical debris flow gullies help explain the mechanism behind the correlation between debris flow recurrence interval and dry-wet cycles. The dry-wet cycle characteristics are utilized to construct regional debris flow susceptibility assessment models. The responsive relationship between the climatic dry-wet cycles and debris flow susceptibility is further validated by promoting the machine learning model performance by 1-4%. The importance of dry-wet cycle characteristics in debris flow susceptibility assessment is quantitatively explained. Relative influence and partial dependence based on model structure further disclose the main drivers and their impacts on debris flow susceptibility. Factors affecting the performance of dry-wet cycle characteristics in debris flow susceptibility assessment models

have been disclosed by comparing the model performance from different study regions.

This study reveals the responsive relationship and explains the mechanisms between extreme weather events and regional debris flow susceptibility. A method is proposed to assess the debris flow susceptibility by considering dry-wet cycle characteristics. The contributions of various factors to debris flow susceptibility are quantified, enabling targeted disaster prevention and mitigation plans.

Keywords: Rainfall-induced debris flow; Dry-wet cycle; Recurrence interval; Susceptibility assessment; Wavelet analysis; Multifractal; Machine learning

PUBLICATIONS ARISING FROM THE THESIS

1. Jierui Li, Basanta Raj Adhikari, Xiaoli Ding, Shaolin Wu, Xiangrui Meng, Zhipan Niu, Xiangjun Pei, Yu Zhan, Baofeng Di. 2024. Frequent dry-wet cycles promote debris flow occurrence: Insights from 40 years of data in subtropical monsoon region of Sichuan, China. *CATENA*, 238, 107888.

ACKNOWLEDGEMENTS

This work has been completed thanks to the contributions of many individuals, including professors, teachers, staff, groupmates, and various institutions.

I would like to express my profound gratitude to my supervisor, Prof. Xiao-li DING, for his continuous advice and support. Prof. Ding has not only provided comprehensive guidance in my research but has also contributed valuable research data and resources for this thesis. Thanks to my co-supervisor, Prof. Baofeng DI from Sichuan University, for his invaluable advice and support.

I would also like to extend my thanks to Prof. George Z.Z. LIU, Prof. Xintao LIU, Prof. Shuo Wang, Dr. Naeem SHAHZAD, and Dr. Songbo WU for their significant suggestions, data provision, and support for this work. Thanks to Prof. Jiahong Wen from Shanghai Normal University and Prof. Lu Gao from Fujian Normal University for their comments and suggestions.

I am grateful to all the staff in the Department of Land Surveying and Geo-Informatics, with special thanks to Vaness YU, Ziki CHEUNG, Alvin TSE, and Jimmy KWAN, for their indispensable support.My gratitude also goes to my groupmates, including Xuanyu QU, Lei XIE, Zeyu ZHANG, and Guanxin LIU, for their encouragement and help.

I appreciate the funding and support provided by the Research Grants Council of the Hong Kong Special Administrative Region (PolyU 152164/18E and PolyU152233/19E), the Research Institute for Sustainable Urban Development (RISUD), the National Natural Science Foundation of China (Grant No. 42377168), and the National Key Research and Development Program of China (Grant No. 2023YFE0121900). As a joint Ph.D. candidate between The Hong Kong Polytechnic University and Sichuan University, I would like to extend my appreciation for the support from the Hong Kong Jockey Club Charitable Fund.

Finally, I wish to thank all my family and friends for their support of my work.

TABLE OF CONTENTS

LIST OF FIGURES

LIST OF TABLES

LIST OF PRINCIPAL ABBREVIATIONS

Abbreviation	Term	Page
ACF	Autocorrelation Function	73
ADF	Augmented Dickey-Fuller	71
ANN	Artificial Neural Network	127
AR	Autoregression	11
ARI	Average Recurrence Interval	23
ARIMA	Autoregressive Integrated Moving Average	11
ARMA	Autoregressive Moving Average	11
AUC	Area Under the ROC Curve	126
AWC	Available Water Capacity	36
DEM	Digital Elevation Model	36
DT	Depth of Decision Trees	141
DTM	Digital Terrain Model	36
DWCC	Dry-wet Cycle Characteristics	23
ED	Maximum Elevation Difference	44
EDWP	Extreme Dry-Wet Periods	23
ENTLI	Enhanced Natural Terrain Landslide Inventory	38
FN	False Negatives	124
FP	False Positives	124
FS	Factor of Safety	15
GBM	Gradient Boosting Machine	127
GLOF	Glacial Lake Outburst Flood	3

HKSAR	The Hong Kong Special Administrative Region	34
HWSD	Harmonized World Soil Database	44
KNN	K-Nearest Neighbor	49
LLR	Log-Linear Regression	127
LR	Learning Rate	141
MA	Moving Average	11
MNO	Minimum Number of Observations in Terminal Nodes	141
NT	Number of Decision Trees	141
PD	Partial Dependence	174
PDSI	Palmer Drought Severity Index	23
R^2	Coefficient of Determination	51
RI	Relative Influence	135
RMSE	Root Mean Square Error	51
ROC	Receiver Operating Characteristic	126
SARIMA	Seasonal Autoregressive Integrated Moving Average	12
SMCRS	Subtropical Monsoon Climate Region of Sichuan	33
SPI	Standardized Precipitation Index	63
TN	True Negatives	124
TP	True Positives	124
UAV	Unmanned Aerial Vehicle	38
USC	Underlying Surface Characteristics	24
VIF	Variance Inflation Factor	135

Chapter 1 Introduction

1.1 Background

According to statistics from the China Geological Survey, between 2005 and 2022, Mainland China experienced over 320,000 geological disasters of medium scale or higher. These disasters resulted in more than 9,100 deaths, over 2,100 missing persons, and direct economic losses amounting to 70 billion Chinese Yuan. The impacts of geohazards pose a severe threat to the safety of human lives and properties, hindering socioeconomic development. In recent years, technologies such as remote sensing, geographic information systems, and artificial intelligence have been widely applied to disaster prevention and mitigation efforts. Combined with improved policies and increased economic investment, the impacts of geological disasters on human society have significantly decreased.

However, extreme weather events have become increasingly frequent, leading to larger and more intense geological disasters related to climate change (Sung et al., 2020). For one thing, extreme drought events contribute to the accumulation of loose materials, leading to large-scale landslides, collapses, and debris flows. For another, extreme precipitation events can further trigger landslides and collapses, developing into larger-scale flash floods and debris flows (Chen et al., 2014; Chen et al., 2004; Nyman et al., 2019). The distribution of debris flow disasters is extensive, particularly in densely populated regions. Rainfall-induced

debris flows are widely distributed in inland and coastal mountainous regions. In areas influenced by monsoons, extreme precipitation is the predominant triggering factor for debris flows (Dowling et al., 2014; Hürlimann et al., 2019; Jiang et al., 2015). For example, Sichuan Province, located in southwestern China, is one of the inland provinces with the largest records of debris flow events in mainland China. Additionally, extreme precipitation caused by tropical cyclones is more likely to induce larger-scale debris flow disasters in coastal areas (Furuichi et al., 2018; Mizuyama et al., 2010). For example, the Hong Kong Special Administrative Region, situated in southern coastal China, has a long-term debris flow inventory with many records. It is evident that extreme weather events not only complicate the prevention and mitigation of debris flows but also pose threats to the development of human society.

Therefore, it is a challenge for human society to scientifically carry out regional debris flow prevention and mitigation work under extreme climates. A theoretical approach is desired to explain the formation and initiation mechanisms of debris flows related to extreme weather and to apply it to the practical process of regional debris flow early warning.

1.2 Literature review

1.2.1 Responses of debris flow to extreme climate

Debris flows are a type of special gravity flows where solid materials are transported by water. It is a frequent natural phenomenon in mountainous areas. However, due to the threat to the lives and properties of mountain residents and the potential damage to mountain infrastructure, debris flow disasters have attracted high attention from human society. Extreme weather events, including extreme precipitation, extreme drought, and tropical cyclones, play an important role in the formation or initiation of debris flows (Cui et al., 2011; Hürlimann et al., 2019; Keim, 2008). The interactions among these extreme weather events can also contribute to debris flow formation or initiation and can be understood in the context of climate dry-wet cycles (Poljansek et al., 2017). Debris flows can be classified into rainfall-induced debris flows, glacial lake outburst flood (GLOF)-induced debris flows, and snowmelt-induced debris flows based on the triggering mechanisms. GLOF-induced and snowmelt-induced debris flows predominantly occur in cold, high-elevation mountainous regions, whereas extreme precipitation is a crucial factor in triggering rainfall-induced debris flows. Therefore, rainfall-induced debris flows occur worldwide, which have received attention from numerous researchers and practitioners (Cheng et al., 2003; Guzzetti et al., 2020; Vergara Dal Pont et al., 2020).

1.2.1.1 Extreme wet

The rainfall threshold refers to the minimum precipitation level necessary to initiate a debris flow event and is widely utilized in issuing early warnings for rainfall-induced debris flows. A method based on determining regional rainfall thresholds was proposed early for regional debris flow forecasting (Tan et al., 1992). The rainfall threshold is typically determined based on monitoring data such as antecedent precipitation, rainfall intensity, and rainfall duration (Pan et al., 2018). However, current prediction models based on statistics often overlook the variations in rainfall thresholds caused by other relevant factors such as drought, wildfires, earthquakes, etc. Apart from earthquakes, factors that lower the rainfall threshold, such as drought and wildfires, are closely related to extreme weather conditions (Staley et al., 2016). Considering the frequent occurrence of extreme weather events, the issue of missed or false alarms in debris flow early warnings based on rainfall thresholds is difficult to address (Guzzetti et al., 2020). Therefore, incorporating the impacts of extreme weather events on rainfall thresholds may be an innovative and effective idea in reducing missed or false alarms in debris flow early warnings.

Tropical cyclones are also a type of extreme weather events that are highly related to debris flow disasters. Tropical cyclones include typhoons in the western Pacific region, hurricanes in the eastern Pacific and Atlantic regions, and tropical storms in the Indian Ocean region. In terms of the mechanisms of debris flow formation

and initiation, for one thing, like rainfall-induced debris flows caused by monsoons, typhoons bring intense rainfall that reduces the shear strength of the soil, causing the loose soil to slide with runoff and providing source materials for debris flows. For another, tropical cyclone transports debris, trees, rocks, and so on, further increasing the source materials for debris flows. Additionally, tropical cyclones carry a large amount of moisture from the ocean, which leads to heavy rainfall and landfall. The feedback between tropical cyclones and heavy rainfall intensifies the strength of cyclones and rainfalls (Ren et al., 2019). Therefore, tropical cyclones can magnify the scale of debris flows and cause greater impacts.

1.2.1.2 Extreme drought

The initiation of debris flows is highly correlated with preceding extreme drought conditions, as prolonged drought can generate loose materials for debris flows (Chen et al., 2014; Nyman et al., 2019). Research on machine learning-based debris flow susceptibility assessment models has shown that in arid valleys located in seismic zones, the drought index is the third most important factor after topography and precipitation, making it a significant dynamic factor in assessing debris flow susceptibility (Di et al., 2019; Xiong et al., 2020). However, most current debris flow warning models are based on rainfall thresholds and rarely consider pre-disaster long-term drought conditions (Chen et al., 2005a; Pastorello et al., 2020; Segoni et al., 2018). Therefore, although drought contributes significantly to debris flow occurrence, its importance has not been adequately

reflected in disaster prevention and mitigation. More comprehensive research is required from the perspective of the debris flow formation and initiation mechanisms related to extreme drought.

Besides directly affecting soil properties, extreme drought climate increases the likelihood of wildfires, further raising the potential of post-fire debris flow occurrences. For one thing, wildfires contribute to the formation of debris flows (Hu et al., 2011). The extensive death of vegetation following wildfires not only generates the necessary sediment for debris flow occurrences but also leads to ecological damage, reduced vegetation cover, and increased soil erosion, ultimately contributing to source materials for debris flows (Hu et al., 2018). For another, wildfires enhance the debris flow susceptibility. Wildfires heat the soil to high temperatures, altering its physical properties, disrupting soil structure, and increasing soil hydrophobicity. This directly results in the reduction of soil moisture infiltration during heavy rainfall, and increasing surface runoff transports loose materials, eventually leading to debris flow occurrences (Hewelke et al., 2018). Furthermore, the changes in soil properties following wildfires exacerbate the erosion process and promote the accumulation of loose materials (Liu et al., 2020). Therefore, wildfires triggered by prolonged extreme drought increase the risk of debris flow occurrences.

1.2.1.3 Dry-wet cycle

Dry-wet cycles refer to the alternating period of dry and wet in a specific region, which can reflect meteorological, hydrological, or soil-related variations. A dry-wet cycle index not only reflects extreme weather events but also captures the process of changes in underlying surface moisture conditions. Therefore, it can provide a more comprehensive explanation of the debris flow formation and initiation mechanisms (Tian et al., 2022). Laboratory simulation results confirm a significant reduction in soil strength after experiencing the dry-wet cycles (Lian et al., 2022). Mechanistically, the process of reducing soil strength during the dry-wet cycle is complex, multi-stage, and long-term, impacting soil properties in various ways and ultimately reducing soil strength. During the dry phase, as soil moisture is lost, soil particles shrink, creating voids and cracks, reducing soil cohesion, and increasing soil permeability. During the transition from dry to wet phase, the infiltration of water into voids and cracks increases pore water pressure, leading to reduced infiltration and increased hydrophobicity (Chen et al., 2014; Hewelke et al., 2018). During the wet phase, increased pore water pressure acts on soil particles from all directions for an extended period, destroying soil particle structures, the formation of micro-cracks, and a subsequent reduction in pore water pressure. During the transition from the wet to dry phase, internal micro-cracks in the soil rupture, resulting in a further increase of pore voids and cracks (Duan et al., 2023; Wasantha et al., 2014). Therefore, after repeated dry-wet

cycles, the internal structure of the soil is severely damaged, and soil strength significantly decreases. Regarding the entire process of dry-wet cycles, the influence of long-term dry-wet cycles on soil strength can be explained from the perspective of weathering (Hai et al., 2023). In areas with less vegetation cover and lower biodiversity, the weathering process is mainly physical weathering, that is, during dry-wet cycles, temperature fluctuations cause the rock and soil to expand when heated and contract when cooled. The repeated expansion and contraction lead to the fracturing and breakdown of the rock and soil into smaller particles, thereby reducing the soil strength (Wei et al., 2022). In areas with more vegetation cover and higher biodiversity, chemical weathering predominates, where the cyclical crystallization and dissolution of soil-soluble salts during dry-wet cycles cause the destruction of soil structure and an increase in the looseness between particles, ultimately leading to a reduction in soil strength (Cao et al., 2022; Xu et al., 2020). However, although it is known that dry-wet cycles can reduce soil strength and thereby increase the likelihood of debris flow occurrences, current research predominantly focuses on explaining the formation and initiation mechanisms of debris flows based on dry-wet cycles. At the regional scale, constructing long-term series indicators of dry-wet cycles and exploring the relationship between the dry-wet cycles and the debris flow frequency has not been deeply investigated.

1.2.2 Periodicity of climate and debris flows

The recurrence period of debris flows reflects their frequency, and their occurrences may be responsive to dry-wet cycles. Utilizing the responsive pattern between debris flows and climate dry-wet cycles, combined with the short-term predictability of regional meteorological conditions, is a potential new approach to breaking through the bottleneck of low accuracy and specificity in debris flow early warning systems. However, current research on integrating the debris flow cyclicity with climatic periodicity for debris flow early warning is still insufficient.

1.2.2.1 Time series analysis

A time series is a set of data with time information. Time series data often exhibit attributes such as level, trend, seasonality, and cyclicity, which reflect the underlying characteristics like stationarity and autocorrelation, although these features are not universally present in all datasets. The average value of a time series is called the level, while the long-term change in the level is called the trend. Seasonality indicates the regular variation of time series data over a certain time interval, which refers not only to the seasons but also to weeks, months, or years. Cyclicity is like seasonality but with an irregular frequency of fluctuation. In the context of frequent extreme weather events, the study of meteorological time series is of great importance. For example, research on global surface temperature provides various statistical parameters to describe trend characteristics,

quantitatively reflecting the trend of global warming (Mudelsee, 2019), and ultimately proposing various countermeasures such as carbon neutrality. Similarly, the seasonal characteristics of meteorological factors during the dry and wet seasons have been widely applied to the study of natural disasters closely related to extreme weather, including debris flows, flash floods, and wildfires (Özer et al., 2019; Swain, 2021; Zhang et al., 2019), to reduce casualties, economic losses, or ecological damage. Furthermore, some studies have proposed a close relationship between repeated climate dry-wet cycles and regional droughts or floods (Scanlon et al., 2022), but quantitative applications of the cyclicity of extreme dry-wet events are still relatively rare. Meteorological time series studies, besides focusing on trends, seasonality, and cyclicity, also consider homogeneity in geographical space as an important feature applicable to data mining (Afrifa-Yamoah et al., 2020). However, current research on meteorological time series often focuses on single elements such as temperature, air pressure (Southern Oscillation Index), precipitation, etc., with less research on regional meteorological characteristics under the response of multiple factors. Mining and analyzing meteorological time series within a certain geographical space can enhance the understanding of regional meteorological characteristics, thereby facilitating accurate predictions of regional meteorological conditions.

1.2.2.2 Time series forecasting

Common methods for predicting time series data can be divided into two categories including those based on traditional statistical models and those based on artificial intelligence models. The principle of time series data prediction is to estimate future data reasonably by mining and applying the characteristics of time series based on their stationarity and autocorrelation. A stationary time series, with a fixed level and no obvious correlation with time, can be used to construct an Autoregression (AR) model based on historical data from different time points within the series. This model can then be used to predict future time series data. In addition, a Moving Average (MA) model can be built for the noise term in the AR model, combining to form an Autoregressive Moving Average (ARMA) model to further reduce prediction bias. However, for non-stationary time series data, it is necessary to perform differencing to make the data stationary, resulting in an Autoregressive Integrated Moving Average (ARIMA) model. In constructing an ARIMA model, the order of autoregression and moving averages, as well as the number of differencing steps are the three hyperparameters that need to be adjusted. However, the ARIMA model can struggle to make a time series stationary when predicting time series with seasonality or cyclicity, even when increasing the differencing order and steps. A seasonal time series model can be developed by combining the non-seasonal terms of the ARIMA model with additional seasonal terms, resulting in a Seasonal Autoregressive Integrated

Moving Average (SARIMA) model. In addition to the three ARIMA hyperparameters for the non-seasonal terms, the SARIMA model has four seasonal hyperparameters, including the order of autoregression, the order of moving averages, the number of differencing steps, and the additional hyperparameter of the seasonal period (Barman et al., 2020). Compared to time series prediction methods based on traditional statistical models, methods based on artificial intelligence models can capture the complex nonlinear relationships in time series to predict non-stationary time series. Common machine learning-based time series prediction models, such as the support vector machine and artificial neural network, can achieve smaller prediction errors, and their performance is influenced by the characteristics of the time series data (Das et al., 2018; Samsudin et al., 2010). With the development of deep learning, Recurrent Neural Networks (RNNs), including Gated Recurrent Units (GRUs) and Long Short-term Memory (LSTM) models, can capture long-term dependencies in time series data, thus predicting future complex nonlinear relationships, and they usually outperform support vector machine and artificial neural network (Rajagukguk et al., 2020; Zang et al., 2020). However, compared to traditional statistical models, artificial intelligence models have fewer restrictions on data patterns but require more time-series samples, especially those relying on neural networks, which also require a considerable amount of time for training. Therefore, an appropriate time series prediction model should be chosen based

on the characteristics and volume of data, as well as the tradeoff between time consumption and prediction accuracy.

1.2.2.3 Debris flow recurrence interval

It is found that debris flow occurrences exhibit cyclicity, which is closely related to the characteristics of the underlying surface, meteorological conditions, and other influencing factors. Rainfall-induced debris flows coincide with the cyclical pattern of local extreme precipitation events (Cheng, 2002; Tan et al., 1992; Wei et al., 1994). The cyclicity of debris flows can be quantified through the recurrence interval of debris flows. The average recurrence interval of debris flows is a common indicator used to estimate the probability of debris flows in large areas, characterizing the temporal distribution of debris flow occurrences in a certain area. It can be used to reflect the recurrence period of debris flows, and a shorter recurrence interval indicates a higher susceptibility to debris flows (Ouyang et al., 2019). Different methods, such as stratigraphic methods (Coe et al., 2003; Jakob et al., 2005), ecological methods including dendrochronology and lichenometry (Germain et al., 2020; Tie et al., 2014), numerical models based on rains, floods, or other triggering events of debris flows (Cheng, 2004; Phillips et al., 2005), as well as morphological methods combining field measurements and remote sensing by satellites and unmanned aerial vehicles (Garankina et al., 2019; Lin et al., 2004), can all be used to estimate the average recurrence interval. However, estimates based on historical records are more direct and usually have

higher reliability (Hürlimann et al., 2019; Kobiyama et al., 2019), but there is often a problem of incomplete or even missing data in remote areas (Carrara et al., 2003). Therefore, if the average recurrence interval of debris flows is estimated based on a substantial number of events in a certain area, it is possible to quantitatively describe the spatiotemporal pattern of debris flow disasters.

1.2.3 Assessment of debris flow susceptibility

The debris flow susceptibility assessment models based on machine learning are well-suited for evaluating regions with a substantial number of debris flow samples due to the ease of data acquisition, comprehensive assessment factor system, flexible spatiotemporal scale, and good model interpretability.

1.2.3.1 Advantages of machine learning models

Physical models and statistical models are commonly used for assessing the susceptibility of regional debris flows with different strengths and limitations (Bregoli et al., 2015). Physical models simulate the formation and initiation process of debris flows by considering slope stability and potential runoff patterns (Nyman et al., 2019; Stancanelli et al., 2017). However, due to the variability in the mechanisms of debris flow formation and occurrence in different regions, the parameters of physical models need to be adjusted accordingly. Although physical models may perform well in assessing susceptibility at a single gully or medium-small scale, they may have certain limitations when applied to larger

study areas. Statistical models evaluate debris flow susceptibility based on event records and standardized environmental data, such as topography, meteorology, geology, socio-economic activities, vegetation cover, soil properties, erosion, and hydrological conditions (Di et al., 2019; Xiong et al., 2020). These models provide a more comprehensive description of the large-scale regional geographic environmental characteristics, and thus they have a certain generalizability in regional debris flow susceptibility assessment. However, empirical statistical and artificial intelligence models, as data-driven approaches, require a higher volume of data compared to physical models.

In physical models, the infinite slope model is a simple and effective method for studying the stability of shallow slopes. This model assumes an infinitely long slope length, thereby simplifying the calculation and analysis process. Although the model assumptions neglect the impact of factors such as terrain and groundwater levels on boundary conditions, they can still provide valuable estimates of slope stability (Fuchs et al., 2014; Muntohar et al., 2010). Slope stability estimation based on the infinite slope model is typically represented by the Factor of Safety (FS). The FS can be used to reflect the susceptibility of debris flows (Park et al., 2013). The FS is the ratio of the resisting forces against sliding to the driving forces, that is, the proportion of the soil's internal frictional resistance to the gravitational force component acting down the slope (Wang et al., 2014). The internal frictional force can be calculated based on the Mohr-

Coulomb model, which uses experimental measurements of the soil sample shear strength (Di et al., 2021). Common methods for measuring shear strength include the direct shear test and the triaxial shear test, where conditions such as consolidation and drainage are determined based on soil properties and environmental conditions (Bai et al., 2019). For rainfall-induced debris flows, it is assumed that drainage conditions are dominant due to the typically prolonged duration of precipitation (Stamatopoulos, 2015). Prolonged precipitation can lead to an increase in soil pore water pressure, reducing the soil shear strength, and increasing the unit weight of saturated soil, collectively leading to a decrease in the FS and an increased risk of debris flows.

Machine learning is a representative method of artificial intelligence models, and the development and application of individual models have become relatively mature. Linear models, such as log-linear regression, logistic regression, and support vector machines, assume a linear relationship between the dependent variable and multiple independent variables (i.e., evaluation indicators). These models are constructed by fitting the weight coefficients of each independent variable. However, due to their relatively simple structure, linear models do not perform well with complex nonlinear problems. Algorithms based on decision trees, such as random forests and gradient boosting machines, build decision trees that classify samples based on the features corresponding to evaluation indicators. By integrating the classification results of a certain number of decision trees,

these models achieve more accurate classification of samples and can interpret evaluation indicators based on the structure of the decision trees, but they must be monitored for overfitting. Distance-based algorithms like K-means and K-nearest neighbor classify samples based on the distance between evaluation indicators of samples. These models have a simple construction process but suffer from a steep increase in computational resource consumption with increasing data dimensions and are relatively sensitive to outliers. Neural networks, such as the artificial neural network and multilayer perceptron, identify various features of samples through different neurons and build a weighted network, making them suitable for processing high-dimensional large datasets. However, training neural networks consumes substantial computational resources, and interpreting evaluation indicators is more complex. These representative machine-learning models can be effectively applied to large-area debris flow susceptibility assessments (Di et al., 2019; Ng et al., 2021; Xiong et al., 2020). However, the performance of the models may vary with the changing characteristics of the study area, and the degree of model performance needs to be reflected by comparing performance metrics.

1.2.3.2 Factor system

The construction of a susceptibility assessment indicator system for debris flows requires the consideration of the mechanisms behind their formation and initiation, influenced by various factors such as geology, topography,

meteorology, soil, hydrology, vegetation, and human activities (Kumar et al., 2023). Common geological indicators include proximity to faults, indicative of seismic intensity and the frequency of co-seismic landslide deposits (Huang et al., 2020), and rock types, reflecting the impact of lithology on debris flow development (Wang et al., 2015). Topographical indicators such as elevation difference, slope gradient, aspect, and curvature are widely utilized, with elevation difference representing the potential energy of slopes, slope gradient indicating the capacity to convert potential into kinetic energy (Wei et al., 2015), aspect affecting vegetation growth and landslide recovery due to variations in sunlight duration (Li et al., 2020), and curvature influencing the accumulation rate of material sources and flow convergence (Achour et al., 2018; Dash et al., 2022). Meteorological influencing factors involve precipitation, temperature, wind speed, relative humidity, and sunshine duration, alongside derived indicators like dry-wet indices (Achour et al., 2018; Di et al., 2019), with precipitation being a critical trigger for debris flows, necessitating a comprehensive consideration of intensity and duration (Kumar et al., 2023; Wei et al., 2015). In terms of soil, moisture content can reflect the capacity for runoff generation after heavy rainfall, while erosion status is closely related to the soil structure (Hewelke et al., 2018; Kean et al., 2011). Hydrological indicators such as catchment area, distance to water bodies, and river density are used. Vegetation indicators, such as coverage and type, are frequently applied since reduced vegetation cover can ultimately decrease slope stability (Hu et al., 2018), and

different vegetation types vary in their water retention capabilities (Zhang et al., 2021). Human activities are represented by indicators such as land use type, population density, and road density, reflecting the impact of human habitation, exploitation, and construction on soil stability (Di et al., 2019; Xiong et al., 2020). However, the key to enhancing the performance of debris flow susceptibility assessment models lies in the construction of localized assessment indicators based on the geo-environmental characteristics of different study areas. Consequently, the factor system is not fixed, and the contribution of various indicators to debris flow susceptibility varies across different study areas.

According to the debris flow susceptibility assessment results based on machine learning, susceptibility assessment can be conducted using visualization methods, though such assessment is generally static (Nie et al., 2022). The predictive datasets for machine learning models can be divided into constant and dynamic variables, with dynamic variables like meteorological factors being continuously updatable, thereby facilitating the construction of dynamic debris flow susceptibility assessment models based on machine learning (Fischer et al., 2012; Pavlova et al., 2014). Machine learning algorithms can apply big data to explore and quantitatively characterize potential correlations among multiple factors using statistical principles and can elucidate the quantitative impact of these factors on debris flow susceptibility through the model structure. By identifying the most important factors, machine learning models effectively address the

issues of physical mechanism interpretation which traditional statistical models struggle to resolve (Dikshit et al., 2021; Sun et al., 2021). Adjustments in parameters and the selection of assessment factors for the application of debris flow susceptibility models in different regions can provide more targeted and reasonable guidance for regionalized disaster prevention and mitigation measures (Di et al., 2019; Liu et al., 2018; Xiong et al., 2020).

1.2.3.3 Assessment unit

For debris flow susceptibility assessment using machine learning, in addition to the establishment of an indicator system, the selection of an assessment unit is also crucial. This is due to the assessment units typically serving as the fundamental units for implementing disaster prevention and mitigation measures for debris flows when applying susceptibility assessment results. Common assessment units for debris flow susceptibility include watershed units and grid units. A watershed is a geomorphological unit with a single outlet, also serving as the basic unit for the formation and initiation of debris flows, thus more reasonably capturing the influence of geological and geomorphological characteristics on debris flows. However, regional-scale data such as topography, meteorology, and land use are often derived from grid units, making the data from grid units more representative and reliable (Nie et al., 2022; Qin et al., 2019). Therefore, when selecting assessment units, the influence of factors in the indicator system related to geological and geomorphological characteristics must

be considered, while the accuracy of the data sources for the indicators should also be ensured. Moreover, watershed units are a natural geographic division with relatively fixed areas, while grid units can have their resolution adjusted to meet specific needs and adapt to different research scales. The construction of machine learning models requires abundant samples for training, validation, and testing, hence for smaller-scale study areas, which cannot generate enough watershed units as samples, grid-based assessment units are more appropriate.

1.3 Research scope

1.3.1 Research Questions

Regarding the current research gaps in the field of this study, this research aims to address the following two key research questions:

(1) What is the responsive relationship between debris flow susceptibility and climate dry-wet cycles?

(2) Which factors influence the responsive relationship between debris flow susceptibility and climate dry-wet cycles?

1.3.2 Objectives

To answer the questions, this study aims to provide an in-depth analysis of the relationship between debris flow susceptibility and climate dry-wet cycles, with an emphasis on developing methodologies for debris flow susceptibility assessment. The objectives of this research are as follows:

(1) Constructing indicators of dry-wet cycle characteristics to represent the long-term pre-disaster dry-wet cycle characteristics in regions affected by debris flows.

(2) Estimating the recurrence period of debris flows to disclose the responsive relationship between debris flow susceptibility and climate dry-wet cycle characteristics.

(3) Establishing a debris flow susceptibility assessment model to validate the feasibility of predicting debris flow susceptibility using dry-wet cycle characteristics.

(4) Comparing inland and coastal typical regions to explore the conditions affecting the use of dry-wet cycle characteristics in debris flow susceptibility assessment.

1.3.3 Methodology

The following methodologies are included to achieve the research objectives:

(1) By applying geostatistical universal kriging considering terrain for spatial interpolation, this study extends the precipitation data from monitoring stations and potential evapotranspiration data estimated based on the Penman-Monteith equation to the assessment units. Leave-one-out cross-validation is used to quantify the representativeness of the interpolation results. Subsequently, these results are combined with soil data of the study units to construct a time series of the Palmer Drought Severity Index (PDSI), which serves as the dry-wet index in this study. The SARIMA model is used to predict and verify the accuracy of the dry-wet index for the coming month. Further time-series analyses of the dry-wet index include tests for stationarity, autocorrelation analysis, wavelet analysis, and multifractal analysis to ultimately obtain the dry-wet cycle characteristics (DWCC), such as extreme dry-wet periods (EDWP) based on wavelet power spectrum and extreme dry-wet characteristics based on multifractal spectrum parameters.

(2) For each watershed with debris flow records in the subtropical monsoon-affected region of Sichuan Province, debris flow recurrence buffer zones are constructed using two methods: one based on the equivalent diameter of the debris flow watershed and the other based on the nearest neighboring debris flow watershed. Within a buffer zone, the recurrence intervals of the debris flows are calculated and then estimated as the average recurrence interval (ARI) for the corresponding debris flow watershed. The correlation between EDWC and ARI

is then obtained to quantify the relationship between debris flow susceptibility and the climate dry-wet cycle. In addition, through field investigations and soil sampling of debris flow gullies, FS is measured to quantify the debris flow susceptibility. Correlation analyses between the FS and DWCC are conducted to further validate the responsive relationship between debris flow susceptibility and climate dry-wet cycles.

(3) Taking the subtropical monsoon area in Sichuan Province as an inland typical region, this study uses K-means clustering based on the geological and topographical conditions of watersheds. The number of clusters corresponding to the maximum average silhouette coefficient is used to divide the subtropical monsoon area in Sichuan Province into a corresponding number of zones with different underlying surface characteristics (USC). For the coastal typical region represented by the Hong Kong Special Administrative Region, this study divides assessment units based on the scale of historical debris flow gullies. Positive and negative samples are constructed based on the presence or absence of debris flow records within a month, and assessment factors required for debris flow susceptibility, including geology, topography, meteorology, DWCC, vegetation cover, and human activities, are extracted for each assessment unit. Four representative machine learning methods are compared, and the best-performing model is selected based on model performance metrics. The model generalizability is ensured through cross-validation with different fold numbers.

Model optimization involves selecting assessment factors through collinearity diagnosis and tuning model hyperparameters to simplify and enhance model performance. The model is tested on datasets not involved in training, and the performance of the DWCC predicted by SARIMA when applied to model testing is evaluated.

(4) Based on the established debris flow susceptibility models in the subtropical monsoon area in Sichuan Province and the Hong Kong Special Administrative Region, the relative influences of assessment indicators are calculated according to the model structure to quantify their contributions to debris flow susceptibility assessments. Partial dependence plots are drawn to reveal the main controlling factors and characteristics of debris flow susceptibility based on various assessment factors. Adaptation measures for disaster prevention and reduction of debris flows are formulated according to the performance of each main controlling factor in the susceptibility assessment and the characteristics of different study areas. Focusing on the role of DWCC in debris flow susceptibility assessment, the study discusses factors that may affect the response of debris flows to dry-wet cycles by examining the similarities and differences in assessment methods and model interpretation results between the two typical study areas, aiming to reveal the applicable conditions of the debris flow susceptibility assessment model based on DWCC.

Based on the methodologies involved, a flowchart is shown in Fig. 1-1:

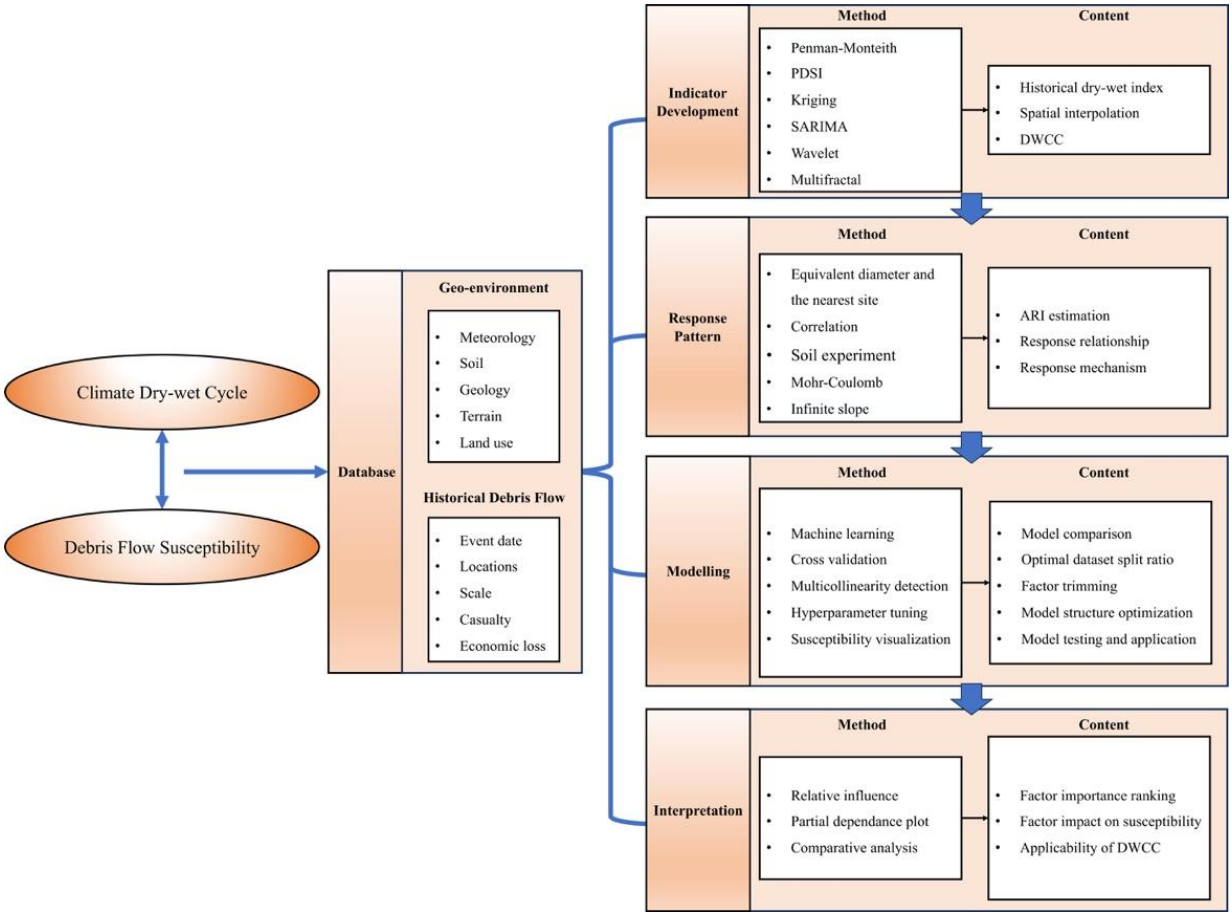

Fig. 1-1. Flowchart of research methodology

1.3.4 Significance

Currently, it is difficult to quantitatively characterize the mechanisms of debris flow formation and initiation, resulting in frequent missed or false alarms in debris flow early warning. It is still challenging to obtain accurate and targeted debris flow early warning on a large regional scale due to the lack or low accuracy of basic data. The significance of this study is utilizing meteorological data within a regional scope, combined with geographical and environmental information, and applying theories or technologies including statistical analysis, fractal theory,

time series analysis, remote sensing, geographic information systems, and machine learning to explore the responsive relationships and mechanisms between debris flow susceptibility and extreme weather events. The aim is to develop new technologies for debris flow susceptibility assessment in different typical regions, considering extreme climate factors, and providing scientific guidance for debris flow conducting prevention and mitigation measures under the background of increasing extreme weather events.

Debris flows triggered by extreme precipitation have drawn significant attention due to their widespread occurrence in both inland and coastal regions with different climatic characteristics. Especially, for regions with a larger population density, the impacts of debris flow events on human society will be more concerned. In this study, the sub-tropical monsoon climate region of Sichuan Province, China, is selected as a representative inland monsoon area, while the Hong Kong Special Administrative Region is chosen as a typical coastal monsoon area. According to data from the China Geological Survey, Sichuan Province consistently records the highest level of debris flow disasters among all provincial administrative regions in China. Within the monsoon climate region, the potential risk of debris flows is further amplified due to its high population density. Significant progress has been made in geological disaster prevention and mitigation work in recent years due to increased financial investment and improved regulations, but the large-scale and frequent debris flows caused by

extreme weather events still result in fatalities, missing persons, and injuries during the rainy season. Therefore, conducting studies on the regional debris flow susceptibility considering the impacts of extreme weather events in the sub-tropical monsoon climate region of Sichuan Province is of great practical significance and an important aspect of addressing the impact of extreme climate on human society. Although the area of the Hong Kong Special Administrative Region is relatively small compared to the sub-tropical monsoon climate region of Sichuan Province, the debris flow prevention and mitigation work in Hong Kong still deserves concentration. For one thing, due to the scarcity of land resources, Hong Kong experiences significant slope development, which greatly increases the risk of debris flows. The government thus attaches great importance to slope safety. For another, the Hong Kong Special Administrative Region has a long history of debris flow records and has made sufficient investments in debris flow prevention and mitigation measures, ultimately achieving significant success in debris flow risk control. Additionally, considering the factor of typhoons that occur in Hong Kong every year is also an important aspect of considering the impacts of extreme weather events on debris flow disasters. By selecting the two typical rainfall-induced debris flow regions, one inland and one coastal, this research not only verifies the spatial adaptation of the debris flow susceptibility assessment model in different study areas but also explores the performance of various assessment indicators in different locations.

1.4 Overview of structure

This thesis is structured into 7 chapters:

(1) Introduction. The first chapter introduces the background of this study and reviews related research progress, based on which the research scope including research questions, objectives, methodologies, and significance is summarized. The structure of this thesis is shown in this chapter.

(2) Study Area and Data. The second chapter introduces two study areas involved in this paper, i.e., the subtropical monsoon climate region of Sichuan Province and the Hong Kong Special Administrative Region. Debris flow susceptibility models that consider climate dry-wet cycles will be constructed in both study areas for comparisons in the following chapters.

(3) Representation of dry-wet cycle characteristics. The third chapter describes the process of extracting daily monitoring data from meteorological stations to the assessment unit and calculating its dry-wet index. It also includes the monthly forecast of dry-wet index time series. DWCC including EDWP and extreme dry-wet characteristics are quantified in this chapter.

(4) Impact of dry-wet cycle characteristics on debris flow susceptibility. The fourth chapter proposes two methods based on historical debris flow records to

estimate the ARI of debris flows and explores the correlation between it and EDWP. In this chapter, soil experiments in typical debris flow gullies validate the responsive patterns of debris flow susceptibility to DWCC and explain the responsive mechanisms.

(5) Debris flow susceptibility model based on dry-wet cycle characteristics. The fifth chapter focuses on the subtropical monsoon climate region of Sichuan Province and the Hong Kong Special Administrative Region as study areas. It divides the subtropical monsoon climate region of Sichuan Province into different zones based on USC. A debris flow susceptibility assessment model based on dry-wet cycle characteristics is established in each study area (zone). This chapter includes model comparison, model optimization, model testing, and model application.

(6) Main drivers of regional debris flow susceptibility. The sixth chapter, based on the debris flow susceptibility assessment models constructed in the two typical study areas, identifies the main drivers and quantifies the characteristics of debris flow susceptibility according to the performance of assessment factors in the models. It also compares the performance of DWCC in different study areas when assessing debris flow susceptibility, summarizing the conditions affecting the applicability of DWCC.

(7) Conclusions and Future Work. The seventh chapter summarizes the entire research and points out the current limitations and future research directions.

Chapter 2 Study Areas and Data

2.1 Overview of study areas

This study will focus on the impact of climate dry-wet cycles on rainfall-induced debris flows. Due to the varying effects of the climate dry-wet cycle on the mechanisms of three types of debris flows, i.e., rainfall-induced, GLOF-induced, and snowmelt-induced, the exploration of their respective responsive patterns will be impacted in this study. Rainfall-induced debris flows, which are more widely distributed in areas with dense human activities, pose a greater impact on human society. Consequently, this research focuses on the responsive patterns of rainfall-induced debris flows to the climate dry-wet cycle, particularly in the typical regions of the subtropical monsoon climate zone. The study ultimately selects the monsoon-affected region of Sichuan Province in Southwest China as a typical inland study area and the Hong Kong Special Administrative Region in Southern China as a typical coastal study area. The comparisons between the two study areas aim to investigate the responsive relationship between climate dry-wet cycles and debris flow susceptibility in different terrestrial or marine locations. Both study areas have extensive records of mostly rainfall-induced debris flows and abundant geographical environmental data. By conducting comparative research, this study can identify the applicable conditions under which the climate dry-wet cycle affects debris flow susceptibility and develop a more generalized susceptibility assessment model for debris flows. This proposed

model will provide reasonable and targeted disaster prevention and mitigation references for decision-makers in different regions.

2.1.1 Inland monsoon region

Sichuan Province, located in the southwest of China (26°03′ - 34°19′N, 97°21′ - 108°12′E), was preliminarily selected as a typical inland monsoon study area (Fig. 2-1). With a total area of approximately 485,000 square kilometers, Sichuan lies upstream of the Yangtze River, spanning the first and second topographical steps of China, featuring significant elevation differences with a maximum variation exceeding 7,000 meters. The province is primarily composed of mountains, hills, plateaus, and plains, with mountains accounting for about 85% of its total area (Wang et al., 2020). Sichuan incorporates multiple fault zones and has experienced several major earthquakes in the past years, including the Ms. 8.0 Wenchuan earthquake (2008), the Ms. 7.0 Lushan earthquake (2013), and the Ms. 7.0 Jiuzhaigou earthquake (2017), which destabilized mountain slopes and generated loose materials (Fan et al., 2021). The climate of Sichuan Province is dominated by the subtropical monsoon climate in the Sichuan Basin and the plateau climate in the western Sichuan Plateau. The vegetation in the Sichuan Basin is primarily subtropical evergreen broadleaf forests, while the western Sichuan plateau is characterized by shrub meadows. Influenced by the monsoon climate, the Sichuan Basin receives about 75% of its annual precipitation,

approximately 1100 millimeters, from June to October, which is prone to triggering debris flows in the surrounding mountain areas (Di et al., 2019). The various climate types of Sichuan result from its considerable elevation differences and diverse micro-terrain, with monthly average temperatures ranging from -30.6°C to 36.4°C, according to data from the China Meteorological Data Service Center. Annually, Sichuan Province suffers from debris flow disasters that lead to casualties and economic losses. For example, the widespread flash floods and debris flows in July 2022, resulted in 8 deaths, 10 missing persons, and direct economic losses of 679 million Chinese yuan, particularly affecting infrastructure, local houses, and agriculture. The coupled effects of topography, seismic activity, and meteorological events create favorable conditions for the frequent occurrence of debris flows in this region (Chen et al., 2014; Di et al., 2019; Fielding et al., 2012).

In this study, the focus is on the influence of the climate dry-wet cycle on rainfall-induced debris flows. Therefore, the study area was narrowed down to the subtropical monsoon climate region of Sichuan (SMCRS) to mitigate the impact of GLOF-induced and snowmelt-induced debris flows which are more prevalent in the regions affected by plateau climate. The study area under investigation encompasses an area of approximately 266,000 square kilometers, accounting for 54.8% of the total area of Sichuan Province.

2.1.2 Coastal monsoon region

The Hong Kong Special Administrative Region (HKSAR) of southern China (22°08' - 22°34' N, 113°49' - 114°30' E) was selected as a typical study area located within the coastal monsoon region (Fig. 2-1). Covering a land area of about 1,100 square kilometers, the HKSAR is situated at the estuary of the Pearl River and its bedrock primarily consists of granite and volcanic rocks, with some areas exposing metamorphic sedimentary rocks (Lee et al., 1997). Approximately 75% of the undeveloped terrain in the HKSAR is classified as hills or mountains. Despite being a coastal region, it has an average elevation of about 100 meters, with the highest peak exceeding 900 meters, indicating substantial elevation differences. The dominant vegetation type is the South Asian tropical evergreen broadleaf forest, which includes various vegetation layers such as trees, shrubs, and herbs, as well as unique plant communities like mangroves found in intertidal zones (Zheng et al., 2018). The HKSAR has a subtropical monsoon climate with rainfall occurring more frequently at mountaintops and the city center compared to nearby coastal areas, with about 90% of its annual rainfall occurring between April and October (Shu et al., 2021). On average, the HKSAR experiences 5 to 7 typhoons annually, typically resulting in extreme precipitation (Sewell et al., 2015). The average temperature during the summer season is 28.4 °C, and due to subsidence airflows caused by tropical cyclones, daily maximum temperatures can exceed 35°C (Chang et al., 2021). The mountainous terrain and extreme

rainfall of HKSAR also lead to debris flow disasters. For instance, a severe rainstorm on June 7, 2008, triggered approximately 900 debris flow occurrences (Zhou et al., 2019).

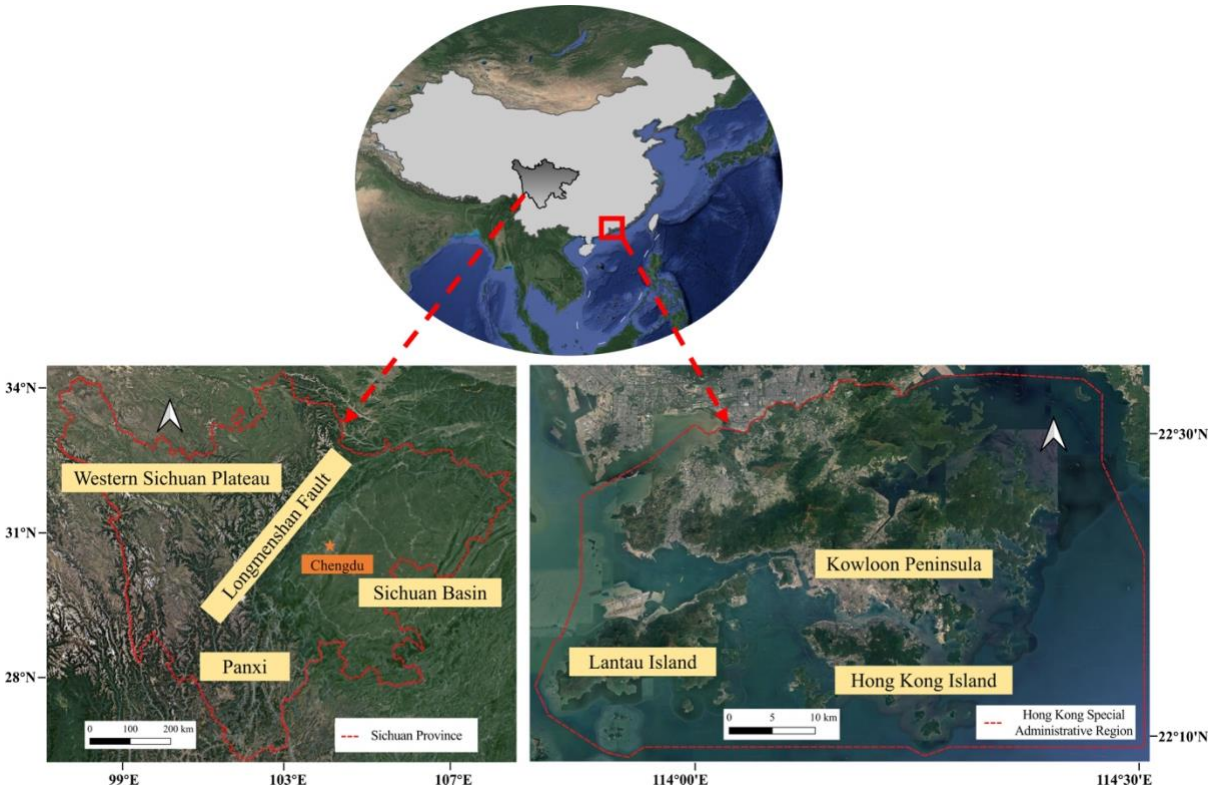

Fig. 2-1. Locations of study areas

2.2 Data

The research data required for this study encompasses two distinct areas, i.e., SMCRS and HKSAR. The debris flow data include details on the timing of events, geographical location, scale, and impact of the occurrences. Meteorological data comprise daily records from ground-based weather stations, including precipitation, temperature, relative humidity, wind speed, and sunshine duration.

Geological data incorporate rock types and fault information. Topographic data are extracted based on the Digital Elevation Model (DEM) or Digital Terrain Model (DTM). Soil data encompass information on the available water capacity (AWC) of soil. Land use data are primarily employed to characterize human activities and vegetation cover.

2.2.1 Debris flow data

Debris flow records in the SMCRS from 1981 to 2020 were compiled by combining disaster inventories prepared by the Sichuan Geo-Environment Monitoring program, news reports, and literature (Di et al., 2019; Fan et al., 2019). Hydrological analysis tools based on ArcGIS were used to divide SMCRS into 16,195 watersheds (Xiong et al., 2020). These were further refined based on the distribution of valley topography to correct the delineation of the watersheds (Fig. 2-2). The average area of the watersheds within SMCRS is 16.4 ± 0.1 km^2 (mean ± standard error). To avoid oversampling, duplicate records of debris flows occurring within the same watershed in a single month were removed, resulting in a final selection of 772 debris flow records for the calculation of the regional ARI and pre-disaster DWCC. For the construction of a debris flow susceptibility prediction model, 743 records from 1981 to 2019 were used as positive samples for the training dataset. Watersheds with debris flow records were excluded, and an equal number of non-debris flow sites were randomly determined as negative

samples. Each negative sample was randomly matched with a positive sample to assign a pseudo-occurrence date. The 29 debris flow cases from 2020 were used to test the proposed models, ensuring no overlap with the training dataset. This approach was taken to validate the generalizability of the developed debris flow susceptibility assessment model to different datasets.

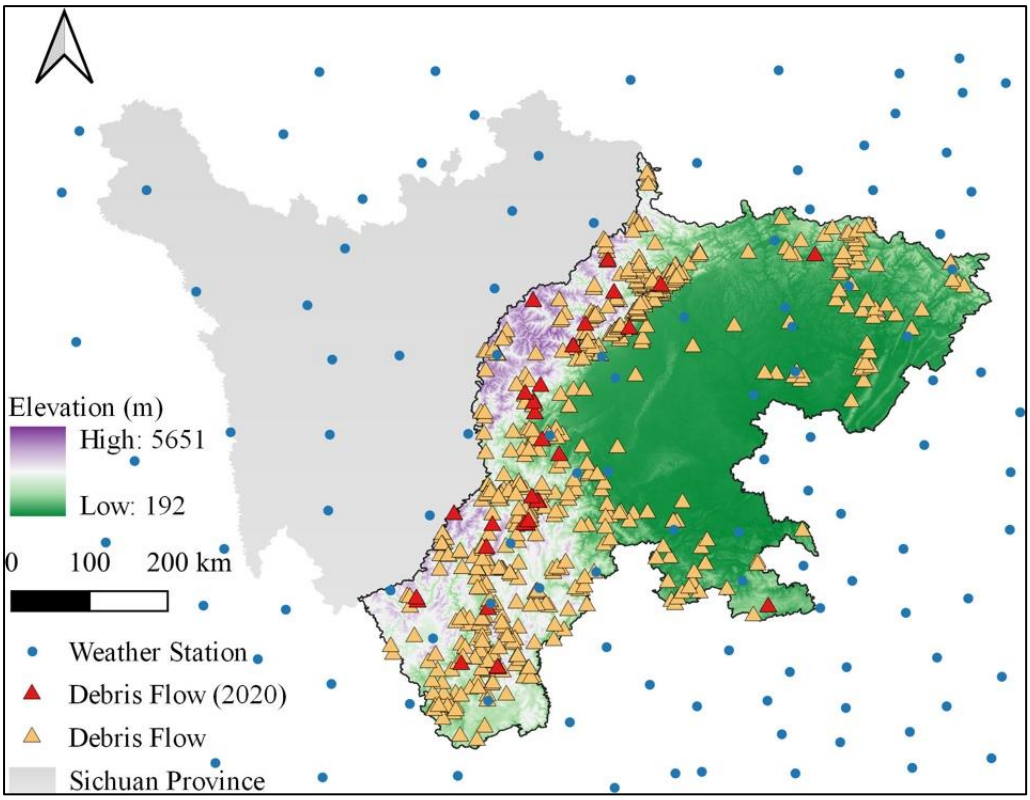

Fig. 2-2. Debris flow distribution in the SMCRS (area with elevation data)

Debris flow records for the HKSAR were obtained from the Civil Engineering and Development Department, encompassing 1,848 events from 2010 to 2019 (Fig. 2-3). These records include the occurrence date of the event, geographical coordinates, volume of the collapsed material (m^3), casualty and injury numbers,

evacuated population, and the number of closed roads. The Enhanced Natural Terrain Landslide Inventory (ENTLI) dataset, compiled by the Geotechnical Engineering Office of Civil Engineering and Development Department, identifies debris flow channels through unmanned aerial vehicle (UAV) imagery, spanning from 1924 (the first year debris flows were observed from aerial photography) to 2018, with a total of 7,091 records. Each record includes the width of the main scarp (m), the length of the source area (m), and the elevation difference between the crown and toe of each debris flow (m). The maximum length of the source areas (117 m) was used as the radius for the debris flow buffer zones, and the highest precision debris flow susceptibility assessment unit grid resolution was set at 250 m to ensure that the assessment unit area was not less than the buffer zone area. This provided a total of 20,451 grids as assessment units. To prevent oversampling, duplicate records within the same grid occurring in a single month were removed. An equal number of non-debris flow points were randomly generated in the study area, ensuring that their buffer zones did not overlap with those of the debris flow sites. Each non-debris flow site was randomly matched with a debris flow site to assign a pseudo-occurrence date. Ultimately, 977 grids with debris flow records and an equal number of grids without debris flow records were selected. In the process of constructing the debris flow susceptibility assessment model, 904 grids with debris flow events from 2010 to 2018 were used as the training dataset, while 73 grids from 2019 were used as the test dataset to ensure the generalizability of the model across different datasets.

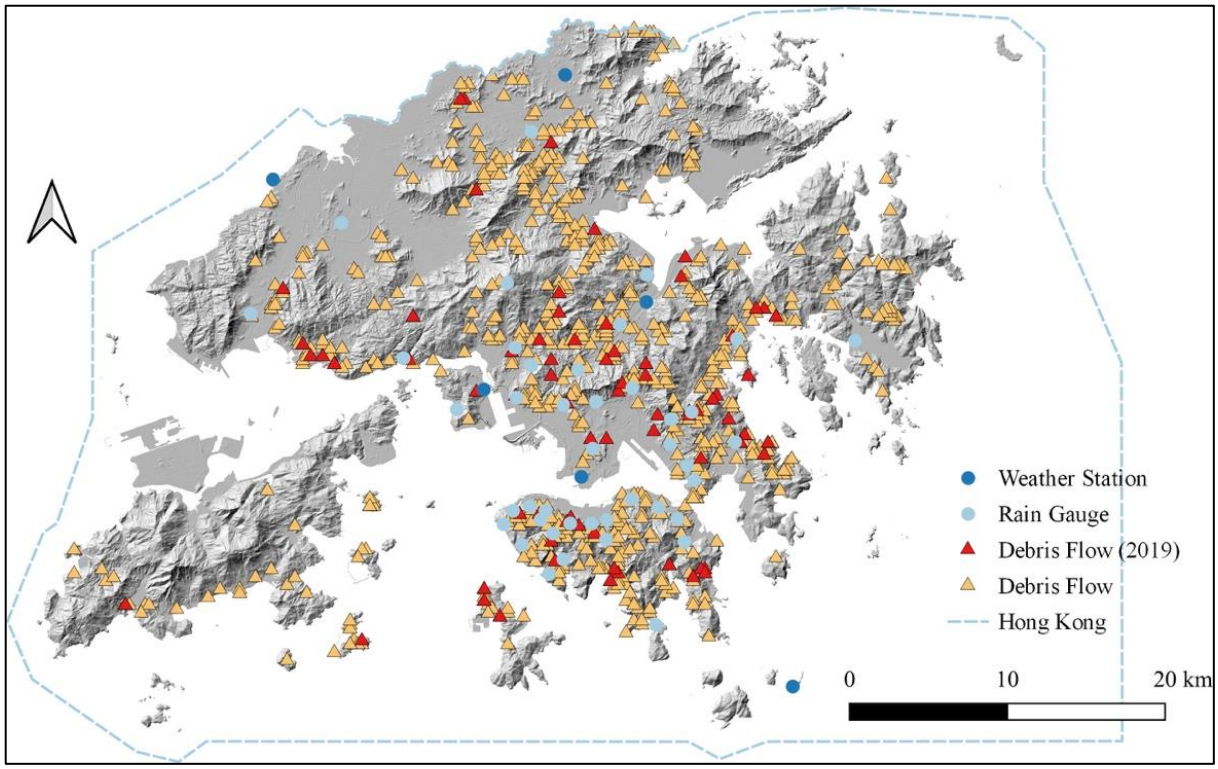

Fig. 2-3. Debris flow distribution in the HKSAR (area in grey)

Although the HKSAR has a land area significantly smaller than the SMCRS, the number of debris flow events impacting human society is comparable to that of the SMCRS. This can largely be attributed to differences in the comprehensiveness of data collection and the standards for data acquisition between the two study areas. In terms of data comprehensiveness, the SMCRS, due to its vast area and the prevalence of debris flows in sparsely populated areas, often has unreported debris flow data, making it challenging to compile a complete record of all debris flow events. In contrast, the HKSAR, with its smaller area, allows for the detailed recording of characteristics for each debris flow occurrence within the entire region based on field investigations or remote

sensing (i.e., UAV). Regarding data collection standards, the debris flow disaster database in the SMCRS, constructed from disaster inventories, news reports, and literature, only includes larger-scale debris flow events that have resulted in human casualties or economic loss. Conversely, the debris flow disaster database in HKSAR also includes records of smaller-scale events, such as those with a collapsed volume of only 0.001m³, even if they do not result in casualties or road closures.

However, the debris flow disaster databases constructed for both the SMCRS and the HKSAR are based on typical debris flow events derived from field surveys. These events are representative enough to reflect the characteristics of the majority of debris flow disasters in these localities. The similarity in the number of debris flow samples between the two study areas is advantageous for the subsequent construction and comparison of debris flow susceptibility assessment models. Therefore, the establishment of the debris flow databases for both the SMCRS and the HKSAR is representative and reasonable for this study.

2.2.2 Meteorological data

Climate zoning data were downloaded from the Resources and Environment Science and Data Center, Chinese Academy of Sciences (https://www.resdc.cn), to delineate the SMCRC in Sichuan Province.

Meteorological data must encompass a period extending at least 20 years before the recorded debris flow events to study the long-term DWCC before debris flow occurrences.

Based on the China Meteorological Data Service Centre (https://data.cma.cn), meteorological data including precipitation, temperature, relative humidity, wind speed, and sunshine duration for Sichuan Province and its surrounding meteorological stations were obtained, encompassing a total of 112 stations with the monitoring period covering 1960 to 2020 (Fig. 2-2). For the verification of typical debris flow gullies, meteorological data for the year 2021 is required. Therefore, the same meteorological items were downloaded based on 412 stations in 2021.

Daily meteorological data for temperature, relative humidity, wind speed, and sunshine duration from 1990 to 2019 were downloaded and filtered from the Hong Kong Observatory (https://www.hko.gov.hk/sc/index.html) for five weather stations within the HKSAR. Additionally, daily precipitation data were combined based on six weather stations from the Hong Kong Observatory and 42 rain gauge stations of the Geotechnical Engineering Office of Civil Engineering and Development Department for the same period (Fig. 2-3). Moreover, 175 tropical cyclone warning signals from 2010 to 2019 for the HKSAR were sourced also from the Hong Kong Observatory, including the intensity, names, signal levels, and the start and end time of the tropical cyclones.

2.2.3 Geological data

The geological data for the two study areas were sourced from the Spatial Database of 1:2500000 Digital Geologic Map of People's Republic of China (Ye et al., 2017), where the data type is a vector format, and each vector feature contains subcategories of rocks primarily present within the region.

Table 2-1. Rock type

Rock Type	Formation	Rock Sub-type
Igneous	Formed by the cooling and solidification of magma from within the earth's crust	Granite, diorite, gabbro, diabase, basalt, andesite, rhyolite, siliciclastic rocks, etc.
Sedimentary	Formed by the processes of weathering, erosion, transportation, deposition, and lithification	Conglomerate, sandstone, siltstone, carbonate rock, clastic rock, mudstone, limestone, etc.
Metamorphic	Formed from pre-existing rocks altered by high temperature and pressure	Quartzite, marble, slate, phyllite, schist, gneiss, mica schist, etc.

To simplify the evaluation indicator system for subsequent debris flow susceptibility models, the principal subcategories of rocks in the dataset were classified according to Table 2-1. Based on the rock formation processes, rock types were divided into three main categories: igneous, sedimentary, and metamorphic rocks. Ultimately, the primary rock types of each research unit were extracted and used as assessment indicators for the respective assessment units.

The fault data for the SMCRS is sourced from the Seismic Active Fault Survey Data Center, China Earthquake Administration (https://www.activefault-datacenter.cn), and is characterized as vector data. This fault information is utilized for the extraction and assessment of the proximity of assessment units to faults, thereby reflecting the intensity of geological activity in the SMCRS (Huang et al., 2020). Additionally, fault data serves as a crucial USC for delineating the SMCRS. This is to mitigate the excessive impact of USC on the study of the relationship between climate wet-dry cycles and regional debris flow susceptibility.

2.2.4 Topographical data

The topographic data for the SMCRS employs the 30-meter resolution DEM from the Shuttle Radar Topography Mission (https://dwtkns.com/srtm30m), as illustrated in Fig. 2-2. The HKSAR utilizes a 5-meter resolution DTM provided by the Lands Department (https://data.gov.hk/sc-data/dataset/hk-landsd-openmap-5m-grid-dtm), which can be seen in Fig. 2-3.

Topographic data will be utilized for obtaining features like the slope, aspect, and curvature. Specifically, within the SMCRS, the Melton ratio will be calculated according to the research units, as seen in equation (2-1). For the HKSAR, the maximum elevation difference will be determined based on the research units.

Through the calculations of these two indicators, the slope within the research units can be derived. Therefore, in comparison to the exclusive use of topographic features such as elevation and slope, both the Melton ratio and the maximum elevation difference serve as relatively comprehensive topographic features for the debris flow susceptibility assessment (Ilinca, 2021).

$$Melton = \frac{ED}{\sqrt{A}} \tag{2-1}$$

where ED is the maximum elevation difference in a watershed (m), and A is the area of the watershed (m^2).

2.2.5 Soil data

Soil data for the two study areas are derived from the Harmonized World Soil Database (HWSD) (Wieder et al., 2014). Within China, the soil data in the HWSD originates from a 1:1,000,000 soil map provided by the Institute of Soil Science, Chinese Academy of Sciences. The HWSD data type is raster, with a spatial resolution of 1 km, and includes parameters such as soil AWC, soil reference depth, and statistics on soil particle types and various physicochemical properties for the topsoil and subsoil layers. Globally, the database categorizes and classifies over 16,000 soil types. In this research, the HWSD data is solely utilized for the extraction of the AWC within the research units. The range of AWC in the HWSD dataset spans from 15 to 150 mm. The AWC is combined with meteorological

data to construct a surface water balance model, which is eventually used to calculate the dry-wet status of the research units within each study area.

For the SMCRS, given that a watershed unit typically encompasses multiple soil data grids, it is feasible to adopt the mean value of several grids to represent the AWC of the corresponding watershed.

2.2.6 Land use data

The land use data for the SMCRS is sourced from the WorldCover provided by the European Space Agency (Venter et al., 2022), with a spatial resolution of 10 m. This data set quantifies the proportion of various land use types within watersheds, including tree cover, shrubland, grassland, cropland, built-up, bare/sparse vegetation, snow and ice, permanent water bodies, herbaceous wetland, mangroves, moss, and lichen. The land use data for the HKSAR is obtained from the Planning Department, which is also mapped at a 10-meter grid resolution. It encompasses 27 categories that cover a range of land uses such as residential buildings, commercial buildings, industrial buildings, governmental buildings, public amenities, transport facilities including roads, railway, ports, and airports, agricultural areas including farmland and fish ponds, vegetation comprising woodland, shrubland, grassland, and mangrove/swamp, rocky shore, water bodies including reservoir, stream, and nullah; and other undeveloped land.

Land use data will be analyzed based on the area proportion of each land use category within the research units of the study areas, reflecting the characteristics of two major land use types such as human activity and vegetation cover (Huang et al., 2022; Xu et al., 2013). Typically, human activities are represented by categories such as cropland and urban development, while vegetation cover is indicated by land use types like woodland, shrubland, and grassland.

Chapter 3 Representation of Dry-wet Cycle Characteristics

This chapter will construct a meteorological dataset related to the hydrological cycle based on ground meteorological monitoring data in the SMCRS and the HKSAR. Incorporating AWC, the study will develop long-term dry-wet indices for research units with and without debris flow records in each study area, spanning at least 20 years before debris flow events. It will then compare the differences in the dry-wet indices between units with and without debris flow records before the events. By extracting temporal characteristics of the dry-wet index time series, the study aims to achieve monthly predictions of these indices. By using methods such as autocorrelation analysis, wavelet analysis, and multifractal analysis, DWCC will be extracted, including EDWP and extreme dry-wet characteristics. By comparing the DWCC of research units with historical debris flow records to those without in each study area, this study attempts to reveal the similarities and differences of DWCC in regions with and without debris flow before the event occurrences.

3.1 Meteorological data preprocessing

Precipitation, temperature, solar radiation, wind speed, and humidity are meteorological factors that influence the hydrological cycle. To construct the meteorological components of the hydrological cycle for assessment units with

and without debris flow records, the process begins by obtaining daily data on meteorological factors such as precipitation, average temperature, maximum temperature, minimum temperature, sunshine duration, wind speed, and relative humidity from ground meteorological monitoring stations in the two study areas. Data imputation is conducted for missing daily meteorological data, and the accuracy of the imputations is verified. Subsequently, potential monthly evapotranspiration values for the meteorological stations are estimated based on meteorological factors like average, maximum, and minimum temperatures, sunshine duration, wind speed, and relative humidity. Finally, the monthly values of precipitation and potential evapotranspiration from the meteorological stations are interpolated, yielding historical data on monthly precipitation and potential evapotranspiration for the assessment units within both research areas for the study period, with the accuracy of the interpolation results being verified.

3.1.1 Meteorological data imputation

It is necessary to conduct imputation for missing meteorological data, ensuring data accuracy to facilitate subsequent time series analysis. Monitoring data from meteorological stations are often subject to missing values due to a variety of unavoidable factors such as instrument failure or operator errors. However, acquiring accurate time series results for dry-wet indices based on discontinuous meteorological data is challenging. Commonly employed methods for missing

data imputation include mean substitution, regression, expectation-maximization algorithm, multiple imputation, and the K-nearest neighbor (KNN) algorithm. Mean substitution is convenient but performs poorly when the proportion of missing data is large. Regression methods depend on the correlation between independent variables and missing values to construct equations, which can be time-consuming when the correlation is not accurately known in advance for multiple meteorological elements. The expectation-maximization algorithm and the multiple imputation have high accuracy in imputing missing values but may consume substantial computational resources for large data samples, as in this study. The KNN algorithm, which is based on machine learning techniques and does not rely on prior knowledge, estimates missing values by calculating the Euclidean distance between the features (such as time, geographic coordinates, elevations, etc.) of the missing and complete data, selecting the K-nearest complete data points, and performing a weighted average based on distance, making it suitable for efficiently and accurately filling in missing data over long time series and large samples (Du et al., 2020; Gan et al., 2018).

In this study, considering both the volume of monitoring data and the accuracy of imputation, the KNN algorithm was chosen to fill in the missing daily meteorological data. Research results indicate that when the missing data constitutes less than 50% of the total dataset, various imputation methods (except for mean substitution) enhance the quality of the data (Farhangfar et al., 2008;

Tsai et al., 2016). However, as the proportion of missing data increases, so does the time consumed. Therefore, when applying KNN for data imputation, the proportion of missing values typically should not exceed 30% (Amiri et al., 2016; Xu et al., 2018). In this research, the proportions of missing values in the meteorological data are shown in Table 3-1. The results demonstrate that within the SMCRS and HKSAR, the proportion of missing values for each meteorological factor does not exceed 10%, with the majority being below 5%, making KNN suitable for accurate and efficient imputation of missing data. Precipitation data include observations of trace amounts less than 0.1 mm, which are negligible for this study when calculating the total monthly precipitation and thus are replaced with zero (Zhou et al., 2017). Finally, the accuracy of the imputations was assessed based on the total monthly precipitation and potential evapotranspiration to quantify the potential impacts of the imputations on the subsequent results of this study.

Table 3-1. Ratio of missing meteorological data to total observations

Study Area	Year	Precipitation	Average Temperature	Maximum Temperature	Minimum Temperature	Relative Humidity	Average Windspeed	Sunshine Duration
SMCRS	1960-2020	<0.001	<0.001	<0.001	0.001	0.003	0.003	0.001
HKSAR	1990-2019	0.028	0.016	0.015	0.015	0.066	0.019	0.083*

* The sunshine duration has been recorded since July 1, 1992, with no subsequent missing observations.

During the imputation of meteorological data using KNN, the initial step involves calculating the Euclidean distance between rows with missing data and rows with complete data, considering various factors such as the date of observation (year, month, and day) and the location of the station (projected coordinates and elevation), which are then used as weights. Given the extensive range of meteorological factors, the large total volume of daily data, and there is not necessarily a positive correlation between the choice of K and imputation accuracy based on previous research (Lai et al., 2019), it was determined that the 10 nearest complete data rows (K = 10) to the missing data row would be selected to calculate a weighted average for data imputation. Additionally, within the HKSAR, due to a significant portion of non-randomly missing sunshine duration data (from 1990 to June 1992), reaching a missing data ratio of 8.3%, the imputation was conducted using the mean substitution of the same period from previous years to minimize the impacts of missing sunshine duration data on the estimation of potential evapotranspiration for the period from January 1990 to June 1992. To further validate the accuracy of the employed imputation method, an equivalent number of complete data rows were randomly selected and imputed using the same technique. Fig. 3-1 presents scatter plots of the imputations versus observations for the precipitation and potential evapotranspiration, with both variables aggregated on a monthly total basis. The performance of the imputation model was assessed by calculating the coefficient of determination (R^2) and the root mean square error (RMSE) between the imputed and observed values (Addi

et al., 2022). The calculations of R^2 and RMSE are shown in equation (3-1) and equation (3-2).

$$R^2 = \left(\frac{\sum_{i=1}^{N}(I_i - \bar{I_i})(O_i - \bar{O_i})}{\sqrt{\sum_{i=1}^{N}(I_i - \bar{I_i})^2 \sum_{i=1}^{N}(O_i - \bar{O_i})^2}} \right)^2 \tag{3-1}$$

$$RMSE = \sqrt{N^{-1} \sum_{i=1}^{N}(I_i - O_i)} \tag{3-2}$$

where i represents the ith missing value, N denotes the total number of missing values, I stands for the imputed value, and O signifies the observed value, with $\bar{I}$ and $\bar{O}$ being the mean of the imputed and observed values, respectively.

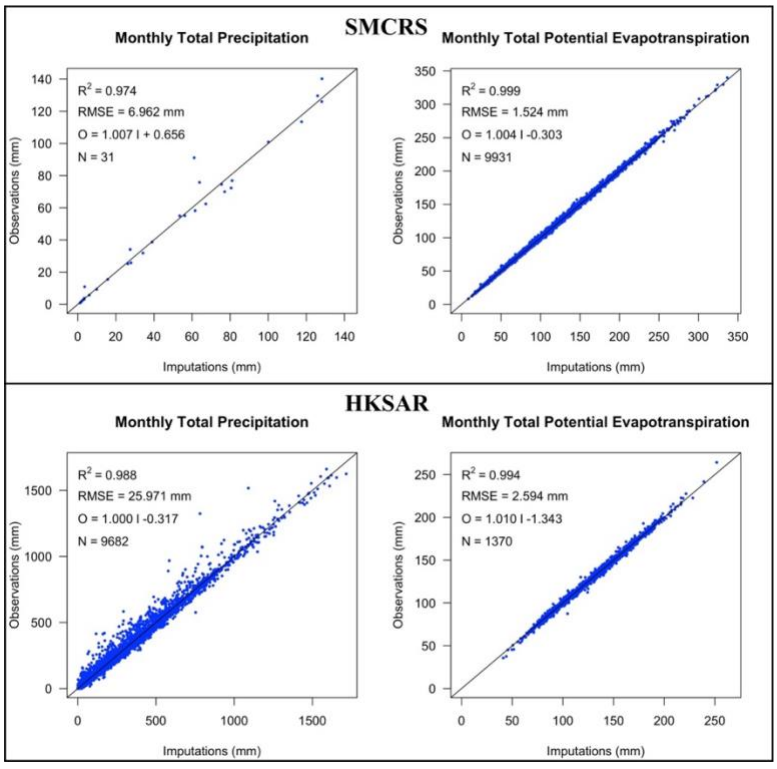

Fig. 3-1. Validation of monthly total precipitation/potential evapotranspiration based on imputations

The results indicate that within the two study areas of the SMCRS and the HKSAR, the imputation of missing precipitation and meteorological factors (excluding sunshine duration in the HKSAR) based on the KNN method for the estimation of total monthly precipitation and potential evapotranspiration is acceptable. In the SMCRS, the imputations yielded high R^2 values (0.974 - 0.999), with the RMSE for total monthly precipitation not exceeding 7 mm and that for potential evapotranspiration not exceeding 2 mm. In the HKSAR, the R^2 values were even higher (0.988 - 0.994), with the RMSE for potential evapotranspiration not exceeding 3 mm, but the RMSE for total monthly precipitation reached nearly 26 mm. Even though the RMSE value is relatively high, it remains within an acceptable margin of error for the total monthly precipitation. This discrepancy may be attributed to the coastal region typically experiencing more typhoons, leading to extreme precipitation events, and resulting in sudden changes in the distribution of precipitation data, which can affect the imputation quality. Therefore, the imputation of missing values for precipitation and potential evapotranspiration using the KNN or mean substitution proved to be highly effective, with the imputed values largely representative of the missing data. Moreover, the representativeness of the imputed values could be further enhanced by employing a linear regression equation between the observed values (O) and the imputed values (I) for adjustment.

3.1.2 Potential evapotranspiration estimation

This study uses the Penman-Monteith equation for estimating potential evapotranspiration due to its comprehensive accuracy in various climates. The estimation of potential evapotranspiration is commonly based on either the Thornthwaite or the Penman-Monteith equation. The Thornthwaite equation relies on temperature and latitude (Thornthwaite, 1948), making it suitable for estimating potential evapotranspiration in regions with sparse meteorological data. However, it struggles to accurately capture the spatial and temporal distribution of potential evapotranspiration, particularly in arid areas (Chen et al., 2005b). In contrast, the Penman-Monteith equation is more comprehensive as it considers a range of meteorological factors including average daily temperature, wind speed, solar radiation, and relative humidity (van der Schrier et al., 2011), and it has been found to align more closely with actual evapotranspiration in both arid and humid regions (Liu et al., 2015). Accordingly, based on the completeness of meteorological station data, this study employs the Penman-Monteith equation, as outlined in the calculation guidelines published by the Food and Agriculture Organization of the United Nations (Allen et al., 1998). This approach uses historical daily monitoring values of meteorological factors like temperature, relative humidity, wind speed, and sunshine duration, along with spatial information such as geographic coordinates and elevation of the monitoring sites,

and temporal information of the monitoring data, to estimate the historical daily potential evapotranspiration at various meteorological stations.

Based on daily observations of maximum temperature (T_{max}), minimum temperature (T_{min}), mean temperature (T_{mean}), and relative humidity (R_h), the daily average saturation vapor pressure (e_s) and the actual vapor pressure (e_a) are estimated according to equation (3-3):

$$\begin{cases} e_s = \frac{e^o(T_{max})+e^o(T_{min})}{2} \\ e_a = \frac{R_h}{100} e_s \\ e^o(T) = 0.6108 e^{\frac{17.27T_{mean}}{T_{mean}+237.3}} \end{cases} \tag{3-3}$$

where e represents the base of the natural logarithm, and e^o is a function of vapor pressure about mean temperature, which can be calculated using equation (3-4) to determine the slope Δ of the e_s curve at various temperatures.

$$\Delta = \frac{4098 e^o(T_{mean})}{(T_{mean}+237.3)^2} \tag{3-4}$$

Based on the elevation of the monitoring station (H), the psychrometric constant (γ) can be obtained employing equation (3-5).

$$\begin{cases} \gamma = 0.665 \times 10^{-3} P \\ P = 101.3 (\frac{293-0.0065H}{293})^{5.26} \end{cases} \tag{3-5}$$

where P is the atmospheric pressure at the monitoring station.

Due to the variations in wind speed measurements resulting from different anemometer heights, it is necessary to standardize the measurement height of

wind speed monitoring data in the calculation of potential evapotranspiration. In the Penman-Monteith equation, the wind speed is measured at a height of 2 meters. For wind speed data recorded at different measurement heights, conversion can be carried out by equation (3-6):

$$u_2 = u_z \frac{4.87}{ln\,(67.8z-5.42)} \tag{3-6}$$

where u_2 and u_z are wind speeds with the anemometer height of 2 and z m above the ground surface accordingly.

To estimate net radiation (R_n), it is necessary to calculate extraterrestrial radiation (R_a) based on the latitude of the monitoring station and the time of the monitoring data, using equation (3-7):

$$\begin{cases} R_a = 24 \times \frac{60}{\pi} G_{sc} d_r [\omega_s \, sin(\varphi) \, sin(\delta) + cos(\varphi) cos(\delta) \, sin(\omega_s)] \\ \delta = 0.409 \, sin\left(\frac{2\pi}{365} J - 1.39\right) \\ \omega_s = arccos[-tan(\varphi) \, tan(\delta)] \\ d_r = 1 + 0.033 \, cos\left(\frac{2\pi}{365} J\right) \end{cases} \tag{3-7}$$

where the solar constant (G_{sc}) is taken as 0.082 MJ/m^2/min, δ represents the solar declination, φ denotes the latitude of the site, ω_s is the sunset hour angle, d_r is the inverse relative distance Earth-Sun, and J signifies the order of date within the year, with values ranging from 1 to 365 (or 366 in a leap year).

Then, based on the sunshine duration (n_s), solar radiation (R_s) is estimated using equation (3-8):

$$\begin{cases} R_s = \left(0.25 + 0.5\frac{n_s}{N}\right) R_a \\ N = \frac{24}{\pi}\omega_s \end{cases} \quad (3\text{-}8)$$

where N is the potential sunshine duration.

By combining temperature data with the elevation of the monitoring station, the net radiation (Rn) can be determined using equation (3-9):

$$R_n = 0.77R_s - \sigma\left[\frac{(T_{max}-T_{K0})^4+(T_{min}-T_{K0})^4}{2}\right]\cdot\left(0.34-0.14\sqrt{e_a}\right)\cdot\left[\frac{1.35R_s}{(0.75+2\times10^5\cdot H)R_a}-0.35\right] \quad (3\text{-}9)$$

where the Stefan-Boltzmann constant (σ) is taken as 4.903×10-9 MJ/K^4/m^2/day, with T_{K0} representing absolute zero.

Eventually, the potential evapotranspiration (PET) is obtained based on equation (3-10):

$$PET = \frac{0.408\Delta(R_n-G)+\gamma\frac{900}{T-T_{K0}}u_2(e_s-e_a)}{\Delta+\gamma(1+0.34u_2)} \quad (3\text{-}10)$$

where G represents the soil heat flux density, which is assumed to be zero in this study. For one thing, the estimation of G is relatively complex, and individual assessment for each monitoring station would be time-consuming. For another, G constitutes the smallest component of the daily surface energy balance models and has a minimal impact on the model (Sauer et al., 2005). Therefore, setting G to zero is considered to have a negligible effect on the estimated values of potential evapotranspiration for this study.

3.1.3 Meteorological data interpolation

This study employs universal kriging spatial interpolation based on meteorological data from weather stations and considers the impact of topographic factors to estimate precipitation and potential evapotranspiration for each research unit. Kriging spatial interpolation is based on geostatistical methods, utilizing the data from observation sites and the spatial information to construct a semi-variogram function of observations and spatial distances within the interpolation range. Based on the semi-variogram function, it estimates the values for sites with known spatial distances from the observation sites, as seen in equation (3-11). Universal kriging interpolation extends upon this by incorporating regionalized variables (such as topographic factors) and leveraging the correlation between meteorological and topographic factors to enhance the accuracy and reliability of the interpolation. The universal kriging spatial interpolation for this study is facilitated by the "sp", "gstat" , and "automap" packages in the R programming language (Bohling, 2005).

$$Z(u) - m(u) = \sum_{i=1}^{n(u)} \lambda_i(u_i)[Z(u_i) - m(u_i)] \quad (3\text{-}11)$$

where Z represents spatial attributes such as precipitation or potential evapotranspiration. u and u_i respectively denote the position vectors for the estimation point and the observation point i. $n(u)$ indicates the number of

observation points required for each interpolation. $\lambda_i(u_i)$ represents the kriging weights determined based on the semi-variogram. $m(u)$ and $m(u_i)$ represent the expected values of the spatial attributes. Within the context of the "sp", "gstat", and "automap" packages in R, it is assumed that the topography and spatial location have a first-order linear relationship, where $m(u)$ is a first-order linear function of the spatial position.

However, given that the HKSAR only has five meteorological stations for estimating potential evapotranspiration, it is not feasible to construct a variogram of the distances between meteorological stations and their observations based on geostatistical methods to fit a semi-variogram that could estimate the variability of observations with distance. Consequently, the interpolation of potential evapotranspiration in the HKSAR opted for the simpler inverse distance weighted interpolation method. To ensure the accuracy of the interpolation results, a leave-one-out cross-validation was conducted for the estimated precipitation and potential evapotranspiration values from all meteorological stations. This involves interpolating the values for each meteorological station in the study area based on the data from all other stations, followed by creating scatter plots of the actual observations (O) against the estimations (E) derived from the interpolations and calculating R^2 and RMSE between the observations and estimations.

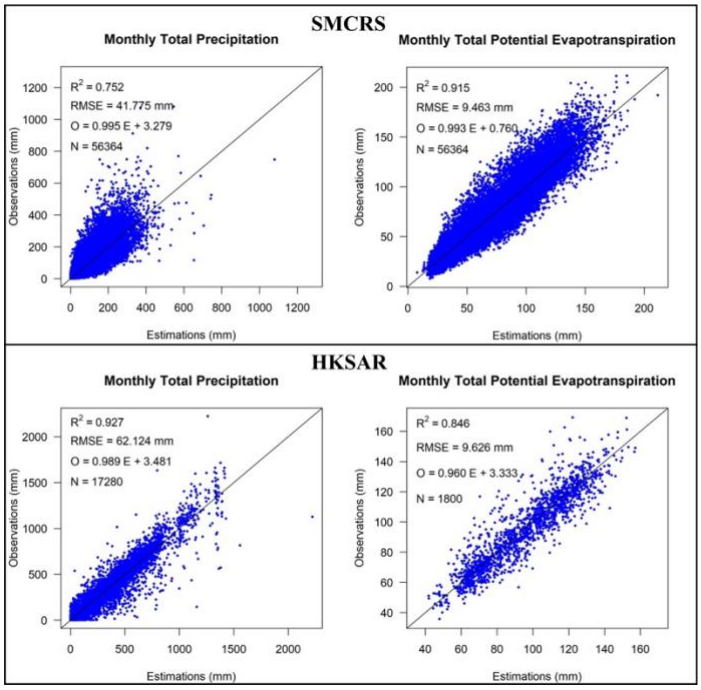

Fig. 3-2. Validation of monthly total precipitation/potential evapotranspiration based on interpolation

The results presented in Fig. 3-2 indicate that within the two study areas of the SMCRS and the HKSAR, the universal kriging spatial interpolation method that takes topography into consideration yields monthly total precipitation and potential evapotranspiration estimates. In the SMCRS, the R^2 value for the comparison between the estimated and observed monthly total potential evapotranspiration reaches 0.915 with an RMSE of less than 10 mm. However, the R^2 for the estimated monthly total precipitation compared to observed values is only 0.752, with an RMSE of less than 42 mm, which is still within an acceptable error range for monthly total precipitation. In the HKSAR, the R^2 for the estimated monthly total precipitation versus the observed values achieves

0.927, but the RMSE reaches 62 mm, exceeding that of the monthly total precipitation estimates in the SMCRS. Meanwhile, in the HKSAR, the R^2 for the estimated monthly total potential evapotranspiration against the observed values is 0.846 with an RMSE of less than 10 mm, which is close to that of the monthly total potential evapotranspiration estimates for the SMCRS.

The relatively lower accuracy of spatial interpolation for monthly total precipitation in the SMCRS is largely due to the complex topography of the area, which has a more significant influence on precipitation than on potential evapotranspiration. This is because topographical relief can affect the flow of warm moist air flows, thereby altering the distribution and intensity of precipitation through changes. However, as indicated by equation (3-11), such nonlinear effects are challenging to represent in the universal kriging interpolation method that considers topography. In the HKSAR, the R^2 between the estimated and observed monthly total precipitation is substantially higher than that in the SMCRS. Nonetheless, the RMSE of the estimated monthly total precipitation in the HKSAR is significantly greater than that in the SMCRS. This discrepancy is largely due to the coastal location of the HKSAR, which is prone to extreme precipitation events influenced by typhoons, and such nonlinear influences are still difficult to characterize through universal kriging spatial interpolation.

Overall, while estimates derived from spatial interpolation methods are subject to certain errors, the metrics of R^2 and RMSE indicate that the estimates can still largely represent the true values of monthly total precipitation and potential evapotranspiration in areas without monitoring stations. Furthermore, the linear regression equation between the observed values (O) and estimated values (E) will be utilized to calibrate the estimates, thereby further enhancing their representativeness.

3.2 Dry-wet index

Following the acquisition of meteorological factors necessary for the hydrologic cycle in assessment units with and without debris flow records, and in conjunction with soil data, a surface water balance model that accounts for the persistent impacts of dry and wet conditions is employed to calculate dry-wet indicators for all assessment units. These indicators are then statistically compared to characterize the differences in the dry-wet status of assessment units with and without debris flow records. Ultimately, predictions of the dry-wet indicators are made based on time-series characteristics, and their accuracy is subsequently validated.

3.2.1 Dry-wet index calculation

A well-established and widely used index is required to quantify the dry-wet status. Drought conditions can be reflected through various drought indices, which primarily take into account factors such as precipitation, temperature, solar radiation, evaporation, and soil moisture (Svoboda et al., 2016). To elucidate the relationship between drought conditions and debris flow activity in this study, considering soil properties is deemed necessary. The standardized precipitation index (SPI) is widely used to describe the dry-wet conditions in debris flow-prone regions due to its relatively simple data requirements and calculations, making it particularly suitable for areas with limited meteorological data (Chen et al., 2014; Hu et al., 2017). PDSI, which accounts for precipitation, potential evapotranspiration, AWC, and the persistent effects of dry-wet conditions, can more comprehensively describe the dry-wet cycles related to debris flows but demands a more complete set of meteorological and soil data (Chen et al., 2020; Mika et al., 2005).

PDSI is a dimensionless index. The nonextreme PDSI values range from -4 to 4, where negative/positive values represent various degrees of drought/wet conditions, with larger absolute values denoting increased severity (Palmer, 1965). However, the range can vary in practice when considering local climate conditions to ensure that the extreme values (-4 or 4) correspond to specific percentiles of the historical distribution rather than being fixed thresholds (Wells

et al., 2004). The historical PDSI for each research unit in the study areas is calculated using the "pdsi" function from the "scPDSI" package in the R programming language. The computation of PDSI requires the establishment of a surface water balance model that correlates precipitation (P) with evapotranspiration (ET), recharge (R), runoff (RO), and water loss (L), as seen in equation (3-12). This calculation necessitates data on precipitation, potential evapotranspiration, and AWC.

$$P = ET + R + RO - L \tag{3-12}$$

The calculation process will consider the persistent effects of dry-wet conditions, as seen in equation (3-13).

$$PDSI_i = qZ_i + pPDSI_{i-1} \tag{3-13}$$

where Z_i represents the moisture anomaly value for the ith month, while p and q are empirical parameters. For the SMCRS and its surrounding areas based on data from the national meteorological stations of China, the empirical parameters can be determined according to the Grades of Meteorological Drought (GB/T 20481-2017) specified in the national standard of China. As for meteorological stations in the HKSAR, in addition to using the parameters from the national standard, it is also necessary to employ the "pdsi" function to calculate self-calibrating PDSI values (Wells et al., 2004).

Comparisons between PDSI and another commonly applied dry-wet index SPI have been conducted. The results (Fig. 3-3, top) show that PDSI can characterize more extreme values compared to SPI, which is calculated based on precipitation data only.

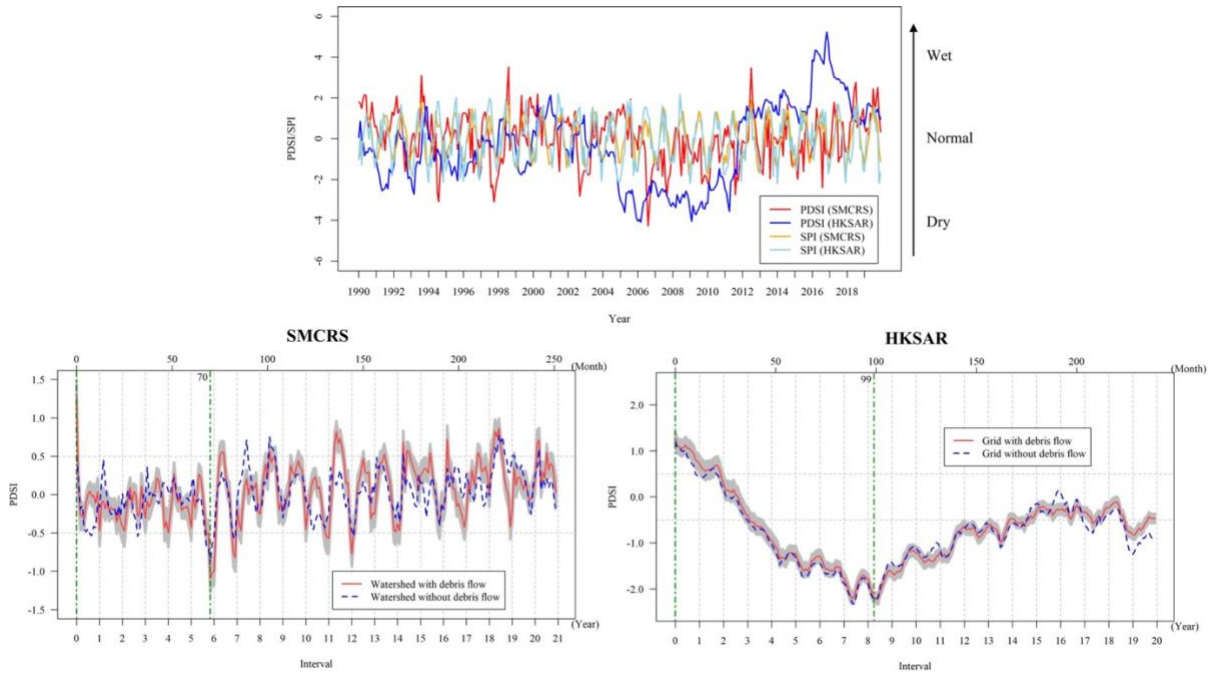

Fig. 3-3. Long-term dry-wet index time series

Assessment units with debris flow records were defined as debris flow samples, while those without debris flow records were defined as non-debris flow samples. Based on 1544 debris flow and non-debris flow samples from the SMCRS, PDSI time series for the 21 years before debris flow disasters were constructed for each watershed unit (Fig. 3-3, bottom-left). Similarly, using 1954 debris flow and non-debris flow samples from the HKSAR, PDSI time series for the 20 years before debris flow disasters were constructed for each grid unit (Fig. 3-3, bottom-right).

In these series, time interval 0 represents the time of debris flow occurrences, and larger intervals indicate greater temporal distance from the debris flow events. The green dashed lines mark the maximum and minimum PDSI values for watersheds or grids with debris flows. The grey area represents the 95% confidence interval calculated using the bootstrap method, which estimates population statistics from data samples through repeated sampling with replacement. With an increasing number of samples, the bootstrap method reflects the population distribution of samples more accurately (Efron et al., 1986). In this study, it was found that resampling data samples 2000 times with replacement could roughly reflect the overall distribution of the data.

The results demonstrated the long-term dry-wet states before debris flow occurrences. In the SMCRS, which encompasses numerous watersheds with complex climate patterns, a sharp increase in PDSI was observed in the months of debris flow occurrence within the watersheds with debris flows. When the time interval was zero, the watersheds were in an extremely wet state during the months of debris flow events. This extreme wet, characterized by high precipitation surpassing low potential evapotranspiration, reflects extreme precipitation conditions in the subtropical monsoon region due to its simultaneous occurrence of heat and rain. The minimum values of PDSI, indicate the extreme drought events, which are occurred around 70 months (approximately 6 years)

before the debris flow events. Watersheds without debris flows generally experienced normal dry-wet states, with PDSI values ranging between -0.5 and 0.5. In contrast, in the HKSAR, despite the highest PDSI values over 20 years being recorded in the months of debris flow occurrences, the driest months occurred approximately 99 months (about 8 years) before the events. Moreover, there is no significant difference in the long-term dry-wet status before the disaster between grids with and without debris flows. This could be attributed to the smaller area and less spatial variability in climatic conditions of the HKSAR. It is thus reasonable to infer that dry-wet cycles before debris flow disasters are a crucial condition for the formation and initiation of debris flows, and in areas with less variability in climatic conditions, the formation and occurrence of debris flows may also be influenced by other factors, which deserves further investigation.

3.2.2 Dry-wet index forecast

The SARIMA model was selected for predicting the monthly PDSI time series due to the obvious periodicity in PDSI and the limited number of monitoring station samples. The forecasted PDSI time series derived from this model can be applied to reflect the short-term dry-wet characteristics in the future. The SARIMA model is constructed using the "auto.arima" function from the "forecast" package in the R programming language.

Based on the debris flow records in the SMCRS, it was found that debris flows all occurred between April and November each year. Consequently, the prediction period for the PDSI time series in the SMCRS is set from April to November 2020. A SARIMA model was established using PDSI time series data from a total of 54 monitoring stations starting from the year 1980, with the model predicting PDSI for only one month at a time.

According to the debris flow records from the HKSAR, debris flows were found to occur every month throughout the year, hence the prediction period for the PDSI time series for the HKSAR is set for the entire year of 2019. Due to the lack of meteorological element records other than precipitation at the rain gauge stations in the HKSAR, which are necessary for the estimation of potential evapotranspiration, the potential evapotranspiration for the rain gauge stations was derived using the interpolation method described in Section 3.1.3. This allows for the construction of a PDSI time series for a combined total of 48 meteorological and rain gauge stations. The SARIMA model was then applied to perform monthly PDSI predictions for these stations.

Ultimately, scatter plots were created for each of the two study areas by plotting all observations (O) against the predictions (P), and the R^2 and RMSE were computed to quantify the agreement between O and P.

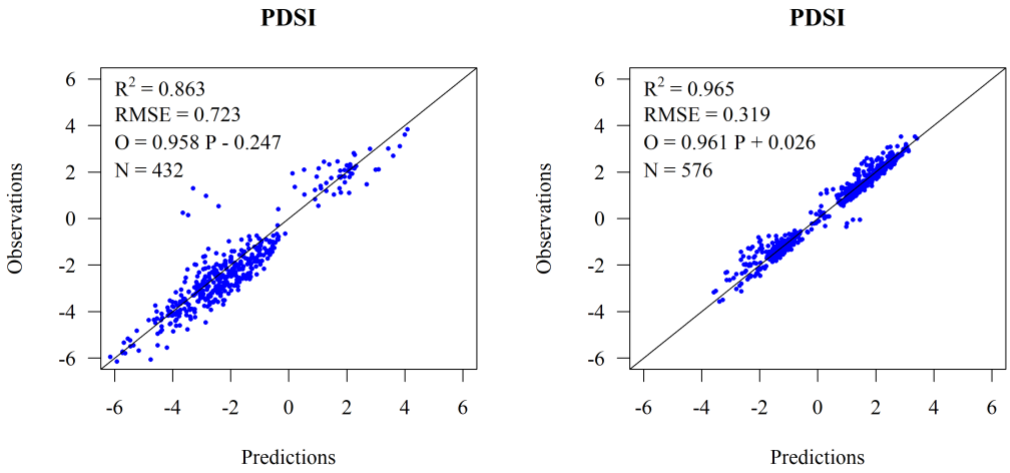

Fig. 3-4. Validation of monthly PDSI predictions using SARIMA (SMCRS: Left; HKSAR: Right)

The results presented in Fig. 3-4 indicate that, within the SMCRS, the R^2 between the PDSI time series predictions based on the SARIMA model and the actual observations reaches 0.863, with an RMSE of 0.723. In the HKSAR, the R^2 between the predicted and observed values reaches 0.965, with an RMSE of 0.319. Consequently, the SARIMA-based PDSI time series forecasted values can largely represent the true values. The linear regression equation between observed values O and predicted values P will be used for the correction of estimated values to further enhance the representativeness of the forecasted values.

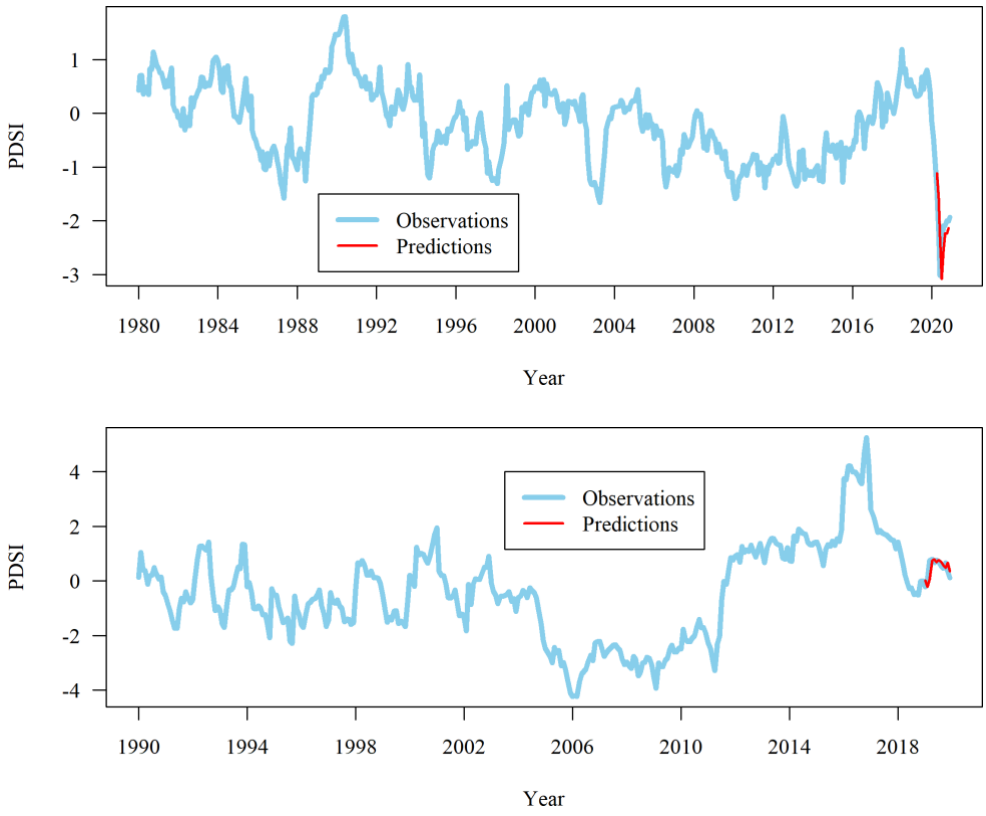

Fig. 3-5. PDSI time series monthly predictions based on SARIMA (SMCRS: Top; HKSAR: Bottom)

However, it is important to note that in the SMCRS, there were significant outliers in the predicted values when the observed values were close to zero. Upon examination, these outliers were all predicted values for July. This result suggests that the PDSI predictions for some areas in July in the SMCRS may be underestimated, potentially misclassifying areas that are in a wet or normal state as dry regions.

The results depicted in Fig. 3-5 show that, based on the average values from 54 meteorological stations in the SMCRS, the forecasted PDSI values for April to November 2020 were generally close to the actual observed values. Similarly,

based on the average values from 48 meteorological stations or rain gauge stations in the HKSAR, the forecasted PDSI values for each month of the entire year of 2019 were also essentially equivalent to the actual observed values. Therefore, it is preliminarily considered that the application of the SARIMA-based PDSI time series for monthly predictions reflects the PDSI for the forthcoming month with representativeness. Nevertheless, attention must be paid to the potential impact of the underestimation of PDSI in certain areas when applying these forecasted PDSI values.

3.3 Dry-wet cycle characteristics

Given that it is challenging to quantify the characteristics of dry and wet indicators solely through the PDSI time series, further time series analyses on the PDSI were conducted to explore the long-term dry-wet cycle periods preceding debris flow occurrences, as well as the severity and frequency of extreme drought and precipitation events in typical inland monsoon and coastal monsoon regions.

3.3.1 Stationarity test

Stationarity tests should be conducted to meet the assumptions required by certain time series analysis methods. The Augmented Dickey-Fuller (ADF) test is

employed to assess the stationarity of the PDSI time series before debris flow occurrences, with the null hypothesis representing non-stationarity due to a unit root, and the alternative hypothesis positing that the time series is stationary (Dickey et al., 1979). The ADF test results for 1544 samples from the SMCRS show that all samples have p-values less than 0.05 (Fig. 3-6, left), indicating that the PDSI time series before debris flow occurrences in the SMCRS is stationary, implying that there are no significant upward or downward trends in the dry-wet conditions preceding debris flow occurrences in the region. Conversely, the ADF test results for 1954 samples from the HKSAR reveal that approximately 86.3% of the samples have p-values exceeding 0.05 (Fig. 3-6, right), indicating that the PDSI time series before debris flow occurrences in the HKSAR is non-stationary, indicating the existence of significant upward or downward trends in the dry-wet conditions preceding debris flow occurrences within the region.

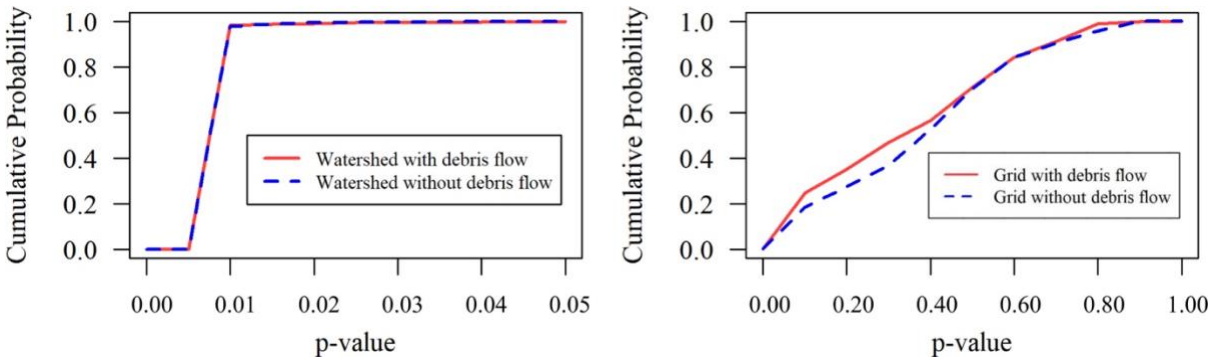

Fig. 3-6. PDSI time series stationary test

(SMCRS: Left; HKSAR: Right)

3.3.2 Autocorrelation analysis

Autocorrelation is a statistical measure used to describe the correlation between data points at different times within a time series. The Autocorrelation Function (ACF) is a function constructed with the time lag as the independent variable and the autocorrelation as the dependent variable. The ACF is applicable for analyzing the correlation of stationary time series at given time intervals. Since the PDSI time series before debris flow occurrences in the HKSAR has been tested and found to be non-stationary, it is not suitable for autocorrelation analysis. Consequently, autocorrelation analysis is conducted exclusively on the PDSI time series before debris flow occurrences in the SMCRS.

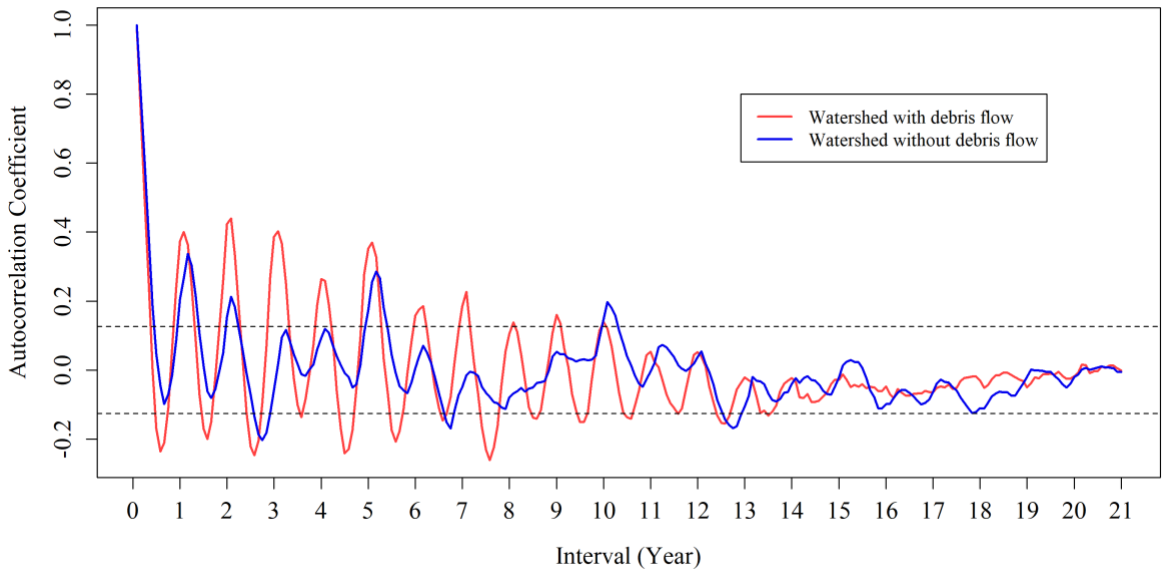

Fig. 3-7. Autocorrelation of PDSI time series

The PDSI time series preceding debris flow events in watersheds within the SMCRS has been verified to be stationary (Fig. 3-6, left). Consequently, the autocorrelation plot for the PDSI time series before the debris flow occurrences in the SMCRS is generated using the "acf" function from the "stats" package in the R programming language. The significance boundary value B (denoted by black dashed lines) is determined based on the length of the time series T using equation (3-14), and the autocorrelations that exceed these boundary values are statistically significant (Fig. 3-7).

$$B = \frac{2}{\sqrt{T}} \tag{3-14}$$

The results indicate that out of 21 years, 14 years (66.7%) in watersheds with a debris flow record exhibit significant negative autocorrelation in the same years as those with debris flow occurrences, whereas watersheds without debris flows showed significant negative autocorrelation in only 3 out of 21 years (14.3%) corresponding with years with debris flow records. Based on the findings presented in Fig. 3-3, watersheds experiencing debris flow events are subjected to extreme precipitation conditions. It can be inferred that the greater the number of years with significant negative autocorrelation associated with debris flow events, the higher the frequency of extreme drought events and the more frequent the dry-wet cycles. Furthermore, the autocorrelations in watersheds with a debris flow record fluctuate more intensely, that is, the extremes have generally larger absolute values, suggesting that watersheds with debris flows have more

pronounced periodicity in their dry-wet cycles. Hence, watersheds that have experienced debris flows present a higher frequency of dry-wet cycles with more distinct periodic characteristics.

3.3.3 Wavelet analysis

Wavelet analysis is utilized to process PDSI time series data by extracting wavelet coefficients at different time scales, thereby quantifying the periodic characteristics of dry-wet cycles. In this study, based on the "dplR" package in the R programming language, the Morlet wavelet function is applied to perform Continuous Wavelet Transform, followed by the construction of a wavelet power spectrum. The wavelet power spectrum illustrates the relationship between time scales and the squared values of wavelet power. A higher squared value of wavelet power at a specific time scale suggests stronger fluctuations in the time series at that scale, while a lower value indicates weaker fluctuations. Hence, the time scales where high values are concentrated in the wavelet power spectrum can be identified as the observation scales of the time series. These observation scales serve as the maximal time scales for observing the PDSI time series and are used to further analyse the periodicity of the time series (Scordo et al., 2018; Zhang et al., 2022).

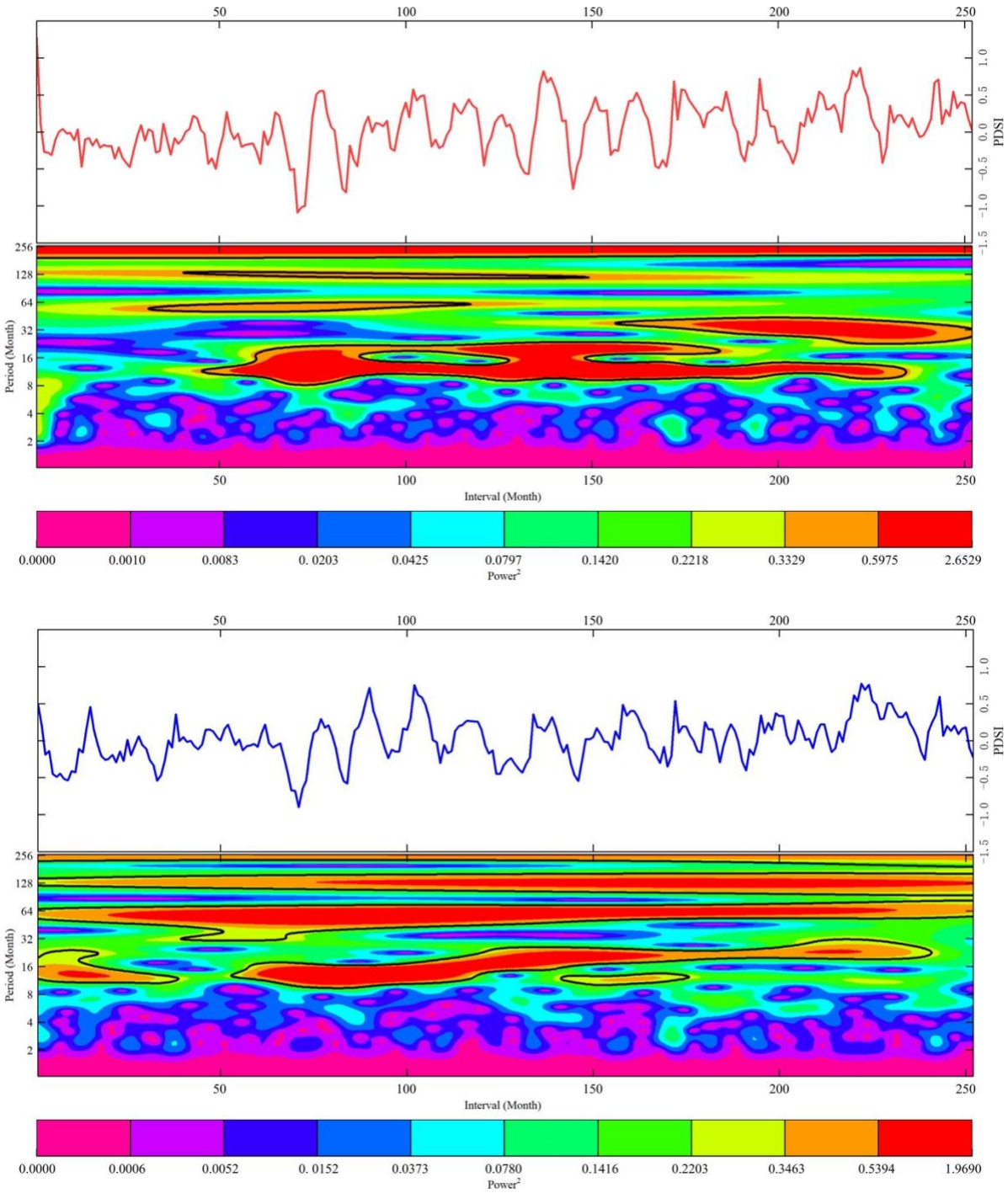

Fig. 3-8. PDSI wavelet power spectra in the SMCRS

(Watershed with debris flow: Top; Watershed without debris flow: Bottom)

The results from the wavelet power spectrum for the SMCRS (Fig. 3-8) reveal that watersheds with a record of debris flows exhibit the highest power squared values during the 252 months (21 years) preceding the debris flow events, indicating that larger observation time scales are associated with more pronounced fluctuations in the PDSI. Consequently, the observation time scale for the PDSI time series is established at 21 years. Although watersheds without debris flow records also observed higher power squared values over the periods of 60 months (5 years), 120 months (10 years), and 252 months (21 years) before the debris flow events, to ensure the comparability of the PDSI time series characteristics between positive and negative debris flow samples and to maintain a high level of power squared values, the observation time scale for the PDSI time series in watersheds without debris flow records is similarly set at 21 years.

Based on the wavelet power spectra of the HKSAR (Fig. 3-9), both the grids with debris flow records and those without exhibit the highest power squared values over the 240 months (20 years) preceding the events, suggesting also that larger observation time scales correlate with more intense fluctuations in the PDSI. Therefore, the observation time scale for the PDSI time series in the HKSAR is determined to be 20 years.

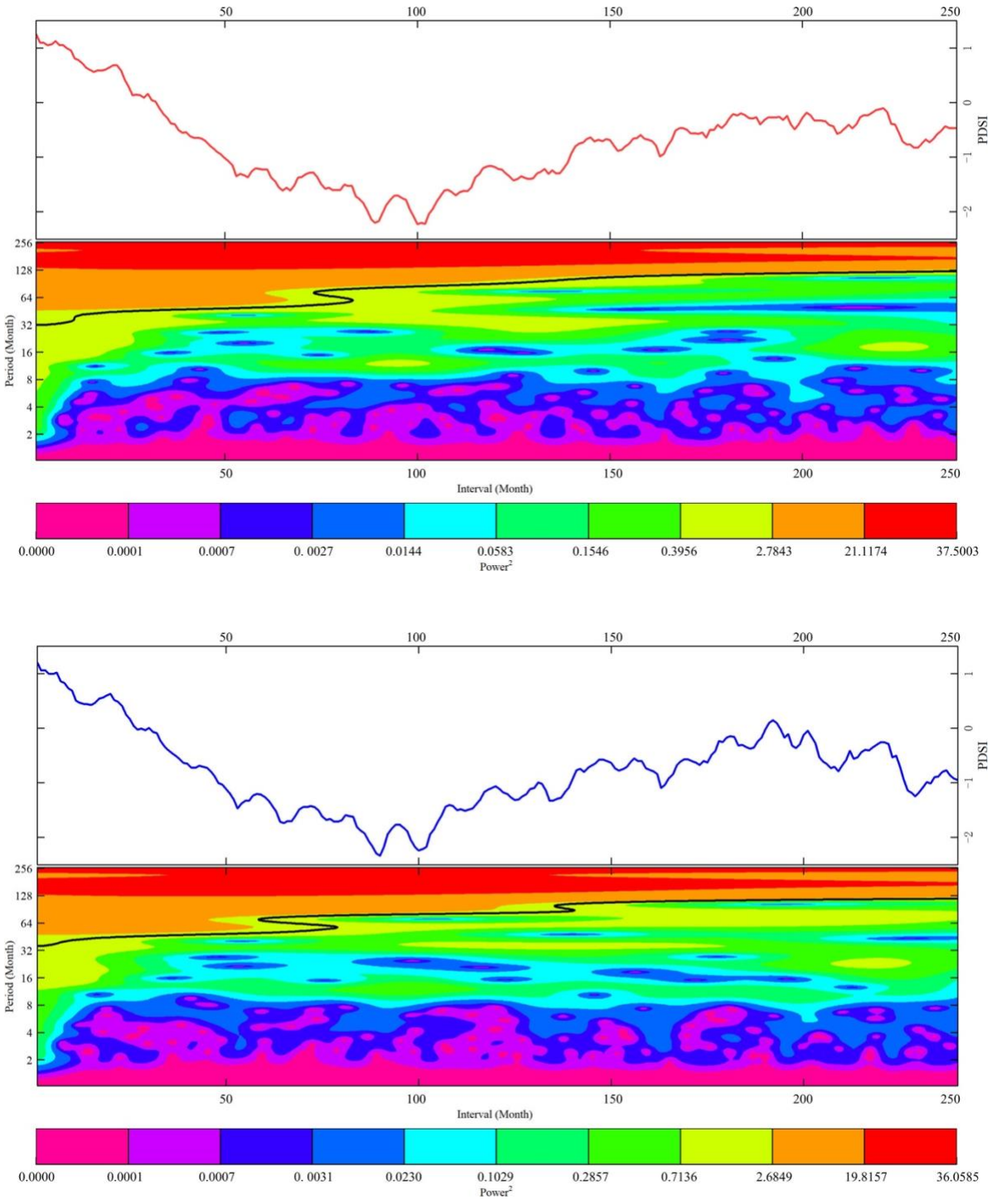

Fig. 3-9. PDSI wavelet power spectra in the HKSAR

(Grid with debris flow: Top; Grid without debris flow: Bottom)

Extracting the wavelet power squared values at the observation scale, curves between these values and the time interval before the onset of debris flows were created, and the periodicity of the PDSI time series at this observation scale was determined based on the maximum wavelet power squared values (Fig. 3-10). The results indicate that the dry-wet cycle period for watersheds with debris flow records in the SMCRS is 8.8 years (106 months), while for those without debris flow records, the cycle period is 15 years (180 months). Furthermore, the power squared values for the positive samples are greater than those for the negative samples, suggesting that watersheds with debris flows experience more pronounced fluctuations in their dry-wet cycles. In the HKSAR, the difference in dry-wet cycle periods between grids with and without debris flow records is not significant, with both approximately around 7 years (84 - 86 months).

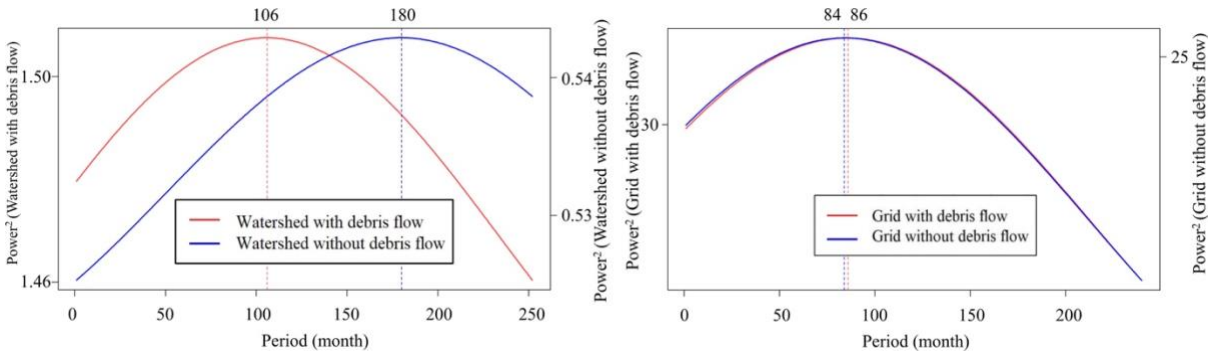

Fig. 3-10. The relationship between the square of wavelet power and dry-wet cycle period (SMCRS: Left; HKSAR: Right)

However, grids with debris flow records exhibit higher wavelet power squared values, implying that within the relatively small area of the HKSAR, where

spatial variability in climate conditions is less pronounced, the difference in dry-wet cycle periods between grids with and without debris flow records is subtle, yet the fluctuation in extreme dry-wet conditions is more intense compared to the SMCRS.

In summary, compared to research units without debris flow records, those with debris flow records exhibit more intense fluctuations in the PDSI, with shorter fluctuation periods in the SMCRS. Specifically, watersheds with debris flow records are characterized by more pronounced dry-wet cycles. This indicates that in regions with greater spatial variability in climate conditions, dry-wet cycles occur more frequently.

3.3.4 Multifractal spectrum analysis

Multifractal analysis divides a time series into intervals of various scales and characterizes the self-similarity of the time series by calculating the variations of moments obtained from mass functions at these different scales. To ensure comparability among the multifractal spectra of the PDSI time series before the occurrence of debris flows across all samples, equation (3-15) is used to standardize all PDSI time series.

$$TS_n = \frac{TS - min(TS_a)}{max(TS_a) - min(TS_a)} \tag{3-15}$$

where TS and TS_n respectively represent the time series before and after normalization, while TS_a denotes the matrix composed of all the time series under consideration. The functions max and min are used to obtain the maximum and minimum values within the time series, respectively.

The partition function $M(q, \varepsilon)$ takes the moment q and the time resolution ε as independent variables, with the normalized PDSI serving as the dependent variable, as shown in equation (3-16).

$$M(q, \varepsilon) = \sum_{i=1}^{n} PDSI_i^q(\varepsilon) \tag{3-16}$$

The observation scale determined by wavelet analysis results, which is 252 months, is taken as the length of the PDSI time series required for multifractal analysis. Based on this length, nine distinct time resolutions ε are established in ascending order according to the ratio of this length to the series $\{2^8, ..., 2^1, 2^0\}$. With the moment q set to 10, the number of data points plotted on the multifractal spectrum is 20.

Mass exponent $\tau(q)$ can be obtained based on the partition function using equation (3-17).

$$\tau(q) = \frac{ln\,[M(q,\varepsilon)] - c}{ln\,(\varepsilon)} \tag{3-17}$$

where c is the intercept of least squares.

The singularity exponent α can be calculated based on equation (3-18).

$$\alpha = \frac{d\tau(q)}{dq} \tag{3-18}$$

Eventually, based on Legendre Transformation, a multifractal spectrum is obtained.

$$f(\alpha) = q\alpha - \tau(q) \tag{3-19}$$

Based on equation (3-19), the multifractal spectrum of the PDSI time series, as illustrated in Fig. 3-11, can be constructed. This multifractal spectrum is a parabolic curve, with its left end representing the transformed maximum PDSI value and its right end representing the transformed minimum PDSI value. The parameter α reflects the intensity of singularity across different time resolutions of the time series, while f corresponds to the probability of occurrence of this intensity. Therefore, this study employs multifractal parameters such as α_{min}, $f(\alpha_{min})$, α_{max}, and $f(\alpha_{max})$ to describe the severity and probability of extreme dry-wet events in a time series. The parameter $\Delta\alpha = \alpha_{max} - \alpha_{min}$ reflects the degree of fluctuation in extreme dry-wet states, meaning that a larger Δα indicates more intense fluctuations, while a smaller Δα indicates milder fluctuations. The parameter $\Delta f = f(\alpha_{min}) - f(\alpha_{max})$ indicates a preference for extreme drought or extreme precipitation events, where $\Delta f > 0$ suggests a tendency towards extreme precipitation events with a larger Δf indicating a stronger preference, and $\Delta f < 0$ suggests a tendency towards extreme drought events with a smaller Δf indicating a stronger preference.

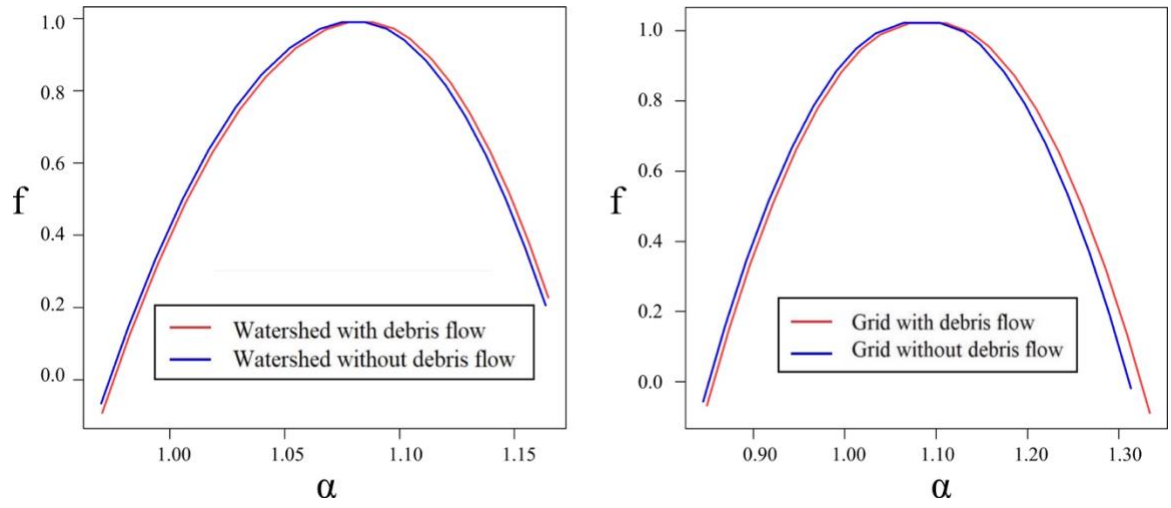

Fig. 3-11. Multifractal spectra of PDSI

(SMCRS: Left; HKSAR: Right)

In the SMCRS, multifractal spectrum analysis results demonstrate that, in comparison to watersheds without debris flow records, those with debris flow records exhibit larger values of α_{max}, α_{min}, $\Delta\alpha$. This indicates that extreme drought events in watersheds experiencing debris flows are more severe, while the extent of extreme precipitation events is relatively milder, and the degree of fluctuation between extreme dry and wet events is more pronounced. Moreover, Δf is consistently less than zero, and the values of $f(\alpha_{min})$ and Δf in watersheds with debris flows are lower than those without debris flows, whereas their $f(\alpha_{max})$ is higher. This suggests that watersheds with debris flow records have a higher probability of experiencing extreme drought events, but a relatively lower likelihood of extreme precipitation events.

In the HKSAR, multifractal spectrum analysis of the PDSI time series reveals that, compared to grids without debris flow records, those with debris flow records exhibit greater values of α_{max} and $\Delta\alpha$, suggesting more severe extreme drought events before the occurrence of debris flows. However, unlike in the SMCRS, the multifractal spectrum Δf of the PDSI time series in the HKSAR is greater than 0, indicating a preference for extreme precipitation events over extreme drought events compared to typical inland areas. This preference is likely due to the potential for extreme precipitation events caused by typhoons. The values of $f(\alpha_{max})$ and $f(\alpha_{min})$ in the HKSAR are relatively small, signifying that the probability of the most severe extreme dry and wet events occurring in coastal monsoon regions is comparatively lower.

By comparing the multifractal spectrum parameters of assessment units with and without debris flow records in the two study areas, it can be observed that frequent and severe extreme drought events may lower the precipitation threshold for the initiation of debris flows. Consequently, even less severe and less frequent extreme precipitation events may be sufficient to trigger debris flows. This finding is consistent with the results of previous research (Chen et al., 2014; Nyman et al., 2019).

Although the PDSI time series for grids in the HKSAR with and without debris flow records do not exhibit significant differences as shown in Fig. 3-3, there is still a marked contrast in their DWCC. Therefore, extracting DWCC is beneficial

for further uncovering potential information embedded within historical dry-wet indices.

However, the present results only reveal from a statistical perspective the reduction of the precipitation threshold under the influence of dry-wet cycles. To interpret how dry-wet cycles affect the formation and initiation mechanisms of debris flows, it is necessary to collect soil samples from typical gullies within the study area and measure their properties. This will allow for a more in-depth analysis of the relationship between the debris flow susceptibility and DWCC.

3.4 Summary

In this chapter, the characteristics of dry-wet cycles are quantified:

A comprehensive meteorological dataset, which is necessary for the calculation of dry-wet indices, was constructed based on daily historical meteorological data related to the hydrologic cycle from ground monitoring stations. To address missing values in meteorological monitoring data, imputation methods based on the KNN algorithm or mean substitution were employed. The obtained total monthly precipitation and potential evapotranspiration, with an R^2 exceeding 0.974, confirmed the strong representativeness of the imputations for the missing data. The Penman-Monteith equation was applied to estimate potential evapotranspiration, considering a variety of meteorological factors such as daily

temperature, wind speed, sunshine duration, and relative humidity, which affect evaporation rates comprehensively. Considering topography, kriging spatial interpolation was used to extend the monitoring station data on total monthly precipitation and potential evapotranspiration to research units with and without debris flow records. The interpolation results, with an R^2 of 0.752 and an RMSE not exceeding 26 mm between imputations and observations, verified the strong representativeness of the interpolated results for the total monthly precipitation and potential evapotranspiration across the research units.

Based on total monthly precipitation, potential evapotranspiration, and combining AWC while considering the sustained impact of dry-wet conditions, the long-term PDSI time series before debris flow events were estimated for research units in two typical regions. The PDSI, in comparison to the SPI that only considers precipitation, comprehensively reflects the surface water balance process and is more closely aligned with the mechanisms of debris flow formation and initiation. By extracting PDSI time series data for at least 20 years before debris flow events, a preliminary comparison between the SMCRS and the HKSAR revealed that extreme precipitation conditions were generally present in the month of debris flow occurrences. Furthermore, extreme drought events were observed 6 to 8 years before the debris flows, indicating that dry-wet cycles are a crucial condition for the formation and initiation of debris flows. In the HKSAR, where climatic spatial variability is relatively small, the formation and initiation

of debris flows may be more influenced by other factors, deserving further investigation. Utilizing the characteristics of the PDSI time series, the SARIMA model was applied to predict the PDSI for the upcoming month. The results showed that in both the SMCRS and the HKSAR, the R^2 values for the predicted versus observed PDSI were 0.863 and 0.965, with RMSE of 0.723 and 0.319, respectively, suggesting that the PDSI predictions for the next month are reasonably representative.

Focusing on the two study areas, this study explores and compares the potential patterns within the PDSI time series of research units with positive and negative debris flow samples, quantifying the differences in dry-wet conditions between units with and without debris flow records. Comparative analyses of the PDSI time series before debris flow events, including autocorrelation analysis, wavelet analysis, and multifractal spectrum analysis for both positive and negative samples, consistently indicate that units with debris flows experienced more severe dry-wet cycles compared to those without. In regions with greater spatial variability of climate conditions, there are also more frequent dry-wet cycles and a tendency for more frequent and severe extreme drought events. While these findings are consistent with previous research, further studies are required in the typical gullies within the study areas to elucidate the mechanisms behind the changes in debris flow susceptibility under the influences of dry-wet cycles.

Chapter 4 Impact of Dry-wet Cycle Characteristics on Debris Flow Susceptibility

This chapter aims to elucidate the impact of dry-wet cycles on debris flow susceptibility from a mechanism perspective. Taking the SMCRS as the study area, two methods were proposed to estimate the ARI of debris flows in watersheds based on historical debris flow records, and the representativeness of the estimated debris flow ARI was validated. The study examined the correlation between debris flow ARI and DWCC including the EDWP and the extreme dry-wet characteristics. The correlations between debris flow ARI and DWCC/maximum daily precipitation were compared. Soil samples collected from typical debris flow gullies in the SMCRS are subjected to soil experiments to measure their soil mechanical properties under extreme precipitation conditions. Combined with historical in situ dry-wet data from the debris flow gullies, the study quantifies the association between extreme dry-wet events and debris flow susceptibility.

4.1 Debris flow average recurrence interval

In this study, given the extensive area of the SMCRS, the spatial variability of debris flow ARI is expected to be more pronounced, making historical records particularly suitable for estimating the ARI of debris flows. Two distinct methods were adopted within the study. The first method derives from calculating the

equivalent diameter of a watershed, while the second method utilizes proximity to the nearest recorded debris flow sites. The two methods were applied to determine the buffer area for the debris flow recurrence in watersheds with debris flow records. By comparing the debris flow ARI obtained from both methods and integrating the existing spatiotemporal distribution patterns of debris flows in the SMCRS, the estimated debris flow ARI are validated for their representativeness in reflecting debris flow susceptibility.

4.1.1 Equivalent diameter-based estimation

A method for estimating ARI using the equivalent diameter of watersheds has been proposed. Based on the 772 historical debris flow events in the SMCRS, the area of the watershed corresponding to each debris flow event was extracted. Subsequently, utilizing equation (4-1), the equivalent diameter D of a circular area with an area A equal to that of each watershed was calculated, which serves as the equivalent diameter for the respective watershed.

$$D = 2\sqrt{\frac{A}{\pi}} \tag{4-1}$$

Then, for estimating the debris flow ARI, the point of the debris flow under consideration, as well as all other debris flow points within a distance not exceeding the equivalent diameter D, were selected. The occurrence times t_i for these n debris flow points, including the point underestimation, were extracted.

These times were then sequenced in the order of the debris flow occurrences to form an array $L = \{t_1, \dots, t_i, \dots, t_n\}$. Utilizing equation (4-2), the ARI for the debris flow point was estimated, which is indicative of the debris flow recurrence period.

$$ARI = \frac{t_n - t_1}{n-1} \tag{4-2}$$

4.1.2 The nearest site-based estimation

Another method for estimating ARI is based on the nearest debris flow sites. For each of the 772 watersheds with debris flow records, its nearest debris flow points i were aggregated into a corresponding group, based on which the debris flow ARI for this watershed was calculated by equation (4-2), and the results were catalogued within a list L_i. Eventually, N such lists were generated as shown in equation (4-3).

$$\begin{cases} L_i = \{ARI_{1,i}, ARI_{2,i}, \dots, ARI_{772,i}\} \\ \dots \\ L_N = \{ARI_{1,N}, ARI_{2,N}, \dots, ARI_{772,N}\} \end{cases} \tag{4-3}$$

To obtain a more comprehensive set of debris flow ARI for watersheds while ensuring representativeness, an increased number of nearest neighbor points were selected for ARI estimation. In this study, based on preliminary results from pre-experiments, the value for N in equation (4-3) was established at 30. Subsequently, the Spearman correlation coefficient r_s was calculated between

each pair of lists within equation (4-3). This approach was chosen since Spearman correlation does not require data to follow a normal distribution, thus obviating the need for prior analysis of data distribution before performing correlation analysis. Ultimately, the optimal number of nearest neighbor points, k, was determined based on which value yielded a higher average/median r_s and a lower overall standard deviation. As illustrated in Fig. 4-1, k equal to 16 best satisfies the set criteria, indicating that the ARI estimated under these conditions is the most representative.

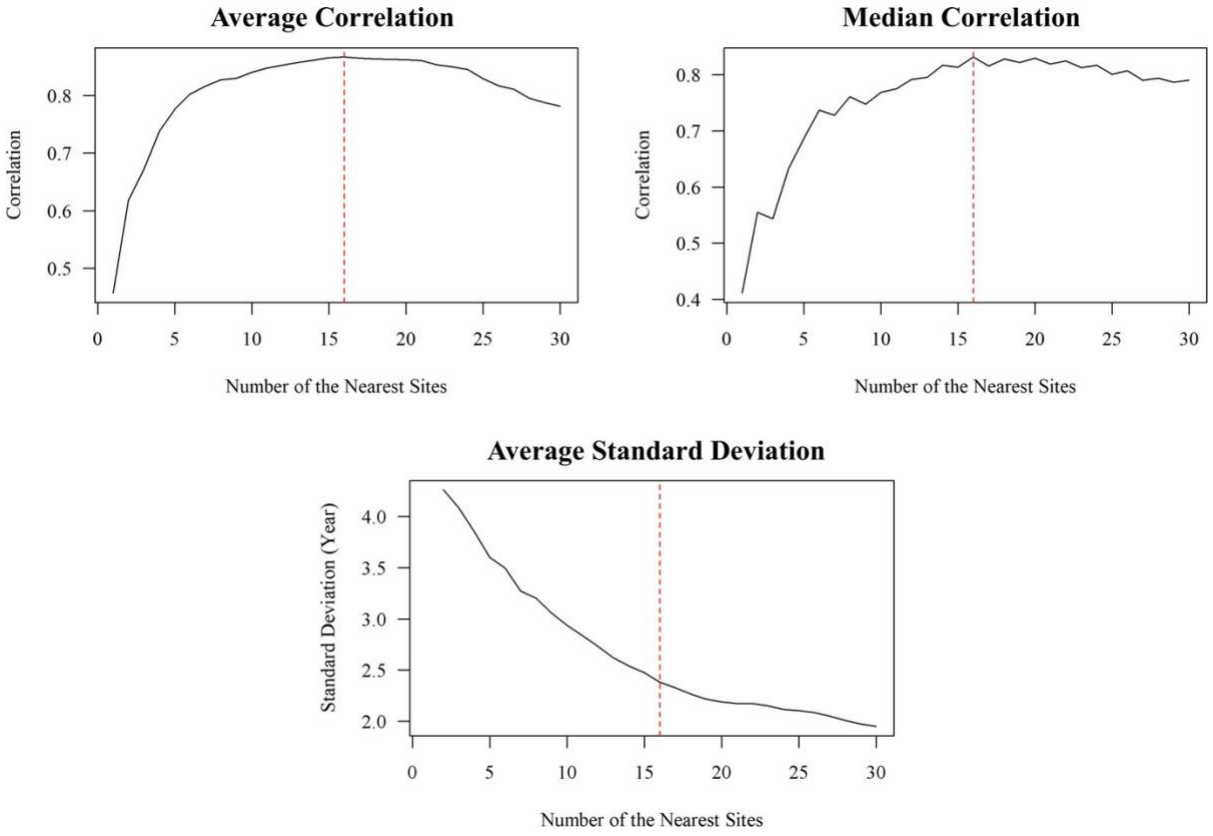

Fig. 4-1. Statistics of correlations between debris flow recurrence period obtained based on different nearest points

4.1.3 Debris flow recurrence period pattern

The estimated ARIs effectively delineate the spatiotemporal distribution of debris flow susceptibility across watersheds in the SMCRS. Spatiotemporal distribution maps of debris flow ARI for watersheds in the SMCRS were generated based on the results obtained from the equivalent diameter and the nearest site estimation methods. When the number of nearest sites was set to 1, as depicted in Fig. 4-2, the results of the two ARI estimation methods based on historical debris flow records were most closely aligned, with a Spearman correlation coefficient of 0.81 ($p < 0.001$). The spatial distribution of ARI across different watersheds revealed that the Longmenshan fault zone, particularly the Wenchuan earthquake region, exhibited shorter ARI with a concentrated distribution. Similarly, shorter ARI were observed in the surrounding mountain areas of the Sichuan Basin and the Panxi region, though with a more scattered distribution. In some watersheds within the Longmenshan fault zone, the eastern surrounding mountain areas of the Sichuan basin, and the Panxi region, the ARIs were less than one, indicating the possibility of multiple debris flow events occurring within a single year in one watershed.

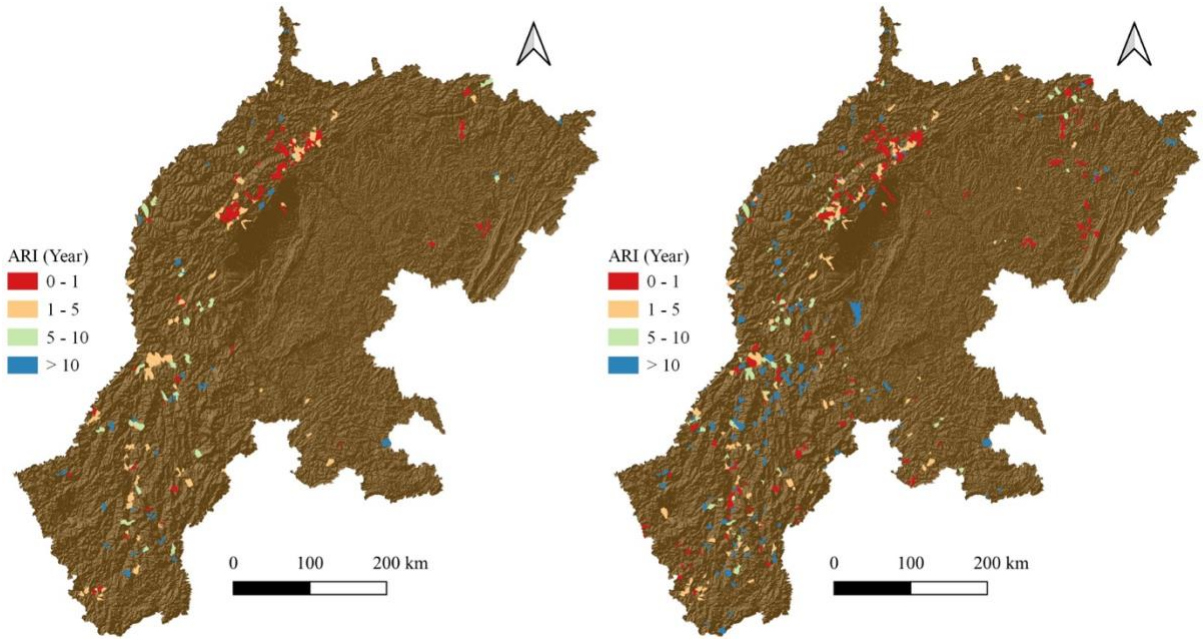

Fig. 4-2. Debris flow recurrence period estimations based on equivalent diameter (Left) and the nearest point (Right) in SMCRS

However, further comparative analysis and discussion are required for the two methods of estimating debris flow ARI based on historical records to ensure that they can more accurately reflect the spatiotemporal distribution patterns of debris flows. For one thing, the estimation method based on equivalent diameter provides a relatively accurate estimation of ARIs for watersheds, but it may fail to estimate ARIs in watersheds with sparse historical debris flow records. For another, the nearest site-based estimation method, while reducing the precision of ARI estimation for each watershed, can still yield ARIs for those with limited historical data. Moreover, the nearest site-based method, without accounting for the area of the watersheds, may lead to undersampling in areas with dense debris flow records and oversampling in regions with sparse records, both of which can

reduce the representativeness of the estimated ARIs. Therefore, in the process of estimating debris flow ARIs, it is necessary to carefully balance the advantages and disadvantages of both methods to ensure as many watershed ARIs as possible are obtained while maintaining the representativeness of the data for each watershed.

4.2 Responsive pattern between recurrence periods and dry-wet cycles

Quantifying the relationship between debris flow ARI and dry-wet cycles can help characterize their impacts on debris flow susceptibility. Due to the complex and nonlinear characteristics of debris flow formation and initiation, grasping the debris flow ARI is challenging. Extensive existing research has identified that dry-wet cycles have impacts on debris flow source material formation, triggering, and transport. Based on these findings, it is possible to quantitatively characterize the impact of DWCC on debris flow susceptibility by elucidating the relationship between the debris flow ARI and DWCC. To validate the feasibility of this approach, it is proposed to quantify the responsive relationship between debris flow ARI and the dry-wet cycles.

Utilizing wavelet power spectrum analysis, the EDWP before debris flow occurrences was estimated for various watersheds in the SMCRS. EDWP was then correlated with the debris flow ARI using Spearman correlation analysis.

The results indicated a correlation of 0.36 ($p < 0.001$) between the EDWP and the ARI calculated based on equivalent diameter, and a correlation of 0.34 ($p < 0.001$) with the ARI based on 16 nearest sites (Table 4-1). These outcomes, derived from different methods of estimating debris flow ARIs, demonstrated a significant moderate correlation between the EDWP and debris flow susceptibility (Ratner, 2009), suggesting that longer EDWP correlates with longer debris flow ARI, thereby indicating a lower frequency and susceptibility to debris flow occurrences. Conversely, shorter EDWP is associated with shorter debris flow ARI, indicating a higher frequency and increased susceptibility to debris flow events.

Table 4-1. Correlations between ARI and EDWP/maximum rainfall

	ARI (Equivalent diameter)	ARI (The nearest site)
EDWP	0.36, $p < 0.001$	0.34, $p < 0.001$
Maximum Rainfall	-0.18, $p < 0.001$	-0.27, $p < 0.001$

To further validate the significant impact of EDWP on debris flow susceptibility, a Spearman correlation analysis was conducted between debris flow ARI and a commonly used triggering factor in rainfall-induced debris flow early warnings, namely the maximum daily rainfall in the watershed before a debris flow event. This correlation was compared with the relationship between debris flow ARI and EDWP. The results indicated a correlation of -0.18 ($p < 0.001$) between the

maximum daily rainfall and the ARI estimated based on equivalent diameter, and a correlation of -0.27 ($p < 0.001$) with the ARI based on 16 nearest sites (Table 4-1). These findings suggest that there is only a weak yet significant correlation between maximum daily rainfall and the ARI. The larger the maximum daily rainfall before a debris flow, the shorter the ARI and the higher the frequency and susceptibility of debris flow occurrences. Although these results are consistent with the general pattern of rainfall-induced debris flow occurrences, the responsive relationship between maximum daily rainfall and debris flow susceptibility is relatively weak.

By comparing the correlation between the EDWP and the debris flow ARI with that between maximum daily rainfall and debris flow ARI, it can be further ensured that the relationship between EDWP and debris flow susceptibility is significantly stronger than that between maximum daily rainfall and debris flow susceptibility. This implies that the DWCC may have greater potential advantages when applied to debris flow susceptibility assessment than the triggering factor of maximum daily rainfall. However, the performance of DWCC in debris flow susceptibility assessment still requires validation through further experimental investigation.

4.3 Mechanism analysis between debris flows and dry-wet cycles

To further explore the mechanisms linking debris flow susceptibility and dry-wet cycles, soil experiments and analysis of historical dry-wet indices are proposed. Although the statistical relationship between debris flow susceptibility and dry-wet cycles has been elucidated through the analysis of ARI and EDWP, the underlying mechanisms between debris flows and dry-wet cycles require further exploration. To investigate this mechanism, soil experiments are proposed to measure the changes in the soil mechanical properties of debris flow source materials under extreme dry-wet conditions. Historical dry-wet indices were applied to identify extreme dry-wet events preceding debris flow occurrences in typical gullies.

4.3.1 Debris flow source material property measurements

Field investigations and soil samplings were conducted to collect representative soil samples for analysis. Two typical debris flow events that occurred in the SMCRS in June 2020 were selected as sampling sites, namely Xiangjiao in Muli Tibetan Autonomous County and Damawucun in Mianning County, with a sampling time of October 2021. Soil samples were collected from four different elevations in each debris flow gully, specifically choosing soil that had moved downslope to ensure the samples were representative of the debris flow source

materials. Samples were taken from depths as close as possible to the debris flow gullies to better represent the characteristics of the slip surface soil. Each sample weighed approximately 0.85 kg, and photographs of the sampling sites were taken. The locations of the samples were documented using GPS, as shown in Fig. 4-3.

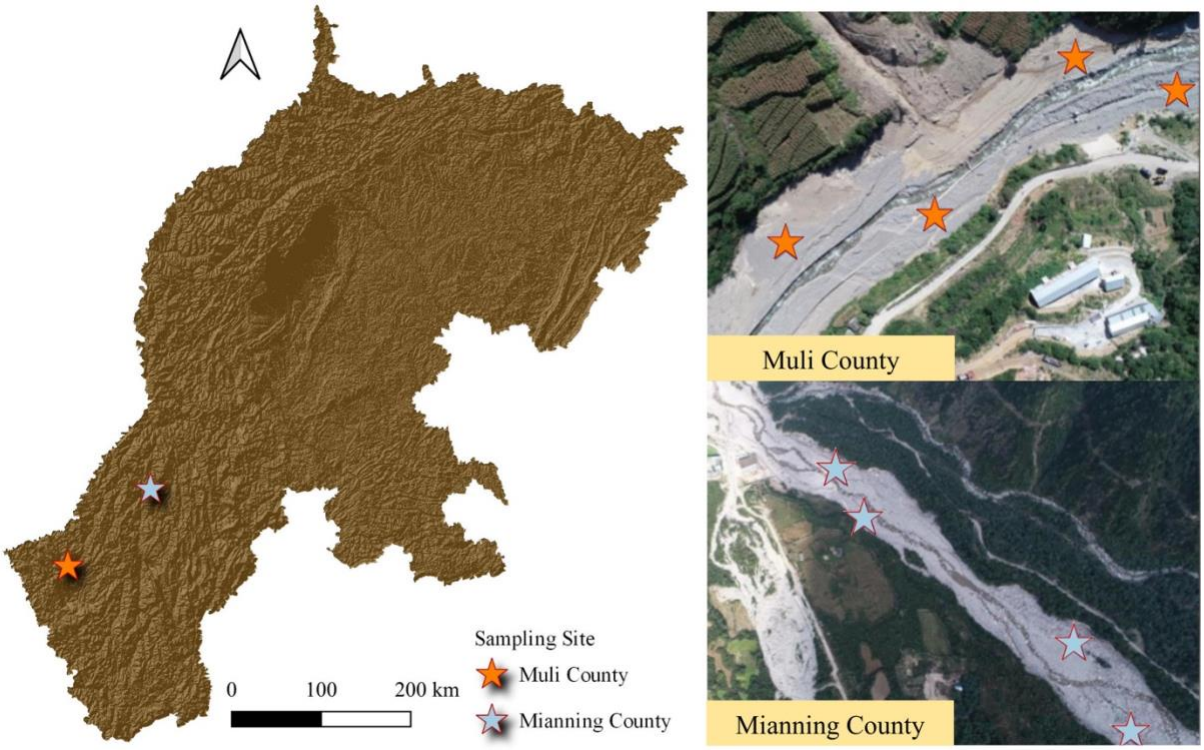

Fig. 4-3. Sampling sites for typical debris flow gullies

The soil particle size characteristics (i.e., gravel percentage, sand percentage, and fine percentage), the density of solids normalized by the density of water (G_s), the water content (w), and the void ratio (e) were determined through sieve analysis, as presented in

Table 4-2. Soil particles were classified based on their size as gravel, sand, or fine. The G_s is the ratio of the unit weight of the soil particles to the unit weight of water at 4°C. The w is the ratio of the mass of water to the mass of dry soil. The e represents the ratio of the volume of voids to the volume of solid particles in the soil.

Table 4-2. Soil properties in typical debris flow gullies

County-Sample	Gravel percentage	Sand percentage	Fine percentage	G_s	w	e	φ (o)
Muli-1	0.41	0.43	0.17	2.73	0.11	0.72	29.00
Muli-2	0.24	0.56	0.20	2.71	0.09	0.75	29.00
Muli-3	0.22	0.63	0.15	2.77	0.10	0.74	30.00
Muli-4	0.00	0.72	0.28	2.75	0.12	0.77	29.00
Mianning-1	0.23	0.75	0.02	2.75	0.17	0.91	28.00
Mianning -2	0.25	0.73	0.02	2.70	0.16	0.87	28.00
Mianning -3	0.12	0.84	0.04	2.72	0.18	0.90	28.00
Mianning -4	0.00	0.95	0.05	2.79	0.15	0.89	27.00

Six specimens from each sample, prepared at their in-situ densities, were subjected to consolidated-drained direct shear tests and consolidated-undrained triaxial tests under pressures of 50, 100, and 200 kPa to measure the soil shear stress (τ) and normal stress (σ). Furthermore, the particle size distribution from

Table 4-2 indicates that all eight samples from the two typical debris flow gullies are predominantly characterized by a higher proportion of sand particles. Therefore, cohesion (c) can be assumed to be zero (Bai et al., 2019; Di et al.,

2021). Using the Mohr-Coulomb failure criterion, as shown in equation (4-4), the angle of internal friction (φ) for the soil mass was further calculated.

$$\tau = c + \delta tan\varphi \tag{4-4}$$

The angle of internal friction reflects the magnitude of the frictional forces between soil particles within a soil sample. A larger angle of internal friction indicates greater soil strength and stability. This parameter will be utilized in the computation of slope material stability, characterizing the debris flow susceptibility of typical debris flow gullies.

4.3.2 Factor of safety calculation

Referring to a physical model built for assessing sandy slopes (Di et al., 2021), based on measured G_s, w, and e, the moist unit weight of soil (γ) and the saturated unit weight of soil (γ_{sat}) can be obtained based on equation (4-5).

$$\begin{cases} \gamma = \frac{\gamma_w G_s (1+w)}{1+e} \\ \gamma_{sat} = \frac{\gamma_w (G_s+e)}{1+e} \end{cases} \tag{4-5}$$

Based on the angle of internal friction (φ), FS for the instability of slope materials is calculated using equation (4-6). An FS greater than 1 implies that the slope materials are in a stable condition, with no risk of large-scale slippage. When FS equals 1, it indicates that the slope materials are at the threshold of slippage. An FS less than 1 signifies a risk of large-scale slippage within the slope material.

$$\begin{cases} FS_o = \frac{tan\varphi}{tan\theta} \\ FS_g = \frac{(\gamma_{sat}-\gamma_w)tan\varphi}{\gamma_{sat}tan\theta} \end{cases} \quad (4\text{-}6)$$

where the FS under conditions without precipitation is denoted as FS_o, while FS_g represents the safety factor under conditions of persistent heavy rainfall. The unit weight of water, γ_w, is taken as 9.81 kN/m³. The inclination angle of the debris flow gully slopes, θ, can be considered a constant within the same natural slope due to relatively uniform geological conditions. This angle θ can be calculated based on the elevation of the sampling points.

Utilizing the calculated data from

Table 4-2, the FS for two typical debris flow gullies under both dry conditions and persistent heavy rainfall conditions were computed, along with the rate of change in the FS, denoted as ΔFS, which is presented in Table 4-3.

Table 4-3. FS of typical debris flow gullies

County-Sample	FS_o	FS_g	ΔFS
Muli-1	1.52	0.75	-51%
Muli-2	1.52	0.74	-51%
Muli-3	1.59	0.78	-51%
Muli-4	1.52	0.74	-51%
Mianning-1	2.13	1.00	-53%
Mianning -2	2.13	0.99	-54%
Mianning -3	2.13	0.99	-54%
Mianning -4	2.04	0.97	-52%

The results indicate that under dry conditions, the FS_o for both Muli County and Mianning County exceed 1, signifying that there is no substantial risk of large-scale slippage for the slope materials. However, under rainfall conditions, the FS_g for the two typical debris flow gullies decrease significantly, with all samples ultimately not surpassing a value of 1, implying a considerable risk of large-scale slippage. These findings demonstrate that persistent heavy rainfall significantly reduces the FS of debris flow gullies, with a reduction rate exceeding 50%. This outcome corroborates the reduction of FS under extreme rainfall conditions for the two typical debris flow gullies, indicating an increased debris flow susceptibility due to the occurrence of extreme precipitation events.

4.3.3 Impacts of dry-wet cycles on debris flow susceptibility

Further analysis using time series of dry-wet indices and meteorological data is needed to assess the impact of long-term dry-wet cycles on debris flow susceptibility. The soil experiments conducted so far have not taken into account the impacts of long-term, repetitive dry-wet cycles on debris flow susceptibility. Consequently, it remained necessary to perform further analysis using a time series of dry-wet indices based on ground monitoring sites within typical debris flow gullies. The meteorological monitoring data in 2021 exhibit no missing values, although there are no records of sunshine duration for the entire year.

Employing the methodology constructed for meteorological elements in Section 3.1, the sunshine duration was initially determined using the mean substitution based on the same period of previous years, followed by estimating the potential monthly evapotranspiration data at the ground meteorological stations using the Penman-Monteith equation. Subsequently, the monthly total precipitation and total potential evapotranspiration for the typical debris flow gullies were estimated using universal kriging interpolation that considers topography. Finally, the PDSI for the typical debris flow gullies was calculated, incorporating the soil AWC to characterize the long-term dry-wet status at the sampling sites. The PDSI time series for the two typical debris flow gullies was extended to October 2021 (i.e., the month of soil sampling) to further investigate the influence of dry-wet cycles on debris flow susceptibility (Fig. 4-4).

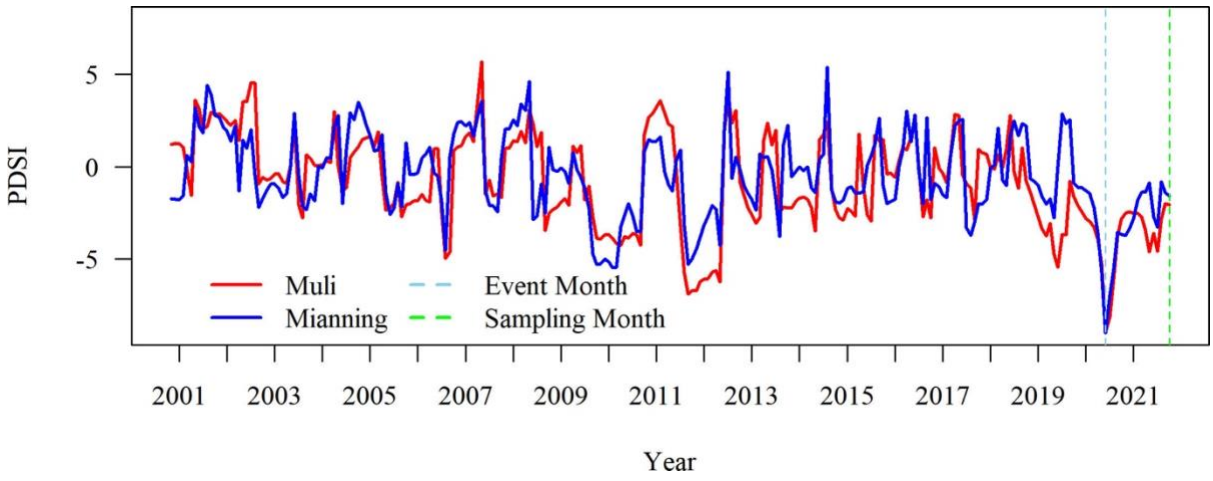

Fig. 4-4. PDSI time series of typical debris flow gullies

The results reveal that before the debris flow occurrences, the two typical debris flow gullies experienced extremely dry conditions that were rare over the preceding 20 years, with the PDSI in the month of the debris flow occurrence (June 2020) reaching the lowest value in nearly two decades, contrary to the maximum PDSI values observed during the debris flow occurrence month depicted in Fig. 3-3. This is due to the first half of 2020, where, despite relatively stable monthly potential evapotranspiration, the monthly total precipitation in both gullies significantly decreased compared to the long-term average (Fig. 4-5), leading to a sharp decline in PDSI and the emergence of extreme drought conditions (PDSI < -4). This process may have lowered the rainfall threshold for triggering local debris flows. Consequently, even with relatively low total precipitation in June 2020 (less than 50 mm), the rainfall threshold for triggering the two typical debris flow events was met, resulting in the debris flows. These findings indicate that relying solely on the PDSI value of a single month is insufficient to accurately determine the relationship between debris flow susceptibility and dry-wet conditions. Therefore, the use of DWCC based on the PDSI time series is essential.

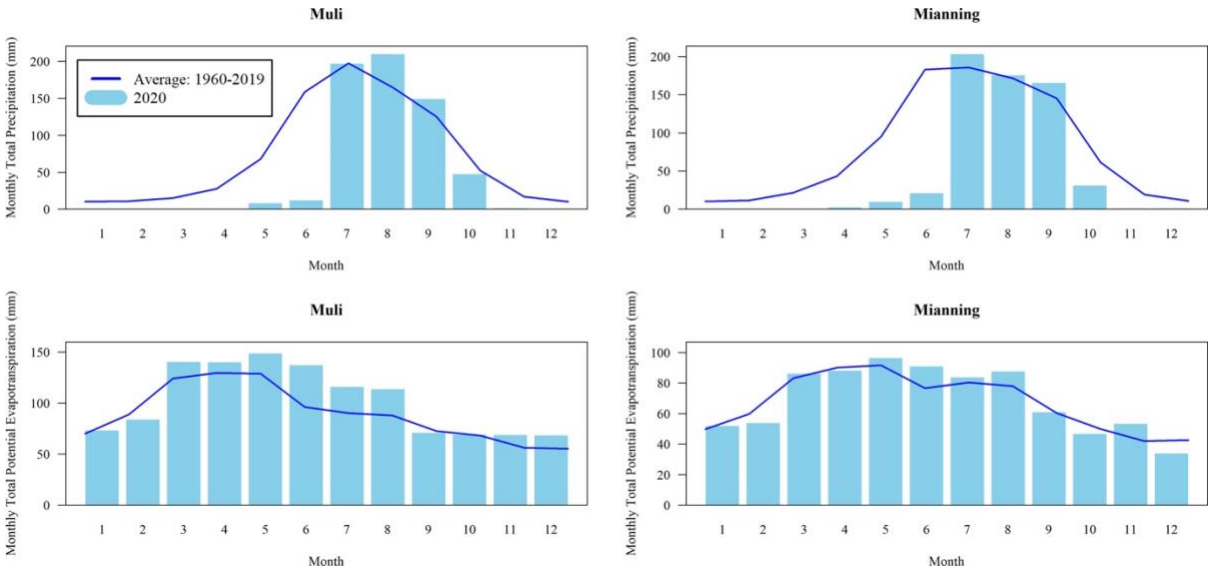

Fig. 4-5. Precipitation and potential evapotranspiration of typical debris flow gullies (2020 and multi-year average from 1960 to 2019)

Since the FS obtained from the soil sample measurements of the debris flow gullies in Muli County and Mianning County are consistent with the actual situation, to further quantify the DWCC before sampling in the two typical debris flow gullies, and to reveal the relationship between the DWCC and the FS of the debris flow gullies, the wavelet analysis method described in Section 3.3.3 and the multifractal analysis method from Section 3.3.4 were employed. These methods were used to calculate the wavelet power spectra and multifractal spectrum parameters of the 252-month PDSI time series before sampling in the two debris flow gullies. The objective is to identify the EDWP and quantify the extreme dry-wet characteristics. Subsequently, the DWCC were correlated with the FS of the debris flow gullies under both dry conditions and persistent heavy rainfall conditions using Spearman correlation analysis (Table 4-4).

Table 4-4. Correlations between FS and DWCC

	EDWP	α_{max}	α_{min}	$\Delta\alpha$	$f(\alpha_{max})$	$f(\alpha_{min})$	Δf (all>0)
FS_o	0.92	-0.92	0.92	-0.92	0.92	0.92	-0.92
FS_g	0.88	-0.88	0.88	-0.88	0.88	0.88	-0.88

The results demonstrate a significant and strong correlation between the FS of debris flow gullies under dry/persistent heavy rainfall conditions and six multifractal spectrum parameters ($p < 0.005$). Overall, the correlation between the FS and multifractal spectrum parameters is minimally affected by precipitation conditions, with a difference of 0.04, which is attributable to the ΔFS of all samples in Table 4-3 being close to each other. Therefore, based on the results in Table 4-4, the correlation between the FS and DWCC can be directly discussed. There is a significant positive correlation between FS and the EDWP, indicating that FS decreases as the EDWP shortens, which suggests that more frequent dry-wet cycles are closely related to the reduction in FS. The FS exhibits a significant negative correlation with α_{max} and $\Delta\alpha$, meaning FS decreases as α_{max} and $\Delta\alpha$ increase, while there is a significant positive correlation with α_{min}, meaning FS decreases as α_{min} decreases, indicating that the reduction of FS in a typical debris flow gully is highly associated with severe extreme dry-wet events. FS shows a significant positive correlation with $f(\alpha_{max})$ and $f(\alpha_{min})$, implying that FS increases with the increase of $f(\alpha_{max})$ and $f(\alpha_{min})$, which could be related to the increased frequency of dry-wet cycles caused by frequent extreme dry-wet

events. FS and Δf are significantly negatively correlated, with FS decreasing as Δf increases. Since Δf is greater than 0, this suggests that there may be a lower FS when the frequency of extreme dry-wet events tends to be associated with extreme precipitation events. In summary, the formation and initiation of debris flows in typical debris flow gullies exhibit a certain pattern of response to dry-wet cycles, where severe and frequent dry-wet events play the most substantial role in promoting the formation and initiation of debris flows.

The validation results from the typical debris flow gullies have ensured the responsive relationship between DWCC and debris flow susceptibility. It has also elucidated the responsive mechanism of dry-wet cycles on the debris flow susceptibility based on FS. The findings indicate that in the SMCRS, intense and frequent dry-wet cycles are highly correlated with a decrease in debris flow susceptibility.

4.4 Summary

This chapter investigates the relationship between debris flow susceptibility and climate dry-wet cycles through statistical analysis and soil mechanical experiments, also inferring its underlying mechanisms:

Drawing on the historical records of debris flows in the SMCRS, two methods for estimating the debris flow ARI are proposed, which are based on either the

equivalent diameter of watersheds or the nearest site. The validity of using debris flow ARI to reflect its susceptibility is confirmed through cross-verification between the two methods and by comparison with the spatiotemporal distribution patterns of debris flows in the SMCRS.

Using wavelet power spectra, the dry-wet cycle periods before the debris flow occurrences in watersheds of the SMCRS are estimated, revealing a significant moderate positive correlation directly between the EDWP and the debris flow ARI. This correlation is numerically slightly stronger than the significantly weak negative correlation between the debris flow ARI and the maximum daily precipitation, suggesting that DWCC have potential advantages when applied to debris flow susceptibility assessment. However, this finding necessitates further experimental work for more comprehensive validation.

To further validate the finding, soil sampling has been conducted in debris flow gullies of two typical debris flow events that occurred in June 2020 in the SMCRS. By calculating the soil mechanical properties of the slope source materials through soil experiments, an infinite slope model is constructed to compute the FS of the two typical debris flow gullies under conditions with and without extreme precipitation. The results confirm that under extreme precipitation conditions, the FS of debris flow gullies significantly decreases, the risk of large-scale slip of slope source materials increases, and consequently, the susceptibility to debris flows rises. Dry-wet indices from January 2001 to October 2021, before

the sampling of the watersheds where the two debris flow gullies are located, show that the debris flow occurrence months are in a state of extreme drought. Further comparison of the total monthly precipitation and potential evapotranspiration of the occurrence months with the long-term average values revealed that the year of debris flow occurrence has experienced a rare extreme drought event in nearly 20 years due to reduced precipitation, potentially leading to a significant reduction in the rainfall threshold required to trigger debris flows. This outcome indicates that a direct application of monthly dry-wet indices for assessing debris flow susceptibility may introduce certain biases. Therefore, extracting DWCC from the time series of dry-wet indices is necessary. Correlation analysis between the FS calculated from the one-dimensional sandy infinite slope model and the DWCC extracted from the PDSI time series shows that there is a definite responsive pattern between debris flow susceptibility and DWCC, where more intense and frequent dry-wet cycles are significantly correlated with the reduction of FS and an increase in debris flow susceptibility.

Chapter 5 Debris Flow Susceptibility Model Based on Dry-wet Cycle Characteristics

This chapter focuses on typical inland and coastal regions affected by monsoons, developing a machine-learning model for assessing the debris flow susceptibility based on DWCC indicators as well as geology, topography, meteorology, human activities, and vegetation cover. By comparing four representative machine learning models, the best-performing model is selected based on performance metrics, and the optimal cross-validation method is determined. The model is optimized through indicator trimming and parameter tuning. Its effectiveness is validated using cases separate from the training set, and the stability of applying DWCC from dry-wet index time series to debris flow susceptibility assessment is tested. This process ultimately verifies the effectiveness and stability of applying DWCC in constructing a debris flow susceptibility assessment model.

5.1 Assessment factors

The establishment of susceptibility assessment indicators for debris flows requires consideration of various geo-environmental factors in typical inland coastal monsoon-affected regions. Besides DWCC indicators and commonly used geological, topographical, meteorological, human activity, and vegetation cover indicators, geological activities in the SMCRS and typhoons in the HKSAR must be considered. Since geological activities can impact DWCC performance

in debris flow susceptibility assessment models, it is necessary to divide the SMCRS based on its USC and establish separate debris flow susceptibility assessment models for each USC zone to mitigate the impact of geological activities on the DWCC-based models. Due to the small spatial variability in the HKSAR, no subdivision is required for the HKSAR to mitigate the impacts of typhoons on the DWCC-based model, and the model can be constructed based on all assessment units in the HKSAR. All assessment indicators are extracted for the research units of each study area.

5.1.1 USC-based zoning for inland monsoon region

The SMCRS is chosen as a typical inland monsoon area, with 16,195 watersheds serving as assessment units for the debris flow susceptibility assessment model. This model, which assesses debris flow susceptibility based on DWCC, will also consider evaluation indicators such as geology, topography, meteorology, human activities, and vegetation cover. However, within the SMCRS, these assessment indicators exhibit considerable spatial variability, and applying a single debris flow susceptibility assessment model to the entire region would hinder accurately elucidating the relationships between debris flow susceptibility and the various assessment factors. Therefore, preliminary zoning of the SMCRS is necessary before constructing the debris flow susceptibility model, and the selection of

zoning indicators needs to significantly influence the representation of DWCC in the debris flow susceptibility assessment model.

This study primarily investigates the impacts of geological activities, such as earthquakes, and complex topographic conditions on the performance of DWCC within the debris flow susceptibility assessment model. For one thing, geological activities like earthquakes generate loose material that accumulates the source materials required for debris flow outbreaks, which are challenging to differentiate from the source materials produced by climatic dry-wet cycles, thereby affecting the representation of DWCC in the debris flow susceptibility model. For another, complex topographic conditions, particularly elevation and slope, determine the gravitational potential energy of source materials during debris flow occurrences and the capacity to convert this potential energy into kinetic energy. The variability in potential energy and its conversion capacity dictates the ease with which loose material accumulated through climate dry-wet cycles can transform into debris flow source materials, thus influencing the contribution of DWCC in the model. Other factors within the assessment factor system, such as meteorology, human activities, and vegetation types, are largely affected by geological activity conditions and complex topographic conditions and are thus not included in zoning the SMCRS at this stage.

Ultimately, it is determined that the clustering of the 16,195 watersheds in the SMCRS should be based on USC such as geology and topography using the K-

means method. For this clustering, the chosen USC are the distance to fault and the Melton ratio, which represent the influence of seismic activity and the relief within the watersheds, respectively. The optimal number of clusters was ascertained based on the maximum value of the Silhouette Score, as depicted in Fig. 5-1.

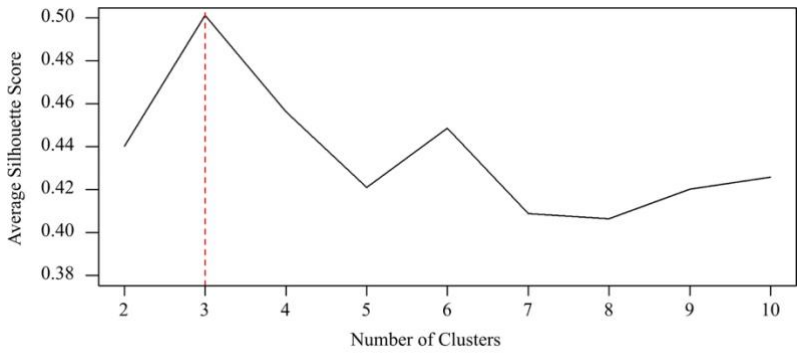

Fig. 5-1. The optimal number of clusters based on the Silhouette Score

The results indicate that when the number of clusters is set to three, the average Silhouette Coefficient is maximized, thereby definitively zoning the SMCRS into three USC Zones, namely Zone I, Zone II, and Zone III, as illustrated in Fig. 5-2. The clustering algorithm ensures that within the same class, the watersheds share more similar geological and topographic conditions, which guarantees a stronger correlation between debris flow susceptibility and the constructed assessment factor system, thereby better identifying the different characteristics between positive and negative examples among debris flow susceptibility indicators within each region (Wu et al., 2022). Consequently, machine learning models are

constructed for each of the three zones within the SMCRS to assess the debris flow susceptibility of the individual watersheds, which will enhance the model performance to successfully identify watersheds that are prone to debris flows.

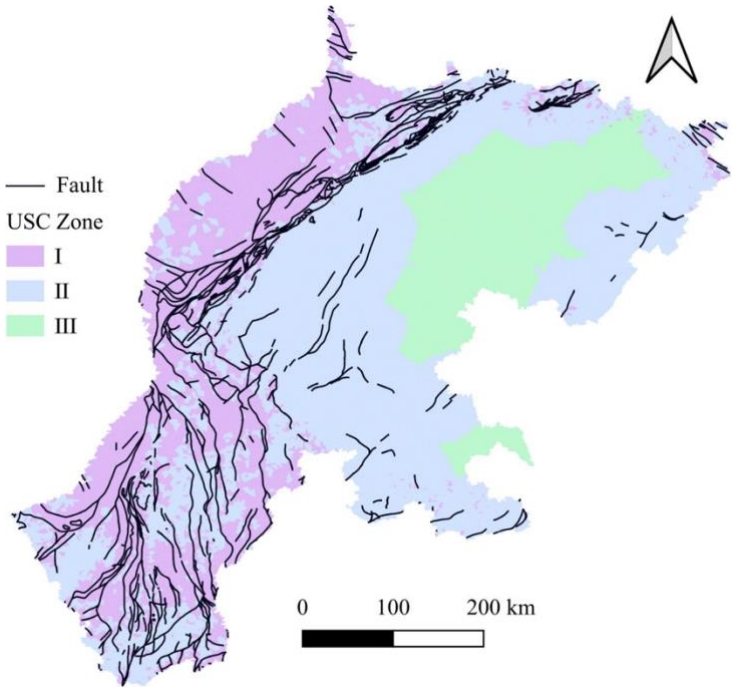

Fig. 5-2. Zoning of the SMCRS based on USC

Based on the three USC zones, a total of 1,486 debris flow positive and negative samples from 1981 to 2019 were respectively allocated to Zone I, Zone II, and Zone III. Specifically, Zone I contains 836 debris flow samples, Zone II comprises 604 samples, and Zone III includes 46 samples. When generating negative samples for debris flows, it was necessary to ensure that the number of positive and negative debris flow samples was equal within each zone.

Table 5-1. Watershed characteristics in different USC zones of the SMCRS

USC Zone	Distance to Faults (km)	Melton Ratio	Amount	Area (km^2)	Debris Flow Record Amount
I	4.3	460.2	5534	81827.4	418
II	11.2	122.9	7894	141265.4	302
III	65.9	90.9	2767	42806.3	23

Table 5-1 presents the USC of the clustering centers for different zones, including the distance to fault and the Melton ratio. The results indicate that within Zone I, Zone II, and Zone III, the watersheds increase in distance from faults and decrease in the Melton ratio, suggesting that watersheds in Zone I are the most affected by geological activities such as earthquakes and possess the steepest terrain. Watersheds in Zone II are less influenced by geological activities compared to those in Class I, and the terrain is relatively flatter. Watersheds in Zone III are the furthest from faults and have the flattest terrain.

Table 5-1 also provides a statistical summary of the number and area of watersheds within each zone, along with a record of debris flow events over the 39 years from 1981 to 2019. Zone II has the highest number of watersheds and the largest area within the SMCRS, yet it has fewer recorded debris flow events than Zone I. Zone III has the fewest debris flow records, averaging less than one event per year for the entire zone. Preliminary conclusions drawn from Table 5-1 suggest that Zone I, characterized by frequent geological activity and large elevation differences within watersheds, has a high frequency of debris flow

events. Although Zone II experiences relatively fewer geological activities and has smaller elevation differences in its watersheds, the large total area contributes to a still significant overall frequency of debris flow events. Consequently, research on the susceptibility of debris flows in the SMCRS should be primarily focused on Zone I and Zone II.

The zoning results derived from the K-means method are largely consistent with the USC of the SMCRS. Zone I encompasses areas concentrated with faults, exemplified by the Longmenshan fault zone, where watersheds exhibit significant elevation differences, and the Melton ratio is notably higher compared to those in Zone II and Zone III. Zone II and Zone III include most areas of the Sichuan Basin and the Panxi region, where the watersheds in both zones have elevation differences similar to each other and are comparatively flatter than those in Zone I. However, the watersheds in the Zone II region are relatively closer to faults.

5.1.2 Record-based assessment unit for coastal monsoon region

The HKSAR was selected as a typical coastal monsoon-affected area for this study, with 20,451 grids serving as assessment units for the debris flow susceptibility assessment model. The sources of debris flow records include UAV imagery interpretation, which lacks precise occurrence times, and geological survey reports that provide relatively accurate occurrence timing. To further

investigate the impact of dry-wet cycles on the debris flow susceptibility in typical coastal monsoon-affected areas, it is necessary to construct a debris flow dataset with accurate occurrence time. Consequently, the debris flow records from the geological survey reports were utilized to build the debris flow susceptibility assessment model.

Debris flow records based on the interpretation of UAV imagery, due to their inclusion of information such as the width of the main scarp, the length of the source area, and the elevation difference between the crown and toe of each debris flow, can be used to approximate the maximum scale of debris flows in the HKSAR. The largest scale identified from historical debris flow records can be employed to determine the highest resolution for the grid assessment units in the region, which was ultimately set at 250 meters.

The method of determining the grid resolution based on the maximum scale of historical debris flow records ensures that each grid assessment unit can completely contain the majority of the debris flow gullies, and also ensures that the number of assessment units delineated for the HKSAR (i.e., 20,451 grids) is roughly on the same order of magnitude as those in the SMCRS (i.e., 16,195 watersheds). This consistency facilitates subsequent comprehensive comparisons between the debris flow susceptibility assessment models of the two typical regions.

5.1.3 Assessment factor system construction

Utilizing watersheds as the assessment unit, models were constructed for different regions including a total of 32 initial indicators (Table 5-2) encompassing geological conditions (distance to faults, and dominant rock type of igneous, sedimentary, or metamorphic), topographical conditions (Melton ratio, curvature, aspect), meteorological conditions (maximum daily rainfall, maximum 3-day rainfall), DWCC (EDWP, extreme dry-wet characteristics), and land use types representing vegetation cover or human activities (woodland, shrubland, grassland, cropland, built-up land, bare land/sparse vegetation, wetlands, mosses/lichens). Among these indicators, some exhibit weak spatial variability. For example, in watersheds of Zone III, the predominant rock type is all sedimentary. In such cases, it becomes necessary to eliminate all indicators related to rock type before constructing the debris flow susceptibility assessment model to avoid the influence of ineffective variables on model development.

Table 5-2 presents the factor system for assessing the debris flow susceptibility in the SMCRS. From a mechanistic perspective, the contribution of each index to the formation and initiation of debris flows, involving the three essential elements of debris flows, i.e., energy, source material, and water is also explained (Wei et al., 2015). Within the 32 indices, 11 are categorical variables, specifically rock type and aspect (where a value of 1 indicates the presence of the category, and 0 indicates its absence), while the remaining 21 are continuous variables.

Table 5-2. Debris flow susceptibility assessment indicators for SMCRS

Factor		Abbreviation in figures	Introduction	Mechanism
Category	Sub-category			
Geology (4)	Distance to faults (m)	D	Distance between the geometric center of a watershed and the nearest fault	Geological activities generate loose materials
	Rock type	GEO_	I: Igneous II: Sedimentary III: Metamorphic	Weathering and erosion of rocks produce loose materials
Terrain (11)	Melton ratio	Melton	The maximum watershed elevation difference divided by the square root of the watershed area	Providing potential energy
	Curvature	CPl, CPr	Plan curvature: Positive/negative values indicate horizontal convexity/concavity Profile curvature: Positive/negative values indicate vertical concavity/convexity	Accumulation and retention of loose materials
	Aspect	A_	I: North; II: Northeast; III: East; IV: Southeast; V: South; VI: Southwest; VII: West; VIII: Northwest	Impact on soil moisture due to sunshine duration
Meteorology (2)	Maximum daily precipitation (mm)	Pre_1d	Maximum daily precipitation for the month	Trigger
	Maximum 3-day precipitation (mm)	Pre_3d	Maximum 3-day precipitation for the month	Trigger
DWCC (7)	Extreme dry-wet periods (month)	EDWP	Period of maximum power squared in dry-wet index wavelet spectrum	Dry-wet cycles promote loose material accumulation, with extreme rainfall as the trigger
	Extreme dry-wet characteristics	α_max, α_min, Δα, f(α_max), f(α_min), Δf	Multifractal spectrum parameters of the dry-wet index	
Human activity/ Vegetation cover (8)	Proportion of area by land use type	LU_	I: Woodland II: Shrubland III: Grassland IV: Cropland V: Built-up land VI: Bare/sparse vegetation VII: Wetland VIII: Moss/lichen	Loose materials accumulation relates to human activities and vegetation cover

Due to the relatively small area, the variability of USC such as geology and geomorphology in the HKSAR is considerably less than that in the SMCRS. However, while geological activity may be negligible, the impact of typhoons, which occur annually, is an important factor to consider for the occurrences of debris flows in the HKSAR. Based on the timing of debris flow records, three evaluation indices, i.e., typhoon frequency, maximum typhoon intensity, and longest typhoon duration, are matched for each debris flow grid. If there are no typhoon records in the month of a debris flow occurrence, the values for typhoon frequency, maximum typhoon intensity, and longest typhoon duration are all set to zero.

Table 5-3 shows the initial 35 factors for assessing the debris flow susceptibility in the HKSAR. A brief explanation of each variable related to energy, source material, and water is also provided. The assessment factors include geological conditions (dominant rock types of igneous and sedimentary), topographical conditions (maximum elevation difference, curvature, aspect), meteorological conditions (typhoon frequency, maximum typhoon intensity, longest typhoon duration, maximum daily rainfall, maximum 3-day rainfall), DWCC (EDWP, extreme dry-wet characteristics), and land use type proportions representing human activities or vegetation cover (reclassified into categories such as built-up land, agriculture land, roads/railways, ports/airports, woodland, shrubland, grassland, mangroves/swamps, bare land, water bodies).

Table 5-3. Debris flow susceptibility assessment indicators for HKSAR

Factor		Abbreviation in figures	Introduction	Mechanism
Category	Category			
Geology (2)	Rock type	GEO_	I: Igneous II: Sedimentary	Weathering and erosion of rocks produce loose materials
Terrain (11)	Maximum elevation difference (m)	ED	The maximum elevation difference for an assessment unit	Providing potential energy
	Curvature	CPl, CPr	Plan curvature: Positive/negative values indicate horizontal convexity/concavity Profile curvature: Positive/negative values indicate vertical concavity/convexity	Accumulation and retention of loose materials
	Aspect	A_	I: North; II: Northeast; III: East; IV: Southeast; V: South; VI: Southwest; VII: West; VIII: Northwest	Impact on soil moisture due to sunshine duration
Meteorology (5)	Typhoon frequency	TY_F	Typhoon frequency for the month	Promoting extreme precipitation and transports loose materials
	Maximum typhoon level	TY_L	The maximum typhoon level for the month	
	Maximum typhoon duration (h)	TY_D	The maximum typhoon duration for the month	
	Maximum daily precipitation (mm)	Pre_1d	Maximum daily precipitation for the month	Trigger
	Maximum 3-day precipitation (mm)	Pre_3d	Maximum 3-day precipitation for the month	Trigger
DWCC (7)	Extreme dry-wet periods (month)	EDWP	Period of maximum power squared in dry-wet index wavelet spectrum	Dry-wet cycles promote loose material accumulation, with extreme rainfall as the trigger
	Extreme dry-wet characteristics	α_max, α_min, Δα, f(α_max), f(α_min), Δf	Multifractal spectrum parameters of the dry-wet index	
Human activity/ Vegetation cover (10)	Proportion of area by land use type	LU_	1: Built-up land 2: Agriculture land 3: Roads/railways 4: Ports/airports 5: Woodland 6: Shrubland 7: Grassland 8: Mangroves/swamps 9: Bare land 10: Water bodies	Loose materials accumulation relates to human activities and vegetation cover

According to the warning signals provided by the Hong Kong Observatory, typhoons are classified into Signal No. 1 (the typhoon is within 800 km of Hong Kong), Signal No. 3 (strong winds with sustained speeds of 41-62 km/h and gusts that may exceed 110 km/h), Signal No. 8 (gale or storm force winds with sustained speeds of 63-117 km/h and gusts that may exceed 180 km/h), Signal No. 9 (gale or storm force winds are increasing or expected to increase), and Signal No. 10 (hurricane force winds with sustained speeds exceeding 118 km/h and gusts that may exceed 220 km/h). For this study, the typhoon signal levels are standardized to ensure they are treated as continuous variables, with Signal No. 1, 3, 8, 9, and 10 corresponding to levels 1, 2, 3, 4, and 5, respectively.

The debris flow susceptibility assessment factors constructed in Table 5-3 are largely consistent with those in Table 5-2. However, in regions affected by typhoons, additional consideration is given to the frequency, intensity, and duration of typhoons. Since the HKSAR does not have delineated watersheds but instead builds models based on grid assessment units, the Melton ratio is replaced by the maximum elevation difference within the grid. The grid resolution was determined based on the length of the largest source area recorded in the historical debris flow records. Therefore, the maximum elevation difference of a grid unit can approximately represent the maximum elevation difference of a debris flow gully. Both the Melton ratio and the maximum elevation difference of debris flow gullies can be converted to slopes, reflecting the ability of the source materials in

a debris flow gully to transform gravitational potential energy into kinetic energy. In terms of land use types, since the HKSAR does not have watersheds delineated by rivers and is a coastal area, additional land use types that reflect the characteristics of the coastal intertidal zone (mangroves/swamps) and those related to water bodies (ponds, rivers, and channels) are incorporated. Out of the 35 assessment variables, 10 are categorical variables, which include 2 rock categories and 8 aspect categories, where a value of 1 indicates belonging to that category and a value of 0 indicates non-belonging. The remaining 25 indicators are continuous variables.

5.2 Model selection

After constructing the assessment factor systems for the two typical regions, it was necessary to select an appropriate model for assessing debris flow susceptibility. Initially, performance metrics for the models were established to evaluate the effectiveness of the models in assessing debris flow susceptibility. Subsequently, a comparison of four representative models was conducted, and the model exhibiting superior performance, as determined by these metrics, was chosen for the susceptibility assessment. Finally, an optimal model validation method was selected with an appropriate ratio of model training and validation datasets to ensure the model performance and generalization capability.

5.2.1 Model performance metrics

This study treats debris flow susceptibility assessment as a classification problem, evaluating machine learning model performance using metrics based on correctly and incorrectly classified samples. The classifier, based on the assessment factors of each sample, outputs the probability that the sample is positive (ranging from 0 to 1). After determining the classification threshold that distinguishes positive from negative samples, the samples can be categorized as positive or negative based on the output probability. Samples with an output probability greater than or equal to the threshold are classified as positive, whereas those with an output probability below the threshold are classified as negative. Correctly classified positive samples are termed True Positives (TP), correctly classified negative samples are termed True Negatives (TN), incorrectly classified positive samples are termed False Positives (FP), and incorrectly classified negative samples are termed False Negatives (FN). These classifications form the basis for deriving metrics to evaluate the performance of the classification model, including recall, precision, and accuracy, as detailed in equations (5-1), (5-2), and (5-3).

$$recall = \frac{TP}{TP+FN} \tag{5-1}$$

Recall, as a performance metric, reflects the capability of a model to correctly identify all positive samples without considering the negative samples. Recall is

particularly important when the consequence of failing to detect a positive sample is significant, as it emphasizes the sensitivity of the model to the presence of positive cases.

$$precision = \frac{TP}{TP+FP} \tag{5-2}$$

Precision is a performance metric that reflects the ability of a model to accurately predict positive samples out of all the positive and negative samples it classifies. Precision is particularly relevant when the cost of a false positive is significant, as it measures the reliability of the classification results of a sample as positive.

$$accuracy = \frac{TP+TN}{TP+FP+TN+FN} \tag{5-3}$$

Accuracy is a performance metric that reflects the ability of a model to correctly predict both positive and negative samples. It represents the proportion of TP and TN out of the total number of samples evaluated. Accuracy is a fundamental metric often used to gauge the general performance of classification models in balanced datasets where each class is equally important.

The metrics of recall, precision, and accuracy have a value range between 0 and 1, with values closer to 1 indicating superior model classification performance. In the context of debris flow susceptibility assessment models, a high recall rate ensures that the model successfully predicts a greater number of debris flow occurrences. However, focusing solely on recall may lead to false positives or false alarms, which in turn could increase the response costs for debris flow

prevention and mitigation. A high recall rate, when combined with high precision and accuracy, can effectively minimize the issue of an excessive false alarm rate. By determining the optimal classification threshold, the recall, precision, and accuracy of the classification model can be enhanced, thereby its overall classification performance.

To determine the optimal classification threshold, the output probability of each sample can be used as a potential threshold, thereby obtaining the corresponding TP rate and FP rate for each threshold value. These rates can be plotted with the TP rate on the y-axis and the FP rate on the x-axis to construct the Receiver Operating Characteristic (ROC) curve. The optimal classification threshold can be selected by balancing the TP rate to the FP rate according to the specific needs regarding the acceptable rate of false alarms. Moreover, the area under the ROC curve (AUC) serves as an additional metric for reflecting the performance of the classification model. When the model performance surpasses that of a random classifier, the AUC value ranges from 0.5 to 1, with larger AUC values indicating a more effective overall classification of positive and negative samples by the model.

5.2.2 Model comparisons

A superior machine learning model for debris flow susceptibility assessment can be selected and optimized from four algorithm types using R programming packages (Anastasiadis et al., 2005; Friedman, 2001; Ripley, 2002). Based on model performance metrics, a machine learning model that demonstrates better classification performance can be selected for further optimization. The selection process encompasses four types of machine learning algorithms including log-linear regression (LLR) representing linear regression models, gradient boosting machine (GBM) representing decision tree models, KNN representing distance-based models, and artificial neural network (ANN) representing the application of neural networks in regional debris flow susceptibility assessments. The construction and evaluation process for these four representative machine learning models involves the use of packages within the R programming language, such as "caret", "nnet", "gbm", "neuralnet", "ROCR", and "verification".

Taking the SMCRS as an example without USC zoning, all positive and negative samples are applied across the four models. The performance of a preliminary model is determined through 10-fold cross-validation, during which ROC curves are generated. The model with the best classification effect is identified based on the maximum average AUC value derived from the 10 ROC curves, thereby obtaining a robust model by using multiple iterations to account for the randomness.

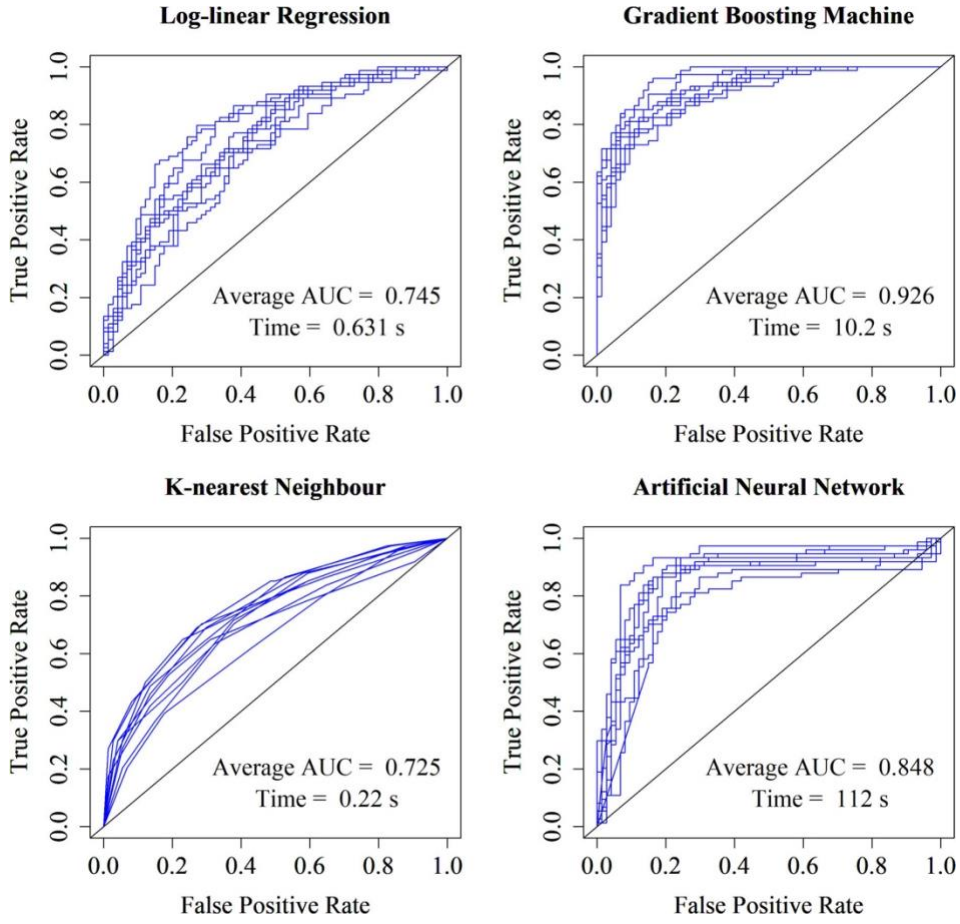

Fig. 5-3. Performance comparisons among different machine learning models

The results indicate that, after tuning the hyperparameters, the GBM, which is based on decision trees, significantly outperforms the other three models with a higher average AUC. Compared to the LLR and the KNN, the GBM, and the ANN possess a relatively larger number of hyperparameters that can be tuned to enhance the model performance. However, ANN is more resource-consuming compared to GBM when tuning the hyperparameters. Therefore, considering both the model classification performance and the time cost for tuning, the GBM based

on decision trees was ultimately selected as the machine learning model for debris flow susceptibility assessment.

The GBM improves prediction by iteratively constructing new decision trees that estimate the residuals of debris flow susceptibility from the predictions of the previous tree. By increasing the number of iterations, the model successively minimizes the prediction error for debris flow susceptibility. The final prediction of debris flow susceptibility (S) is accomplished by summing the predicted residuals from all the decision trees to the initial susceptibility estimate and adding it to the initial susceptibility (S_0). When constructing the GBM model using the "gbm" package in R, the initial susceptibility (S_0) is set to 1. After building a certain number of decision trees to reduce the prediction residuals, the final debris flow susceptibility is obtained. Subsequently, a Sigmoid function is applied to transform the debris flow susceptibility into a probability value ranging between 0 and 1. The computation of debris flow susceptibility is delineated in equation (5-4).

$$S = \frac{1}{1+e^{-[S_0+\sum_{m=1}^{M} f_m(x)]}} \tag{5-4}$$

where e denotes the base of the natural logarithm, M is the total number of decision trees, and $f_m(x)$ represents the predicted debris flow susceptibility residual by the mth decision tree based on different assessment factors x. For each constructed decision tree, the gradient descent of the predicted residuals is

realized by determining the combination of assessment factor weights that minimizes the loss function, which is the binomial deviance in this context.

5.2.3 Cross-validation

Evaluating the effectiveness of different cross-validation methods is crucial for optimizing the model performance and tuning efficiency. The division of the dataset into training and validation sets affects the assessment. Therefore, it is imperative to further evaluate the effectiveness of the 10-fold cross-validation method. Using the SMCRS as an example and employing the GBM, an assessment is made based on Fig. 5-3 by comparing the results of cross-validation with different fold numbers, namely 3-fold, 5-fold, 15-fold, and 20-fold. This comparison is aimed at evaluating the influence of the number of folds in cross-validation on the model classification performance and the time cost associated with tuning (Fig. 5-4).

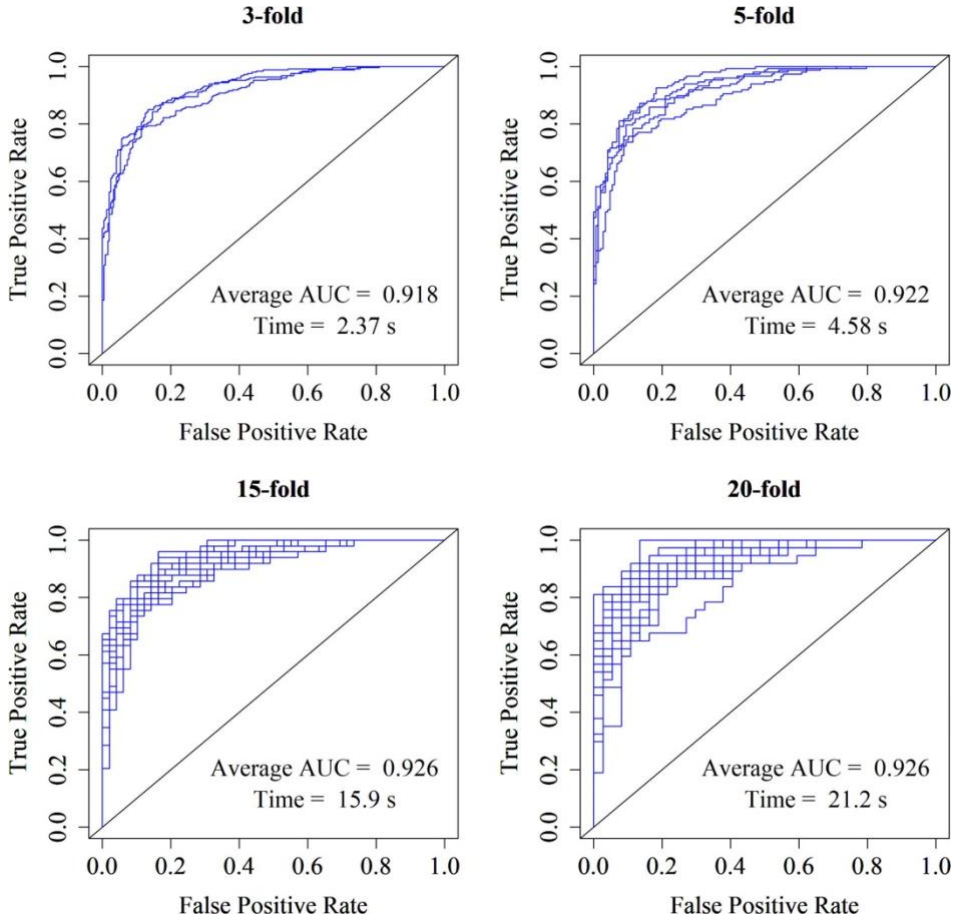

Fig. 5-4. Evaluation of cross-validation with different folds

The results demonstrate that as the number of folds in cross-validation increases, the validation time correspondingly escalates, and the average AUC initially rises and then stabilizes. Considering the 10-fold cross-validation results of the GBM depicted in Fig. 5-3, which exhibit a relatively optimal classification performance as measured by the average AUC, the 10-fold cross-validation method is selected for its balance of high average AUC and the lowest time cost. The optimal number of cross-validation folds determines a balance between training and validation data, thereby ensuring superior classification performance of the model during

the training process and its generalization capability when subsequently tested on different datasets.

To ensure comparability between models for the two study areas, it is advisable to employ the same debris flow susceptibility assessment model and cross-validation method in the HKSAR as chosen for the SMCRS. There are three reasons for conducting the established GBM and the 10-fold cross-validation method in the HKSAR as in the SMCRS. First, the process of model selection based on performance metrics does not involve constructing separate debris flow susceptibility models for each underlying surface subdivision within the SMCRS, and thus, the number of assessment units (16,195 watersheds) in the SMCRS is of the same order of magnitude as that in the HKSAR (20,451 grids). Second, the number of positive debris flow samples from 1981 to 2019 in the entire SMCRS (743 samples) is comparable to that in the HKSAR from 2010 to 2018 (904 samples). Lastly, a comparison of the results from Table 5-2 and Table 5-3 indicates that the debris flow susceptibility assessment factor systems for the SMCRS and the HKSAR are closely aligned. Therefore, for the construction of models across the whole study area of both regions, the same model and validation method can be appropriately utilized.

5.3 Model construction and optimization

Debris flow susceptibility assessment models can be constructed for the SMCRS and the HKSAR based on the DWCC after determining the model choice and validation method. Specifically, for the SMCRS, according to the USC partitioning depicted in Fig. 5-2, separate debris flow susceptibility models will be developed for Zone I, Zone II, and Zone III. This approach aims to mitigate the influence of complex USC on classification effectiveness within the SMCRS while placing greater emphasis on the impacts of DWCC on different USC zones. Despite the analysis results from Table 5-1 indicating that only Zone I and Zone II, which are prone to debris flows, require focus, models have still been constructed for Zone III to ensure the completeness of the debris flow susceptibility assessment results for the entire study area. However, due to the smaller sample size in Zone III, the comparability of the debris flow susceptibility model for Zone III with that for Zone I or Zone II is limited. Therefore, from the aspects of debris flow susceptibility and data representativeness, it is advisable to focus more on Zone I and Zone II.

5.3.1 Application of dry-wet cycle characteristics

For the SMCRS and the HKSAR, models based or not based on DWCC were compared to evaluate the effect of using DWCC in debris flow susceptibility assessment (Fig. 5-5).

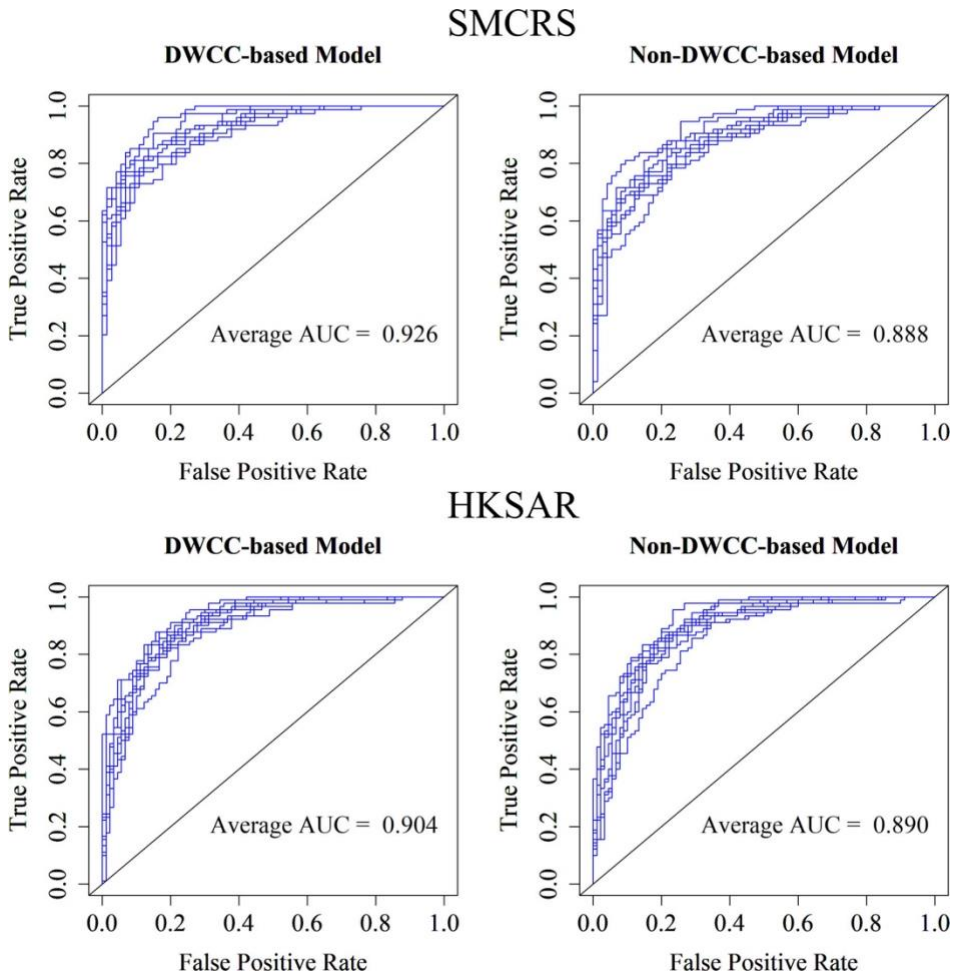

Fig. 5-5. Evaluation of DWCC-based models

The results show that the AUC of models based on DWCC have been improved by 1.4% - 3.8% in the two study areas. Based on equation (5-3), the accuracies of correctly identifying the samples reach 83.6% (SMCRS) and 82.3% (HKSAR) after using DWCC, indicating the effectiveness of applying DWCC in debris flow susceptibility assessment.

5.3.2 Multicollinearity detection

Addressing the multicollinearity among assessment factors is essential to ensure model stability and interpretability in debris flow susceptibility assessments. Severe multicollinearity among assessment factors, characterized by high intercorrelations, can significantly disrupt the weighting process of these factors, reducing the model interpretability and increasing model sensitivity to the assessment factors, thereby leading to unstable model performance. Consequently, it is crucial to detect and address multicollinearity among assessment factors before constructing the model and eliminate those with strong collinearity to ensure the interpretability and stability of the model performance. The diagnosis of multicollinearity among assessment factors is conducted using correlation matrices and the variance inflation factor (VIF) method. Initially, relative influence (RI) scores were calculated based on the structure of GBM, and indicators with RI scores below 1% were discarded to minimize their marginal contribution to debris flow susceptibility and their potential confounding impact on other indicators. A correlation matrix was then constructed for the remaining indicators. If the Spearman correlation coefficient between any two indicators exceeds 0.7, the indicator with the lower RI will be eliminated. Finally, the VIF was applied as a linear regression model to further refine the assessment factor system, discarding any factor with a VIF exceeding 5. The filtered set of assessment factors (19 for Zone I, 17 for Zone II, and 19 for Zone III) was used

to generate a correlation matrix, as shown in Fig. 5-6, along with the VIF values of each assessment factor, as presented in Fig. 5-7.

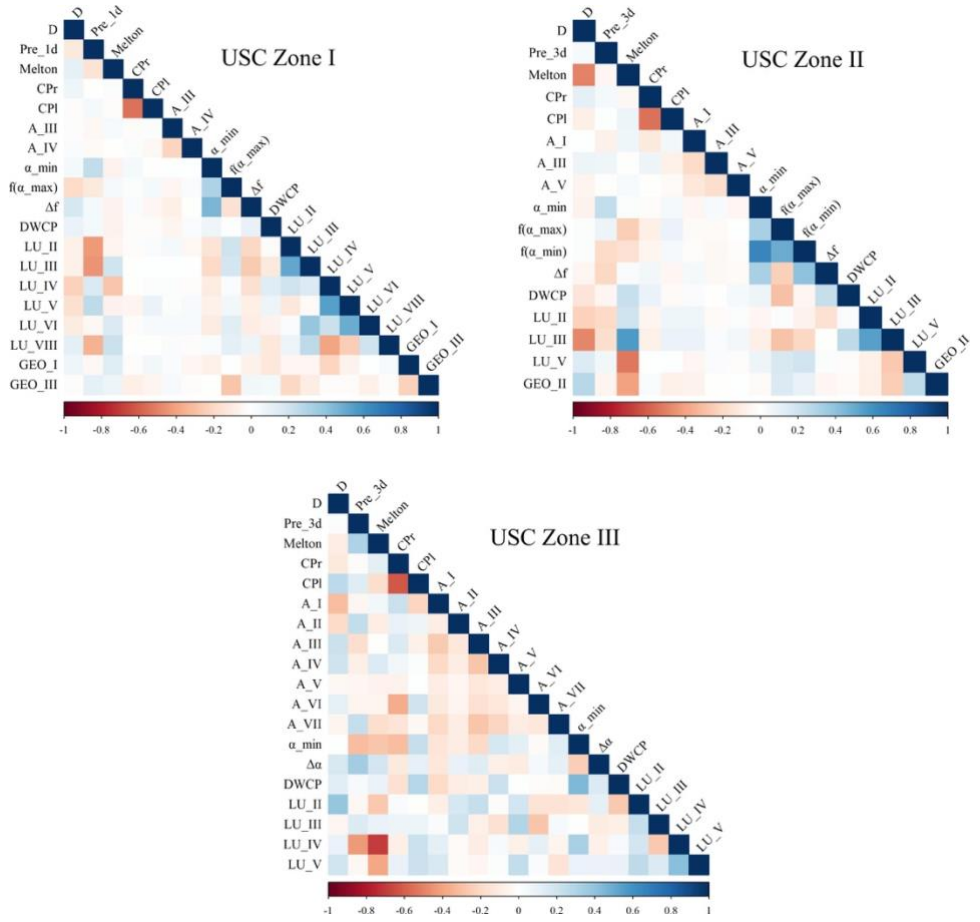

Fig. 5-6. Correlation matrix of assessment variables

The results indicate that, after the removal of assessment factors with high correlations and low RI scores from the dataset, the inter-correlations among the assessment factors for Zone I range between -0.54 and 0.54, for Zone II between -0.54 and 0.66, and Zone III between -0.69 and 0.44. Consequently, there are no instances where the correlation between any two assessment factors exceeds 0.7, thus ensuring that the assessment factor systems for the three USC zones are free

from severe multicollinearity. This outcome validates the robustness of the assessment factor systems and supports the stability and interpretability of the models developed for each zone.

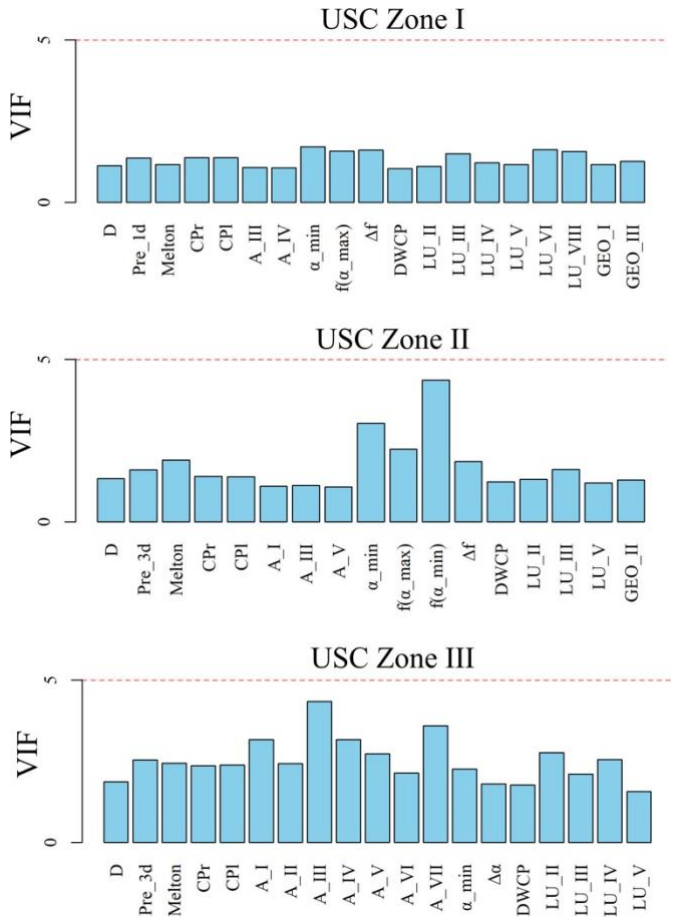

Fig. 5-7. Variance inflation factor of assessment variables

The results demonstrate that after the selection process, the VIF values for the assessment factors within Zone I range from 1.05 to 1.71, within Zone II from 1.07 to 4.36, and within Zone III from 1.57 to 4.34. Consequently, for Zone I, Zone II, and Zone III, the remaining assessment factors all exhibit VIF values

less than 5, signifying that multicollinearities within the refined assessment factor systems are not significant and can be considered negligible.

The common and unique assessment factors of debris flow positive and negative samples among different USC zones can be discerned by comparing their similarities and differences. The common indicators reflect factors potentially related to the debris flow susceptibility in the SMCRS, while the unique factors reveal those that may influence debris flow susceptibility within each specific USC zone. Comparative analysis of common indicators shows that for all three USC zones in the SMCRS, distance to fault, maximum daily/3-day precipitation, Melton ratio, curvature, east-facing slopes, severity of extreme precipitation events, EDWP, shrub coverage, grassland coverage, and built-up land coverage are essential common assessment factors required for the debris flow susceptibility assessment model. Exclusively focusing on Zone I and Zone II, the probability of extreme drought events and the preference for extreme hydrological events are additional common factors for these two USC zones. The unique indicators identified for Zone I include maximum daily precipitation, bare land/scant vegetation coverage, moss/lichen coverage, dominance of igneous rocks, and dominance of metamorphic rocks. The unique indicators identified for Zone II include the probability of severe extreme precipitation events and the dominance of sedimentary rocks. The unique indicators identified for Zone III include northeast-facing slopes, southwest-facing slopes, west-facing slopes, and

the fluctuation of extreme hydrological events. When specifically considering the differential assessment factors for Zone I and Zone II, it is found that maximum daily precipitation, southeast-facing slopes, arable land coverage, bare land/scant vegetation coverage, moss/lichen coverage, dominance of igneous rocks, and dominance of metamorphic rocks in Zone I differ from those in Zone II, whereas maximum 3-day precipitation, north-facing slopes, south-facing slopes, the probability of severe extreme precipitation events, and dominance of sedimentary rocks in Zone II present differences from those in Zone I.

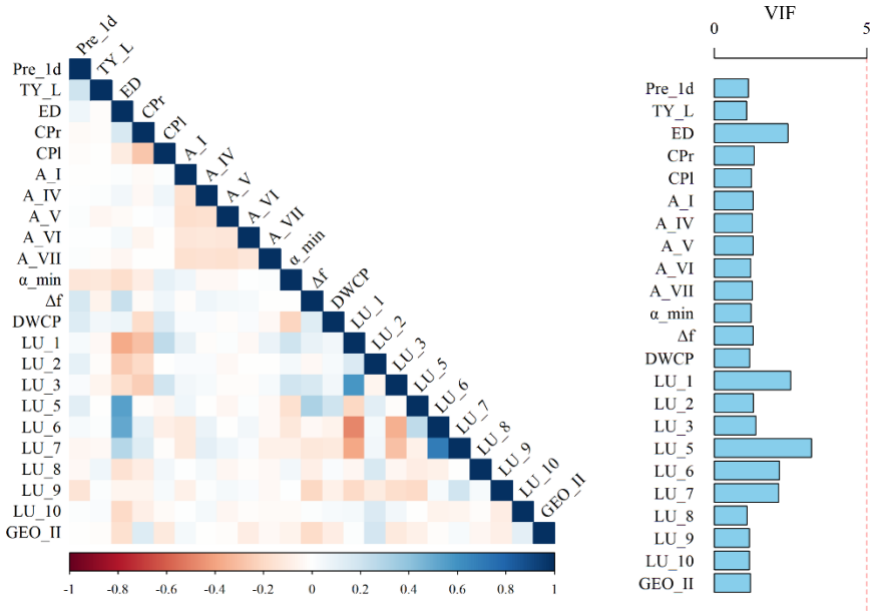

Fig. 5-8. Correlation matrix (Left) and variance inflation factor (Right) for assessment variables

For the assessment factor system of debris flow susceptibility in the HKSAR, the same multicollinearity detection methods as that used for the SMCRS were applied, resulting in a final set of 23 assessment factors. The correlation matrix

and the VIF values for these indicators are illustrated in Fig. 5-8. The results reveal that, after the removal of indicators with high intercorrelations and minimal impact on susceptibility assessment, the correlations between the remaining indicators for the HKSAR range from -0.48 to 0.69, with the highest correlation of 0.69 observed between the coverage ratios of shrublands and grasslands. Since none of the intercorrelations exceed the threshold of 0.7, the assessment factor system is deemed free of severe multicollinearity. Furthermore, the VIF values of the selected indicators range from 1.07 to 3.18, with the woodland coverage ratio exhibiting the highest VIF value. However, all VIF values are below the threshold of 5, indicating that multicollinearity within the assessment factor system can be considered negligible.

Comparing the assessment factor systems before variable trimming for the SMCRS and the HKSAR, the common and unique assessment factors based on positive and negative debris flow samples in typical inland and coastal monsoon areas have been understood initially. It was found that in the SMCRS, indicators such as distance to fault, dominance of igneous rocks, dominance of metamorphic rocks, the probability of extreme drought events, and the probability of extreme precipitation events serve as unique assessment factors that were not included in the construction of the debris flow susceptibility assessment model for the HKSAR. Conversely, in the HKSAR, indicators like the highest typhoon level, the proportion of mangroves/swamps, and the proportion of water bodies act as

unique assessment factors that were not incorporated in the construction of the debris flow susceptibility assessment model for the SMCRS.

However, further research is required to quantitatively assess the impact of each assessment factor on the debris flow susceptibility in different study areas.

5.3.3 Model tuning

Adjusting hyperparameters is crucial to prevent overfitting and underfitting while ensuring stable and efficient debris flow susceptibility assessment. For the GBM based on decision trees, four hyperparameters were adjusted, including the number of decision trees (NT), the depth of decision trees (DT), the learning rate (LR), and the minimum number of observations in terminal nodes (MNO). An excess in NT or DT can lead to overfitting, resulting in instability of the model performance, whereas insufficient values might cause underfitting, preventing the model from identifying the optimal solution. A high LR can accelerate the convergence to the optimal solution but may also lead to overfitting, while a low LR slows down the convergence and increases training time. An overly large MNO can result in underfitting, whereas an excessively small MNO tends to cause overfitting. Therefore, it is necessary to continuously adjust the combination of these four hyperparameters to avoid both overfitting and underfitting, while minimizing training time to construct a debris flow

susceptibility assessment model that is efficient, stable, and has an acceptable training duration.

Given that the debris flow susceptibility assessment model prioritizes the accurate classification of positive samples while maintaining overall optimal performance for both positive and negative samples, recall is adopted as the primary model performance metric, with the AUC serving as a secondary metric, to ensure the model applicability for debris flow susceptibility assessment. However, to guarantee the ability of the model to correctly classify negative samples, it is still necessary to consider precision and accuracy as model performance metrics and ensure that both precision and accuracy reach sufficiently high levels.

Based on 1,486 training samples from 1981 to 2019, hyperparameter tuning was conducted for the debris flow susceptibility assessment models of three USC zones in the SMCRS. The enhancement of model performance through the tuning process was quantified using four model performance metrics calculated via 10-fold cross-validation. The changes in recall, AUC, precision, and accuracy as model performance indicators before and after tuning are presented in Table 5-4.

The results indicated that after hyperparameter tuning, there is a significant enhancement in all four model performance metrics, demonstrating that the models constructed for the three different USC zones each exhibit performance improvements. Despite this, the model for Zone III, which has the fewest samples compared to Zone I and Zone II, displays the lowest performance metrics and

shows less pronounced improvements after hyperparameter tuning, indicating that the debris flow susceptibility model performance for Zone III is not as effective as that of Zone I and Zone II. However, the absence of debris flow records in Zone III for the year 2020 implies that this would not affect the accuracy of identifying watersheds prone to debris flows during subsequent model testing for that year.

Table 5-4. Model performance metrics before and after tuning in 3 USC zones

USC Zone	Recall		AUC		Precision		Accuracy	
	Before	After	Before	After	Before	After	Before	After
I (836 samples)	0.883	0.900 (+2%)	0.938	0.952 (+1%)	0.850	0.877 (+3%)	0.862	0.887 (+3%)
II (604 samples)	0.857	0.910 (+5%)	0.941	0.968 (+3%)	0.866	0.905 (+4%)	0.860	0.907 (+5%)
III (46 samples)	0.750	0.800 (+5%)	0.850	0.875 (+3%)	0.783	0.800 (+2%)	0.750	0.775 (+3%)

Focusing on Zone I and Zone II, after hyperparameter tuning, the recall rates for both exceed 0.9, indicating that the models could correctly identify over 90% of the watersheds prone to debris flows. The AUC values for both Zone I and Zone II after tuning are greater than 0.95, reflecting the excellent classification performance of the GBM model for debris flow susceptibility assessment when there is a balance in the number of positive and negative samples. Additionally, the precision and accuracy rates for both regions are around 0.9, which is a

relatively high level, and are also relatively stable, further indicating a comparatively low FP rate for the models.

Employing the same method as used for the SMCRS, the debris flow susceptibility assessment model for the HKSAR was subject to hyperparameter tuning. Similarly, the four model performance metrics were calculated using 10-fold cross-validation, and the changes in these metrics before and after tuning are depicted in Table 5-5.

Table 5-5. Model performance metrics before and after tuning

Metrics	Recall	AUC	Precision	Accuracy
Before tuning	0.836	0.902	0.821	0.826
After tuning	0.849	0.920	0.830	0.837
Increase rate	+1.3%	+1.8%	+0.9%	+1.1%

The results indicate that after hyperparameter tuning, all four model performance metrics for the debris flow susceptibility model are improved, with the most significant increase observed in the recall rate. This enhancement suggests that the model performance, particularly its ability to recognize debris flow samples, is improved after tuning. The AUC reaches 0.92 after tuning, demonstrating the effective classification of grids susceptible to debris flows under a balanced distribution of positive and negative samples. The recall rate increases notably to 0.85 following tuning, indicating that parameter adjustment effectively enhances the capacity of the model to identify debris flow grids, ultimately enabling it to

correctly recognize approximately 85% of those grids. Additionally, the model exhibits precision and accuracy rates above 0.8, indicating a relatively low false alarm rate.

After hyperparameter tuning, the debris flow susceptibility assessment model has been constructed based on the training dataset. However, to assess the generalization ability of the model across different datasets, further tests are required.

5.4 Debris flow susceptibility assessment

Based on the established debris flow susceptibility assessment model, tests were conducted with datasets excluded from the training set to assess the model generalization capability and its accuracy in identifying units with recorded debris flow events. The performance of DWCC, constructed based on predicted values of dry-wet indices, was also tested within the susceptibility assessment model to affirm the stability and reliability of using these characteristics in assessing debris flow susceptibility. The debris flow susceptibilities in different months for two typical study areas were visualized based on the results of the susceptibility model.

5.4.1 Model testing

Model testing carried out based on 29 cases from June to September 2020 ensured the effectiveness and stability of using predicted DWCC for debris flow susceptibility assessment. Initially, the pre-disaster PDSI time series for these watersheds were derived from the ground meteorological monitoring data and characterized as DWCC for application in the model test. Subsequently, the pre-disaster DWCC for these 29 recorded watersheds were calculated based on the one-month ahead forecast data from the PDSI using the SARIMA model outlined in Section 3.2.2, for their application in model testing. A comparison of the test results for DWCC derived from these two different data sources was conducted to explore the effectiveness of using predicted DWCC in the debris flow susceptibility assessment and to validate the stability of applying DWCC in the susceptibility assessment (Table 5-6).

Table 5-6. Testing of susceptibility models based on DWCC in the SMCRS

USC Zone	DWCC Source	Watershed Amount	Number of Successful Identifications	Identification Accuracy
I	From monitoring data	19	17	89.5%
II	From monitoring data	10	10	100%
I	From forecasting data	19	17	89.5%
II	From forecasting data	10	10	100%

The results of the model testing show that for the 29 watersheds with debris flow records in the SMCRS, the accuracy of the debris flow susceptibility assessment

model, based on actual DWCC, reached 93.1%. Specifically, the accuracy for Zone I is 89.5%, while for Zone II is 100%. This indicates that when using actual DWCC, the model could correctly identify most of the watersheds that have experienced debris flows in the SMCRS, and it could perfectly identify all the watersheds with debris flows in areas with larger distances from faults and flatter terrain. Moreover, when predicting the susceptibility of debris flows for the upcoming month using forecasted DWCC, it is found that the use of predicted data will not lead to a decrease in model performance, suggesting that the forecasts of DWCC for the coming month can be applied to predict debris flow susceptibility without significantly reducing the accuracy of identifying watersheds with high debris flow susceptibility. These findings confirm the effectiveness of applying DWCC in debris flow susceptibility assessment.

The comparative results indicate that the debris flow susceptibility model, based on DWCC, demonstrates an excellent classification performance for identifying watersheds with high debris flow susceptibility in the typical inland monsoon region. Moreover, although there are biases in the prediction of DWCC, these biases have an insignificant impact on the model accuracy of identifying susceptible watersheds, suggesting that the DWCC extracted from the PDSI time series through wavelet analysis and multifractal spectrum analysis are relatively stable and less affected by the biases in PDSI prediction.

To further substantiate this discovery, the constructed debris flow susceptibility assessment model was tested using 73 grid samples with recorded debris flows from the HKSAR in 2019. Similarly, the efficacy of the model in recognizing grids with recorded debris flows was tested using DWCC calculated from the monitoring data and those predicted by the SARIMA model, as described in Section 3.2.2. The performance parameters of the model are presented in Table 5-7.

Table 5-7. Testing of susceptibility models based on DWCC in the HKSAR

DWCC Source	Recall	Precision	Accuracy
From monitoring data	0.767	0.949	0.863
From forecasting data	0.767	0.949	0.863

The results, as reflected in the three model performance metrics from the test, reveal that the model has the lowest recall rate at 0.77, while the precision rate is significantly higher at 0.95. This suggests that the model can correctly identify over 75% of the grids with recorded debris flows and rarely misclassifies grids without debris flow records as having high susceptibility. In other words, the model is more prone to underreporting than overreporting debris flow events. Therefore, while substantially reducing the costs associated with false alarms for prevention and mitigation, still necessitates increased attention to areas with lower susceptibility to debris flows. Overall, these results affirm the effectiveness

of the debris flow susceptibility assessment model constructed based on DWCC in typical coastal monsoon areas.

When employing DWCC predicted by the SARIMA model for the debris flow susceptibility assessment, there are no changes observed in recall rate, accuracy rate, or precision rate. This consistency suggests that the predicted DWCC for the forthcoming month have little impact on identifying the debris flow and non-debris flow grids. Therefore, in typical coastal monsoon regions, the debris flow susceptibility assessment model based on DWCC maintains a strong level of stability.

Based on the comparative results from two typical monsoon-affected study areas, it can be concluded that the debris flow susceptibility assessment model, predicated on DWCC, exhibits both effectiveness and stability. The effectiveness is reflected in the high accuracy of the model in identifying units with a very high susceptibility to debris flows in both typical areas, while the stability is demonstrated by the negligible effect of the biases in predicted DWCC on the debris flow susceptibility assessment. The effectiveness and stability of DWCC in debris flow susceptibility assessment enables the forecast of coming debris flows.

5.4.2 Assessment results

Visualizing debris flow susceptibility using real-time or forecasted meteorological data is essential for debris flow early warnings. Referring to the visualization results, regions with higher susceptibility to debris flows can be identified, and debris flow warnings can be issued for areas with a high susceptibility.

Given the effectiveness and stability of using forecast data to construct DWCC for debris flow susceptibility assessment have been verified, the forecast data is not applied for creating debris flow susceptibility maps. Instead, real-time monitoring data was applied to construct DWCC, thereby enabling dynamic assessment of debris flow susceptibility and the visualization of the results.

In the SMCRS in 2020, 29 typical debris flow events were recorded between June and September. Consequently, an assessment and mapping of debris flow susceptibility were conducted for these four months to visualize the susceptibility of all watersheds. Utilizing a debris flow susceptibility assessment model that incorporates DWCC and based on the latest monthly meteorological monitoring station data, the assessment factors related to meteorology and DWCC were updated. This facilitated a dynamic assessment of debris flow susceptibility from June to September 2020, providing a month-by-month susceptibility assessment for each watershed unit within the SMCRS. The susceptibility was classified into five categories, namely very low, low, moderate, high, and very high, using the

Jenks natural breaks, as depicted in Fig. 5-9. The natural breaks method classifies susceptibility by considering the distribution pattern of susceptibility values, ensuring maximum differences between the various categories of debris flow susceptibility.

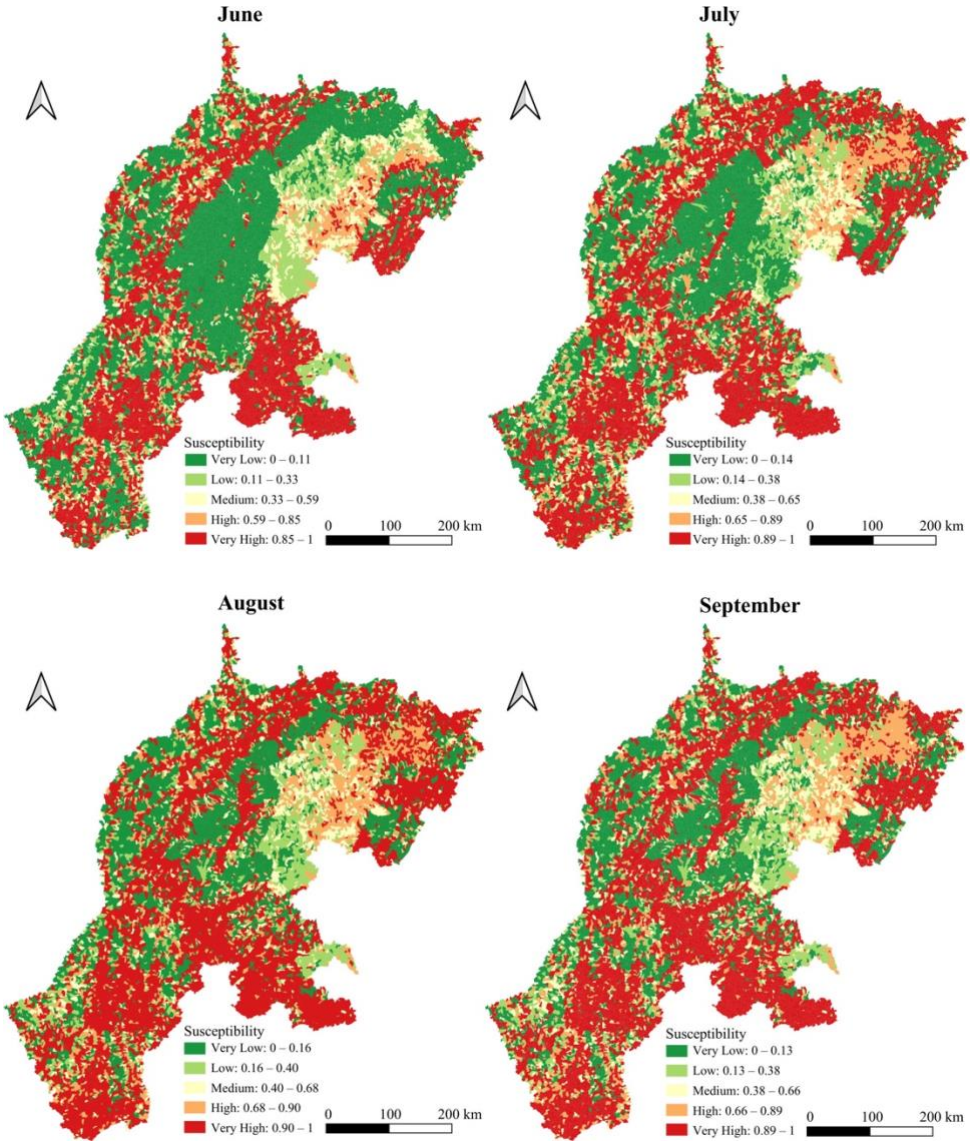

Fig. 5-9. Dynamic debris flow susceptibility mapping in the SMCRS

The results indicate that in the SMCRS, the total area of watersheds with high susceptibility to debris flows exhibited a trend of initial increase followed by a

decrease from June to September, with August identified by the model as having the largest amounts and the total area of watersheds with very high susceptibility. Most of these watersheds are in the Longmenshan fault zone, the surrounding mountain areas of the Sichuan basin, and the Panxi region, which is generally consistent with the spatiotemporal distribution pattern of debris flow susceptibility reflected by the debris flow ARI results. Furthermore, when considering the spatiotemporal patterns of the rainy season precipitation in the SMCRS, it is found that the predicted results of debris flow susceptibility for watersheds based on DWCC largely align with the actual conditions.

Based on the dynamic map of debris flow susceptibility and focusing on the 29 watersheds with typical debris flow records from 2020, it is possible to calculate the proportion of the total area of watersheds within different USC zones that fall into various debris flow susceptibility categories. If the debris flow susceptibility assessment model can classify most of the watersheds with typical debris flow records as very high susceptibility zones, and the total area of these classified watersheds is minimal, then the proposed model demonstrates potential application value for debris flow early warning. A three-dimensional histogram can be drawn with the five debris flow susceptibility levels on the x-axis, the four months with debris flow records on the y-axis, and the total area of watersheds corresponding to each level of debris flow susceptibility for the different months on the z-axis. The color of the bars represents the frequency of debris flows, with

frequencies that can be referred to in the legend, and the results are presented in Fig. 5-10.

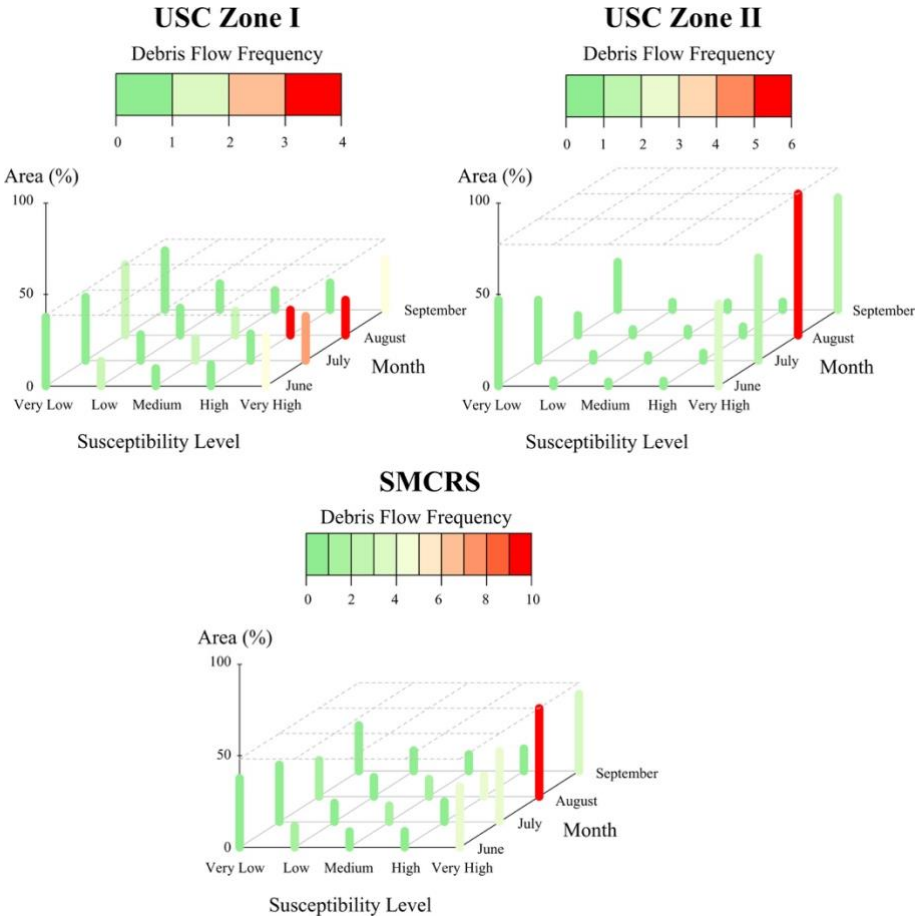

Fig. 5-10. Evaluation of debris flow susceptibility assessments in the SMCRS

The results demonstrate that the majority of the 29 typical debris flow watersheds in the SMCRS for 2020 are identified as having very high susceptibility, highlighting the robust capability of the model to recognize positive samples. However, in Zone I, some watersheds are identified as high susceptibility rather than very high susceptibility in August, suggesting that debris flow prevention policies based on susceptibility assessment maps must consider also certain high-

susceptibility watersheds during months of heavy precipitation, which may increase the cost of implementing debris flow mitigation measures. Similarly, in Zone II regions, most watersheds are identified as having very high susceptibility in August, raising the possibility of false alarms that may also inflate mitigation costs. Overall, the area of very high susceptibility watersheds reaches the largest in August for the SMCRS, yet the case is opposite in the Zone I, potentially due to lower precipitation thresholds resulting from complex terrain, indicating that higher rainfall may not necessarily correlate with higher debris flow susceptibility. This suggests that spatial differences in USC may lead to temporal disparities in debris flow occurrence. For the whole study area in the SMCRS, nearly 50% of the watersheds are classified as having very high debris flow susceptibility, and while this accurately identified most typical debris flow events, the potential false alarm rate may increase the cost of implementing specific mitigation measures. Consequently, while utilizing dynamic debris flow susceptibility assessment results for early warning and guiding mitigation efforts is feasible, the specific complexities of watersheds necessitate the integration of real-time monitoring data from local rain gauges to reduce the cost of potential false alarms.

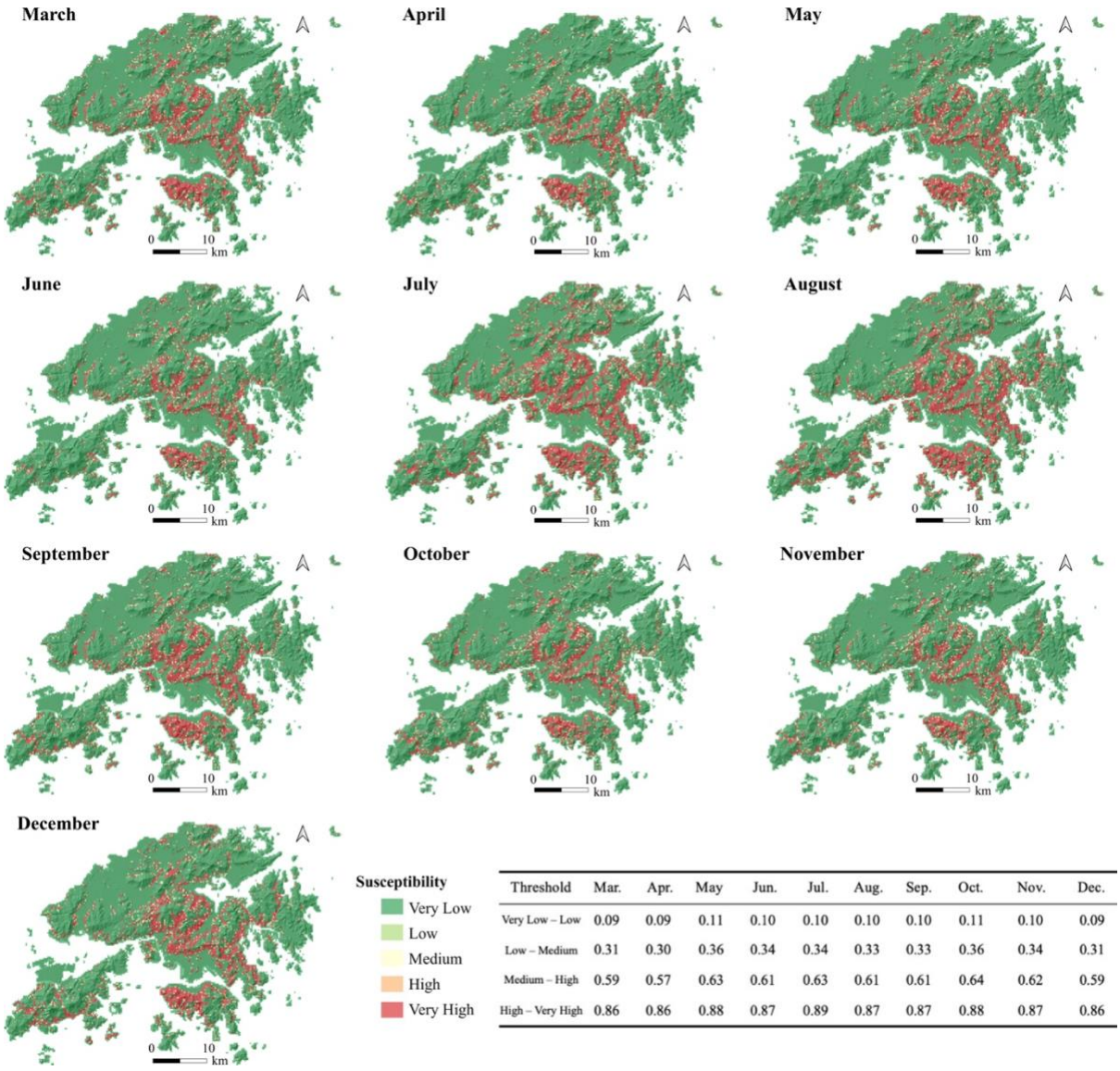

Threshold	Mar.	Apr.	May	Jun.	Jul.	Aug.	Sep.	Oct.	Nov.	Dec.
Very Low – Low	0.09	0.09	0.11	0.10	0.10	0.10	0.10	0.11	0.10	0.09
Low – Medium	0.31	0.30	0.36	0.34	0.34	0.33	0.33	0.36	0.34	0.31
Medium – High	0.59	0.57	0.63	0.61	0.63	0.61	0.61	0.64	0.62	0.59
High – Very High	0.86	0.86	0.88	0.87	0.89	0.87	0.87	0.88	0.87	0.86

Fig. 5-11. Dynamic debris flow susceptibility mapping in the HKSAR

To further confirm the potential application value of the debris flow susceptibility assessment model based on DWCC for regional debris flow early warning, a grid-based visualization of debris flow susceptibility was conducted for the HKSAR. Debris flow records in the HKSAR for the year 2019 span from March to December. Therefore, mapping of debris flow susceptibility on a grid-cell basis was performed for the ten months of 2019 to facilitate the visualization of debris

flow susceptibility in the region. Similarly, the debris flow susceptibility of grid-cell was classified into five categories, very low, low, moderate, high, and very high, using the Jenks natural breaks. By utilizing the monthly updated meteorological monitoring station data from the HKSAR, the latest meteorological data and DWCC were obtained, enabling a dynamic debris flow susceptibility assessment from March to December 2019, as shown in Fig. 5-11.

The results indicate that the total area of high-susceptibility debris flow grids in the HKSAR exhibits a trend of increasing and then decreasing from March to December, with July and August showing the largest area of very high-susceptibility grids. High-susceptibility debris flow grids in the HKSAR are concentrated in mountainous areas, while regions with the densest populations, namely the Kowloon Peninsula and the northern coast of Hong Kong Island, generally exhibit lower debris flow susceptibility. Furthermore, the Hong Kong International Airport, a key infrastructure located in the northern part of Lantau Island, also has very low debris flow susceptibility. These findings are largely consistent with previous studies conducted in Hong Kong (Fuchu et al., 1999; Ko et al., 2016; Ng et al., 2021). In summary, the frequency of debris flow disasters in the HKSAR is closely related to the spatiotemporal distribution of rainfall and predominantly occurs in mountainous regions, yet the threat to human life and property safety is usually relatively low. This reflects the substantial investment

and effective outcomes of slope management efforts in the HKSAR (Cheung, 2021; Kjekstad et al., 2009).

Based on the dynamic map of debris flow susceptibility, utilizing the 73 grids with typical debris flow records from 2019, the proportion of the area of grids with very high debris flow susceptibility can be calculated to reflect the potential value of applying the debris flow susceptibility assessment model based on DWCC to debris flow early warning in the HKSAR. A three-dimensional histogram is constructed also with the five debris flow susceptibility levels on the x-axis, the ten months with debris flow records on the y-axis, and the total area of grids corresponding to the susceptibility levels for different months on the z-axis. The color of the bars represents the frequency of debris flows, with the frequency indicated in the legend, and the results are presented in Fig. 5-12.

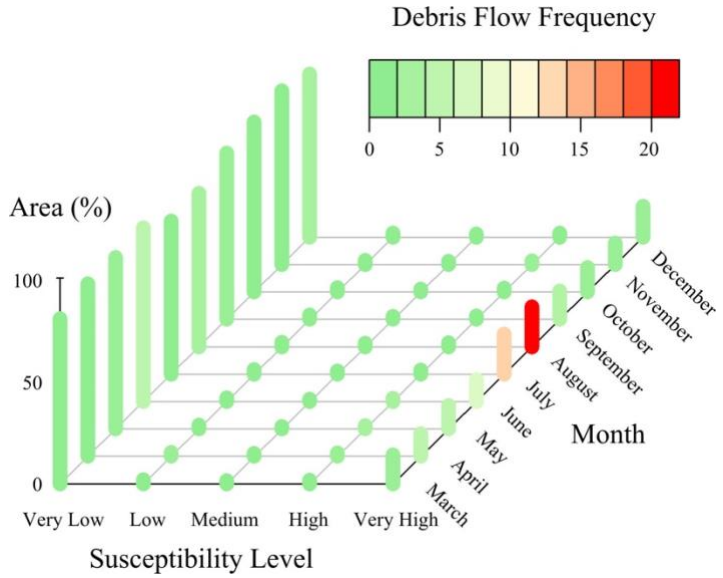

Fig. 5-12. Evaluation of debris flow susceptibility assessments in the HKSAR

The results demonstrate that, for the 73 typical debris flow grids in the HKSAR in 2019, the majority are identified as having very high susceptibility, with the total area of these grids being significantly smaller than that of the grids with very low susceptibility. This indicates that the model possesses a relatively high capability to distinguish both debris flow and non-debris flow samples. The smaller area of grids with very high susceptibility reflects a lower incidence of false alarms for the debris flow susceptibility assessment model in the HKSAR compared to that in the SMCRS. This is primarily due to the smaller assessment units in the HKSAR and a more comprehensive debris flow inventory, which facilitates the accurate construction of debris flow disaster samples. However, the HKSAR model identified 76.7% of the debris flow grids as having very high susceptibility in 2019, which is lower than the 93.1% recognition rate of the model tested in the SMCRS. This discrepancy may be influenced by both the size of the assessment units and the density of the samples. Regarding the assessment units, the HKSAR typically contains grid units with only one debris flow gully as opposed to the watershed units in the SMCRS that may contain multiple debris flow gullies, requiring higher accuracy in the debris flow susceptibility assessment in the HKSAR and hence increasing the difficulty of achieving completely accurate predictions. In terms of sample density, the SMCRS, being larger in area than the HKSAR and with extensive sparsely populated areas, poses greater challenges in comprehensively collecting debris flow disaster records, leading to a lower data density and potentially affecting the performance of the

debris flow susceptibility assessment model. Overall, the results of the dynamic debris flow susceptibility assessment based on DWCC can provide a scientific reference for identifying target areas for slope management in response to extreme weather events in the HKSAR.

Based on the results of the debris flow susceptibility assessment models informed by DWCC for typical inland and coastal monsoon regions, it is evident that the application of DWCC in assessing debris flow susceptibility holds the potential for providing reference information for regional debris flow early warning systems. To further apply the results of debris flow susceptibility assessment to early warning systems, it is necessary to divide the susceptibility maps according to different levels of debris flow susceptibility, particularly targeting high-susceptibility areas, to guide the implementation of necessary disaster prevention and mitigation measures in advance, thereby reducing the casualties and economic losses caused by debris flow occurrences. However, the rate of false alarms (false positive rate) inherent in the DWCC-based debris flow susceptibility assessment model hinders its widespread application, with the issue being more pronounced in inland monsoon regions where debris flow record data density is relatively low. For one thing, although the negative samples in the model are watersheds distant from historical debris flow records, incomplete labeling of positive samples due to unreported debris flow events in the test dataset may still result in positive samples being incorrectly marked as negative,

leading to the inclusion of positive sample characteristics within the negative sample set and thus affecting the classification performance of the model. For another, to ensure the accuracy of the classification, maintaining a balance between positive and negative samples in the training set is necessary, which inevitably leads to undersampling of the negative sample set, potentially resulting in incomplete characteristics labeling of the negative samples. Therefore, differing distributions between training and test datasets may lead to higher false alarm rates during model testing. While false alarm rates are difficult to avoid, they can be mitigated by implementing engineering measures only in assessment units where debris flows pose a threat to the residents or infrastructure, thus reducing the cost of false alarms. Furthermore, since the assessment factor system has not yet considered various prevention measures already implemented in each assessment unit, the impact of these measures on debris flow susceptibility is overlooked, which could lead to an overestimation of local debris flow susceptibility. Therefore, it is also necessary to ensure that the debris flow susceptibility map is integrated with the implementation status of existing local debris flow prevention projects to assess more accurately the susceptibility of local debris flows.

5.5 Summary

In this chapter, a debris flow susceptibility assessment model based on DWCC was developed for watersheds in the SMCRS and grids in the HKSAR, and its potential application value for debris flow early warning was assessed from multiple perspectives:

To mitigate the impact of USC on the debris flow susceptibility assessment, the K-means clustering method was employed to divide the SMCRS into three USC zones based on geological and topographical conditions, and a debris flow susceptibility assessment was conducted for each zone. Owing to the relatively small area, the high data precision, and the low spatial variability, the HKSAR could be modeled directly, ensuring that each model could more accurately extract the characteristics of positive and negative debris flow samples for each study area or zone. Based on the mechanism of debris flow formation and initiation, a preliminary debris flow susceptibility assessment factor system was established, which besides DWCC, also includes geological, topographical, meteorological, vegetation cover, and human activity conditions, with consideration given to the effects of earthquakes in the SMCRS and typhoons in the HKSAR. The performance of the models in classifying positive and negative debris flow samples was measured using model performance metrics such as recall, AUC, precision, and accuracy. A comparative analysis was conducted among representative machine learning algorithms, including the LLR based on

a linear model, the GBM based on decision trees, the KNN based on distance, and the ANN based on neural networks. The analysis revealed that the GBM demonstrated the optimal balance between classification performance and model construction time costs. Consequently, the GBM was selected to construct debris flow susceptibility assessment models for each study area or zone. Different cross-validation methods for the debris flow susceptibility assessment model were compared to determine the optimal ratio of training data to validation data, ensuring the classification performance and generalization ability of the model.

DWCC-based models have effectively promoted the identification accuracy of debris flows by 1.4% - 3.8%. Collinearity detection and relative influence analysis were employed to filter assessment factors for each study area or zone, and models were constructed based on the selected indicators, preliminarily identifying common and unique assessment factors that may affect debris flow susceptibility in each study area or zone. Beyond the DWCC, common factors for both inland and coastal monsoon typical areas included rock type, maximum daily rainfall, human activity, vegetation type, and topographical conditions such as elevation difference, slope, and curvature. However, the inland monsoon typical area required additional consideration of the impact of earthquakes on debris flow susceptibility, while the coastal monsoon area required consideration of the impacts of typhoons and unique vegetation communities like mangroves in the interlaced land-sea zones. The constructed models, after hyperparameter

tuning, showed comprehensive improvements in classification performance on the training datasets, particularly in the correct classification capacity of assessment units with debris flow records, which increased by 1.3 - 5.0%, correctly identifying 80 - 91% of the assessment units with debris flow records. At the same time, by referring to model performance metrics such as accuracy and precision, the models ensured that the rate of false alarms remained at a relatively low level.

To evaluate the generalization ability of the debris flow susceptibility assessment model based on DWCC across different datasets, assessments were conducted using indicators from 29 typical debris flow watersheds in the SMCRS in 2020 and 73 typical debris flow grids in the HKSAR in 2019. The results demonstrate that the assessment model achieved an identification accuracy of 93.1% for the 29 typical debris flow watersheds in the SMCRS in 2020, and an accuracy of 76.7% for the 73 typical debris flow grids in the HKSAR in 2019. The high identification accuracy rates of assessment units with debris flow records in both inland and coastal monsoon typical areas affirmed the effectiveness of using DWCC in debris flow susceptibility assessments. In the two study areas, despite some deviation in the predicted dry-wet indices based on the SARIMA model, the performance metrics of the debris flow susceptibility assessment model remained stable, which demonstrated the reliability of incorporating DWCC in debris flow susceptibility assessments. Overall, the model testing outcomes confirmed the

efficacy and stability of debris flow susceptibility assessments based on DWCC. To further apply climatic dry-wet cycles to the assessment of debris flow susceptibility and provide a scientific reference for regional debris flow early warning in response to extreme weather events, a dynamic debris flow susceptibility assessment based on DWCC was carried out for all assessment units from June to September 2020 in the SMCRS and from March to December 2019 in the HKSAR. Monthly debris flow susceptibility maps for each typical area were subsequently generated. These maps accurately reflected the spatiotemporal patterns of debris flow occurrences in both regions. Spatially, the SMCRS area saw debris flow occurrences concentrated along the Longmenshan fault zone, the surrounding mountainous regions of the Sichuan basin, and the Panxi area, while in the HKSAR, debris flows were concentrated in less densely populated mountainous regions. Temporally, both inland and coastal monsoon areas exhibited the largest total area of assessment units with high susceptibility during the rainy season. The dynamic susceptibility maps for the two regions were assessed for their potential application value in regional debris flow warnings by considering both the classification accuracy of typical debris flow assessment units and the total area of units with very high susceptibility. The results indicated that the DWCC-based model successfully identified the most typical debris flow assessment units as having very high susceptibility in both SMCRS and HKSAR. Consequently, the dynamic susceptibility maps could facilitate the formulation of debris flow prevention and mitigation measures for

watersheds of varying susceptibility levels, aiming to minimize the impacts of debris flow occurrences. However, in the SMCRS, nearly 50% of the assessment units were identified as having very high susceptibility, a proportion significantly larger than that in the HKSAR, suggesting the potential for false alarms in the region. Therefore, when using dynamic susceptibility maps for regional debris flow warnings in the SMCRS, it is necessary to integrate real-time monitoring data from local assessment units to balance life and property safety with cost-effective prevention and mitigation measures.

Chapter 6 Main Drivers of Regional Debris Flow Susceptibility

This chapter interprets the results of the debris flow susceptibility assessment model previously established for the SMCRS and the HKSAR based on the model structure. It prioritizes the assessment factors based on their importance to debris flow susceptibility, thereby identifying the main drivers for assessing debris flow susceptibility. The chapter quantifies the characteristics of debris flow susceptibility in response to variations in these main drivers. By quantifying the impact of each driver on debris flow susceptibility, the results provide targeted and adaptive references for disaster prevention and mitigation for different study areas. A particular focus is placed on comparing the performance of DWCC in the debris flow susceptibility assessments of the two typical regions, to reveal the conditions that influence the applicability of DWCC in regional debris flow susceptibility assessments.

6.1 Identification of main drivers

Quantitative analysis of a GBM model structure helps identify the main drivers of debris flow susceptibility and formulate targeted prevention and mitigation measures. After validating the performance of the DWCC-based debris flow susceptibility assessment model in identifying assessment units with debris flow records, further exploration is carried out to elucidate the contributions of various

assessment factors to debris flow susceptibility. To determine the main drivers for debris flow susceptibility assessments in different typical areas, a quantitative interpretation can be conducted utilizing the structure of a GBM model. Based on the performance of various assessment factors, this approach can assist in the formulation of targeted pre-disaster prevention and mitigation measures for different study areas.

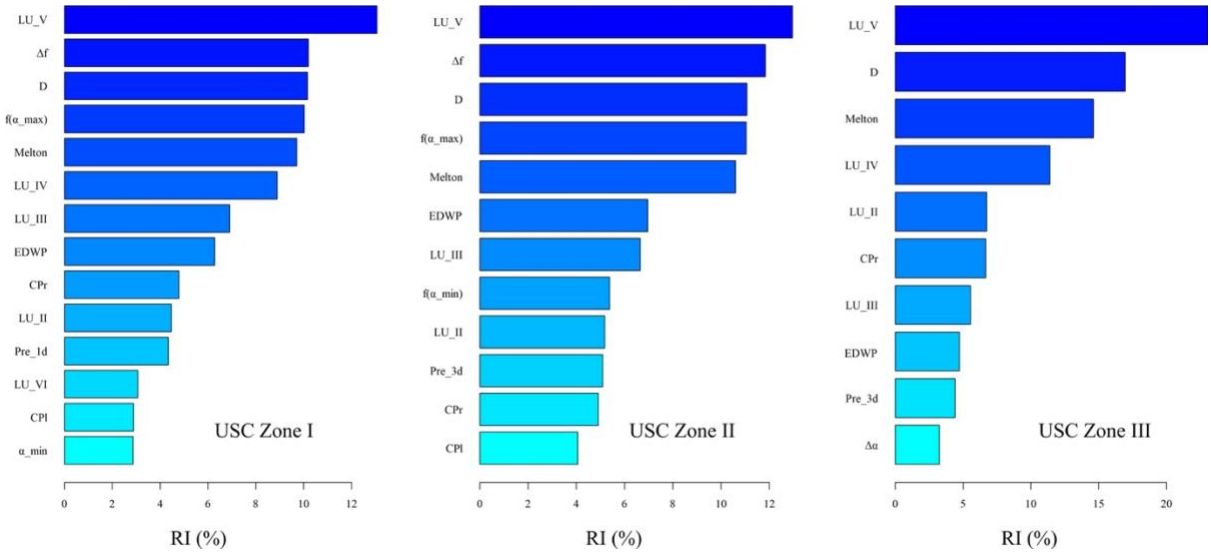

Fig. 6-1. RI of main drives in different USC zones in the SMCRS

For GBM, the RI of assessment factors is calculated by measuring the contribution of different indicators to the improvement of model performance during the node-splitting process in decision tree construction. By employing the GBM model built with the "gbm" package in the R programming language, the RI of assessment factors can be computed using the permutation-based approach, where the sum of the RI of all assessment factors amounts to 100% (Friedman,

2001). To focus on the main drivers affecting debris flow susceptibility, the RI ranking chart will not display indicators with minimal RI. Moreover, it ensures that the total RI of the displayed assessment factors exceeds 95%, which implies that these indicators are considered the main drivers for assessing debris flow susceptibility.

Fig. 6-1 presents the ranking of the RI of main drivers for the debris flow susceptibility model in the SMCRS. In Zone I, there are 14 main drivers, of which four are related to DWCC, including Δf, $f(\alpha_{max})$, EDWP, and α_{min}, with a cumulative RI of 29.37%. There are two factors related to human activities, encompassing the proportion of built-up land area and cropland area, with a cumulative RI of 21.97%. Three factors pertain to vegetation cover, including the proportion of grassland, shrubland, and bare/sparse vegetation land, with a cumulative RI of 14.44%. The RI of the distance to faults is 10.16%, the Melton ratio is 9.71%, and two factors related to topographic curvature, including plan curvature and profile curvature, have a cumulative RI of 7.67%. The maximum daily precipitation contributes an RI of 4.34%. In Zone II, there are 12 main drivers, with four related to DWCC, including Δf, $f(\alpha_{max})$, EDWP, and $f(\alpha_{min})$, accumulating an RI of 35.20%. The proportion of built-up land area has an RI of 12.96%, two factors related to vegetation cover, including grassland and shrubland area proportions, accumulate to 11.83%, the distance to faults is 11.07%, the Melton ratio is 10.60%, two factors related to topographic curvature

accumulate to 8.97%, and the maximum 3-day precipitation has an RI of 5.09%. In Zone III, there are 10 main drivers, with two related to human activity, including the proportion of built-up land area and cropland area, accumulating to 34.47%. The distance to faults has an RI of 16.96%, the Melton ratio is 14.63%, two factors related to vegetation cover, including shrubland and grassland area proportions, accumulate to 12.30%, two related to DWCC, including EDWP and $\Delta\alpha$, accumulate to 7.99%, the profile curvature is 6.67%, and the maximum 3-day precipitation has an RI of 4.41%. Overall, the results indicate that in Zone I and Zone II, DWCC are the most significant category of assessment factors for evaluating debris flow susceptibility.

By comparing the similarities and differences of the main drivers in the three USC zones in the SMCRS, this model interpretation can reveal the distinctive characteristics of assessment factors affecting debris flow susceptibility in regions with different USC. In all three USC zones, the proportion of built-up land area, distance to faults, Melton ratio, grassland area proportion, EDWP, profile curvature, shrubland area proportion, and maximum daily/3-day precipitation are common drivers across the SMCRS. In Zone I and Zone II, the preference for extreme dry-wet events, the probability of extreme drought events, and plan curvature are shared drivers. Bare/sparse vegetation and the severity of extreme precipitation events are unique controlling factors for Zone I, while the probability of extreme precipitation events is unique for Zone II, and the intensity

of extreme dry-wet events is a main driver for Zone III. It is evident that the debris flow susceptibility assessment in all three USC zones of the SMCRS is influenced by human activities, geological activities, and topographic factors such as watershed relief and profile curvature, vegetation cover, EDWP, and maximum daily/3-day precipitation, indicating that all these factors need to be considered when assessing debris flow susceptibility in the entire region. The unique drivers for each USC zone reflect the impact of different geological and topographical conditions on debris flow susceptibility. Different DWCC are included as main drivers for each USC zone, highlighting differences in the probability or severity of extreme dry-wet events across these zones. Moreover, in Zone I, the proportion of bare/sparse vegetation land must also be considered in the assessment, and among the common drivers, the maximum daily/3-day precipitation is specifically the maximum daily precipitation in Zone I. These unique drivers suggest that debris flows in Zone I are likely to occur more frequently in areas with lower vegetation cover and can be triggered by intense rainfall with short duration. These findings provide insights for conducting debris flow mitigation measures in Zone I, such as prioritizing eco-engineering approaches in areas prone to intense rainfall during the rainy season. Similarly, Zone II should focus on mitigating debris flows in areas with a higher probability of extreme precipitation events, while Region III should address debris flow prevention in areas where both extreme dry and wet events are severe.

To further reveal the main drivers of debris flow susceptibility assessment in a typical coastal monsoon region, the same methodology was employed to calculate the RI of the main drivers based on the debris flow susceptibility assessment model for the HKSAR, as depicted in Fig. 6-2.

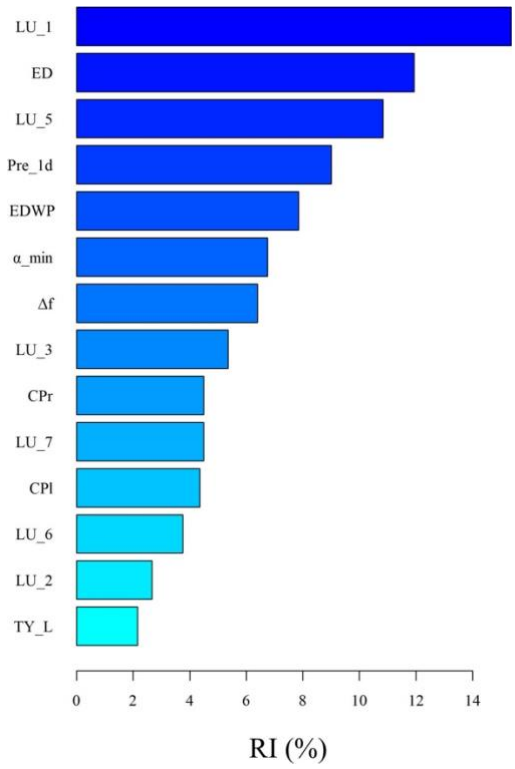

Fig. 6-2. RI of main drives in the HKSAR

The results indicate that there are 14 main drivers for debris flow susceptibility in the HKSAR. Three of these drivers are related to human activities, including the proportion of built-up land area, agricultural land area, and the area of roads/railroads, which collectively contribute 23.39% to the cumulative RI. Three factors are associated with the DWCC, including α_{min}, EDWP, and Δf, with a cumulative RI of 20.99%. Three factors pertain to vegetation cover,

encompassing the proportions of woodland, shrubland, and grassland areas, which together account for 19.08% of the cumulative RI. Elevation differences account for an RI of 11.94%, while the maximum daily precipitation has an RI of 9.01%. Two factors relate to topographic curvature, including plan curvature and profile curvature, with a combined RI of 8.85%. The highest typhoon level has an RI of 2.16%. Overall, the DWCC, aside from human activities, are the most significant class of indicators for predicting debris flow susceptibility in the HKSAR. However, the RI of typhoons is smaller, largely due to only 16.4% of debris flows recorded in the region from 2010 to 2019 coinciding with the period of typhoons, meaning that most recorded debris flows were not related to typhoons. Nonetheless, this does not imply that typhoons have a negligible impact on debris flows. According to estimates based on the volume of debris flow collapses published by the Civil Engineering and Development Department of the HKSAR from 2010 to 2019, it was shown that the scale of debris flows in the HKSAR increased by about 40% under the influence of typhoons.

By comparing the main drivers of the debris flow susceptibility assessment models between the SMCRS and the HKSAR, common and unique factors that affect the debris flow susceptibility assessment in typical inland and coastal monsoon areas can be revealed. Common main drivers shared by both regions include the proportion of built-up land area, preference for extreme dry-wet events, elevation differences, the proportion of agricultural land area, the

proportion of grassland area, EDWP, topographic curvature, the proportion of shrubland area, maximum daily rainfall, and severity of extreme precipitation events. Among these, the main drivers in the HKSAR show the closest resemblance to those of Zone I areas in the SMCRS, with 11 common factors identified. However, the model in the HKSAR still possesses unique main drivers, including the proportion of woodland and the highest typhoon level, whereas the model in the SMCRS includes unique factors such as distance to faults, the probability of extreme drought events, and areas of bare/sparse vegetation land. The common drivers stress that in both typical inland and coastal monsoon areas, factors such as elevation differences, curvature, human activities, vegetation cover, maximum daily rainfall, and the EDWP are universal indicators influencing the debris flow susceptibility assessments. The unique main controlling factors highlight that for debris flow prevention, the regions in the SMCRS should consider frequent geological activity, high incidence of extreme drought events, and less vegetation cover, while the areas significantly affected by typhoons in the HKSAR should be focused on, without neglecting the well-vegetated coastal areas.

Although the RI of the main drivers enabled the identification of the primary influences on debris flow susceptibility in both typical inland and coastal monsoon regions, a quantitative analysis of how these drivers act upon the debris flow susceptibility required further investigation.

6.2 Features of main drivers

Partial dependence (PD) plots can elucidate the mechanisms of how the main drivers influence the debris flow susceptibility and provide targeted disaster prevention and mitigation measures that are more aligned with regional characteristics. These plots are derived by assessing debris flow susceptibility corresponding to different values of a single main driver while keeping other assessment factors constant. PD quantifies the relationship between a single assessment factor and debris flow susceptibility. PD plot in this study indicates how the debris flow susceptibility varies with one single main driver reflecting the DWCC, meteorology, human activity, vegetation cover, terrain, and geology. Upon constructing a GBM model with the R programming language, PD plots for assessment factors can be generated using the "pdp" package. For the three USC zones in the SMCRS, PD plots are separately drawn for each zone, with the results presented in Fig. 6-3, Fig. 6-4, and Fig. 6-5, respectively.

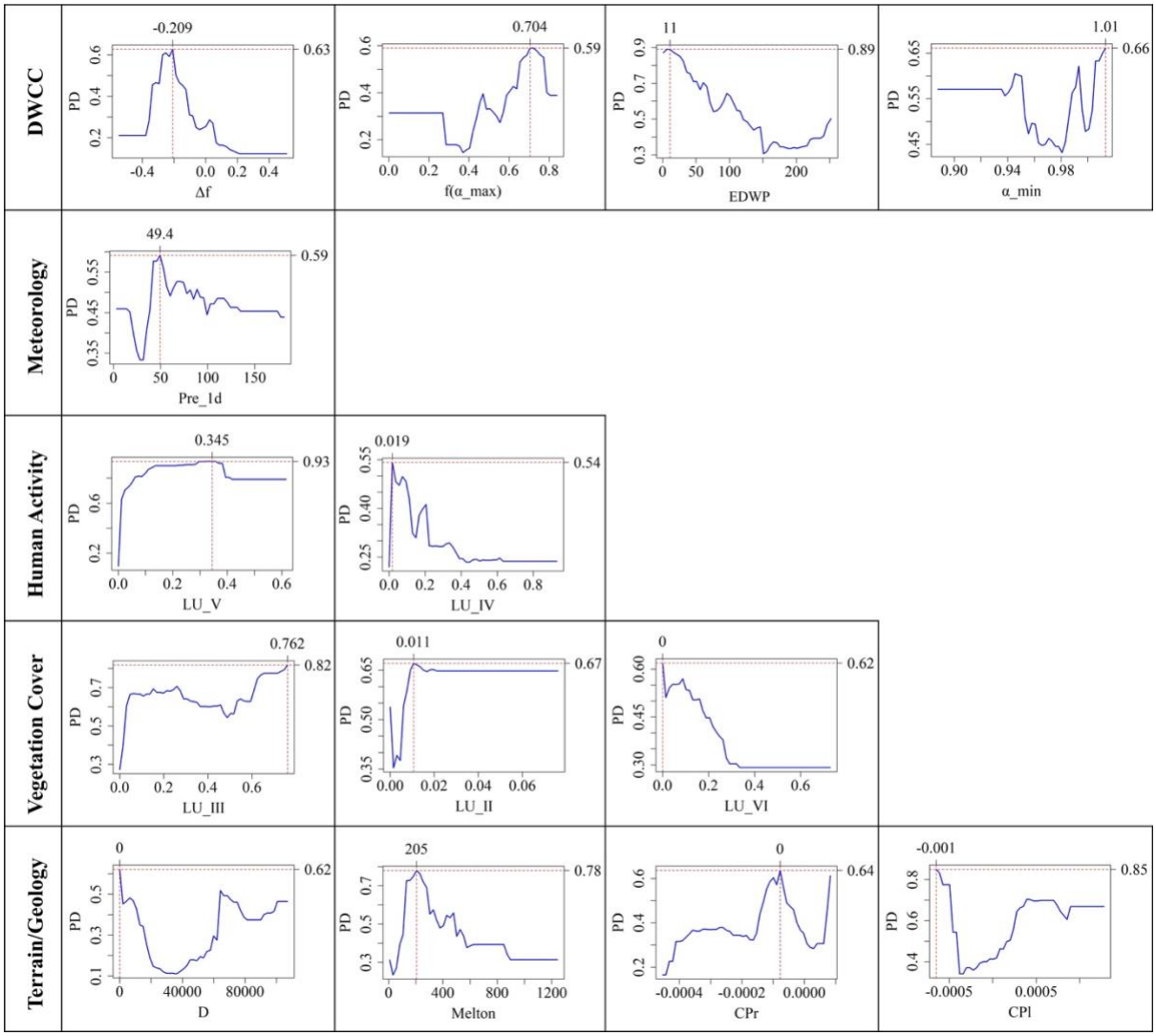

Fig. 6-3. Partial dependence plot for main drivers in Zone I of the SMCRS

Based on the results of the PD plots for DWCC and meteorological assessment factors, in Zone I, the PD value of debris flow susceptibility concerning EDWP is 0.89, indicating a strong correlation between debris flow susceptibility and the dry-wet cycle period. The PD value increases when the EDWP is shorter, Δf is slightly less than zero, and f(α_{max}) is larger, suggesting that a shorter dry-wet cycle period with a preference for a higher probability of extreme drought events is

associated with higher debris flow susceptibility. A larger α_{min} correlates with a larger PD value, implying that the milder the extreme precipitation event, the higher the susceptibility to debris flows. This observation is consistent with the PD plot results for maximum daily precipitation, where the PD peaks at a maximum daily precipitation of 49.4 mm, corresponding to the highest debris flow susceptibility. Furthermore, as the maximum daily precipitation increases beyond this value, the PD value decreases, indicating a reduction in debris flow susceptibility.

According to the results of PD plots for land use types, specifically human activities and vegetation cover assessment factors, in Zone I, the maximum PD value of debris flow susceptibility about the proportion of built-up land within a watershed reaches 0.93. Moreover, debris flow susceptibility generally increases with an increased proportion of built-up land, grassland, and shrubland areas, indicating that regions with larger areas of built-up land, grassland, and shrubland are more susceptible to debris flows. The PD value is maximized when the proportion of cropland in a watershed is 1.9% and there are no bare/sparse vegetation areas. However, as the proportion of cropland and bare/sparse vegetation areas increases, the PD value decreases, suggesting that regions with larger areas of cropland and bare/sparse vegetation land are, in fact, less susceptible to debris flows.

According to the results of PD plots for topographic and geological assessment factors in Zone I, the maximum PD values for various factors all exceed 0.6, indicating a strong correlation between topographic/geological conditions and debris flow susceptibility. From a geological structure perspective, watersheds with faults exhibit the highest PD values and thus the greatest susceptibility to debris flows. Additionally, watersheds located at a certain distance from faults (i.e., approximately 60 km) also display higher PD values and are more susceptible to debris flows. The PD value increases and then decreases with the Melton ratio, suggesting that terrains that are either too flat (i.e., with a low Melton ratio) or too steep (i.e., with a high Melton ratio) have lower susceptibility to debris flows. The PD values reach their maximum when the profile curvature and plan curvature are slightly less than or greater than zero, indicating that slopes with a slight convexity or concavity along the direction of the maximum gradient or perpendicular to it are more susceptible to debris flows.

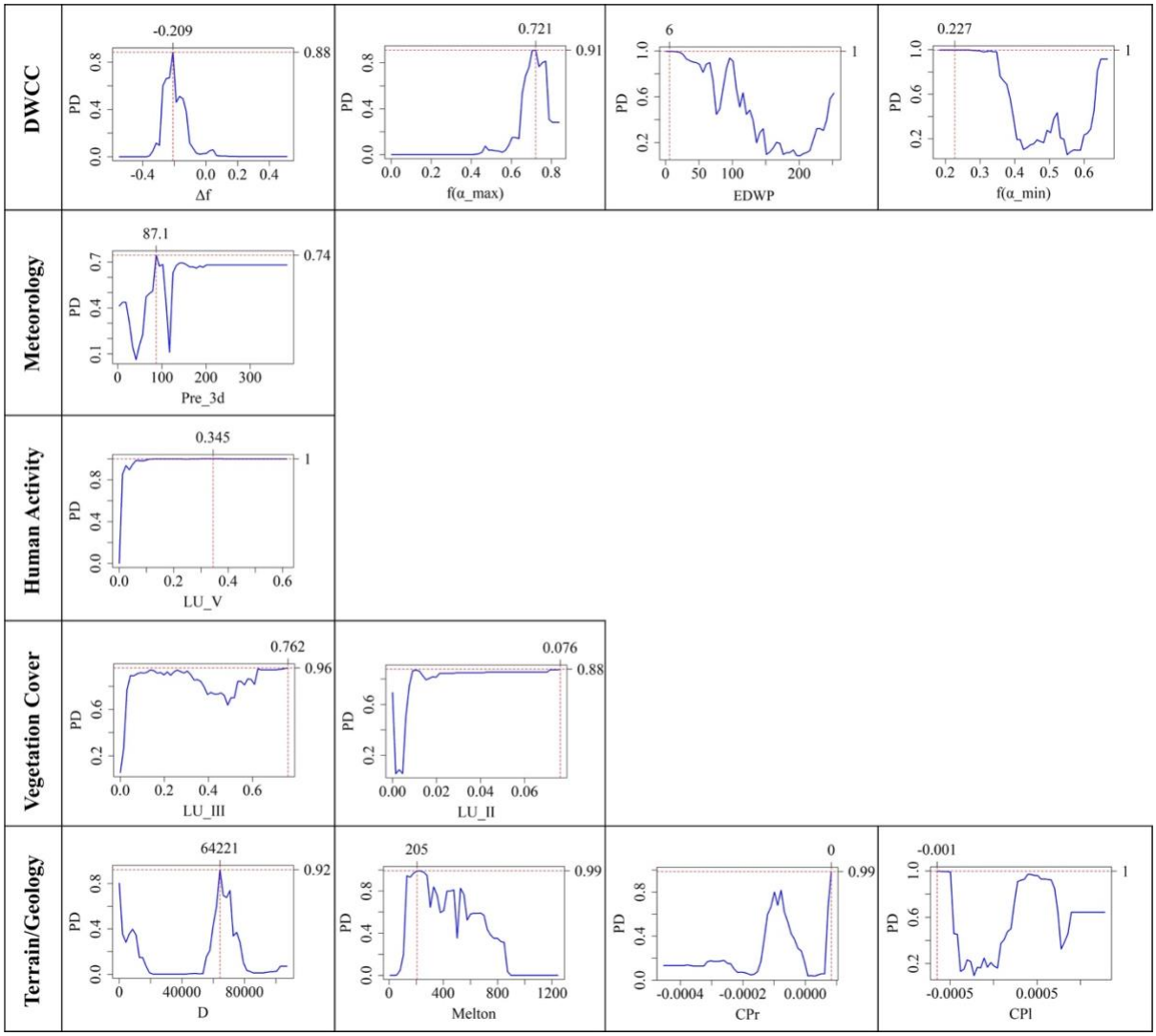

Fig. 6-4. Partial dependence plot for main drivers in Zone II of the SMCRS

According to the results of PD plots for DWCC and meteorological assessment factors in Zone II, the maximum PD values for debris flow susceptibility about the DWCC factors all exceed 0.85, indicating a very strong correlation between debris flow susceptibility and DWCC. Similar to Zone I, in Zone II, the PD value increases with shorter EDWP, slightly negative Δf, and larger f(α_{max}), suggesting that a greater probability of extreme drought events, which are slightly more

probable than extreme precipitation events, correlates with higher debris flow susceptibility. However, differing from Zone I, a larger PD value occurs when $f(\alpha_{min})$ is either small or large, implying that a moderate frequency of extreme precipitation events can reduce the susceptibility to debris flows. The extreme precipitation quantity can be indicated by the maximum 3-day precipitation, where a PD peak occurs at 87.1 mm, corresponding to the highest debris flow susceptibility.

Based on the PD plots analyzing the proportion of land use types, which encompass human activity and vegetation cover assessment factors in Zone II, the maximum PD value for debris flow susceptibility concerning the proportion of built-up land within a watershed reaches 1. Additionally, there is an overall increasing trend in the PD values as the area proportions of built-up land, shrubland, and grassland within the watershed increase. This trend indicates that, similar to Zone I, watersheds with larger proportions of built-up land, shrubland, and grassland are more susceptible to debris flows.

In Zone II, according to the PD plots for topographic and geological assessment factors, the maximum PD values for correlations with debris flow susceptibility are all greater than 0.9, indicating an extremely strong relationship between topographic and geological conditions and debris flow susceptibility. Similar to Zone I, the PD values in Zone II also increase and then decrease with the Melton ratio, suggesting that terrains that are either too flat (with a low Melton ratio) or

too steep (with a high Melton ratio) are less prone to debris flows. Geologically, in Zone II, watersheds with faults show high PD values, with the maximum PD value occurring at a distance of 64 km from a fault, corresponding to the highest debris flow susceptibility. Additionally, in Zone II, the PD values reach maximal points when the profile curvature and plan curvature are slightly greater than or less than zero, indicating that slopes with slight convexity or concavity, either along or perpendicular to the direction of the maximum gradient, have a higher susceptibility to debris flows.

The results depicted in Fig. 6-5 indicate that in Zone III, the PD values for all assessment factors related to debris flow susceptibility are generally low, with the maximum value being 0.64. This suggests that the main drivers in Zone III have a weak correlation with debris flow susceptibility, which could impact the accuracy of susceptibility assessments in these areas. This phenomenon might be attributed to the limited number of samples from Zone III, as evidenced by the scant historical record of debris flows (i.e., only 23 incidents recorded from 1981 to 2019). Consequently, when further interpreting the contribution of main drivers to debris flow susceptibility, the focus should be directed more toward Zone I and Zone II. However, it should be noted that some findings in Zone III are consistent with those in Zone I and Zone II, such as higher debris flow susceptibility in watersheds that have shorter EDWP, larger proportions of built-up land, grassland, and shrubland, and relatively flat terrain.

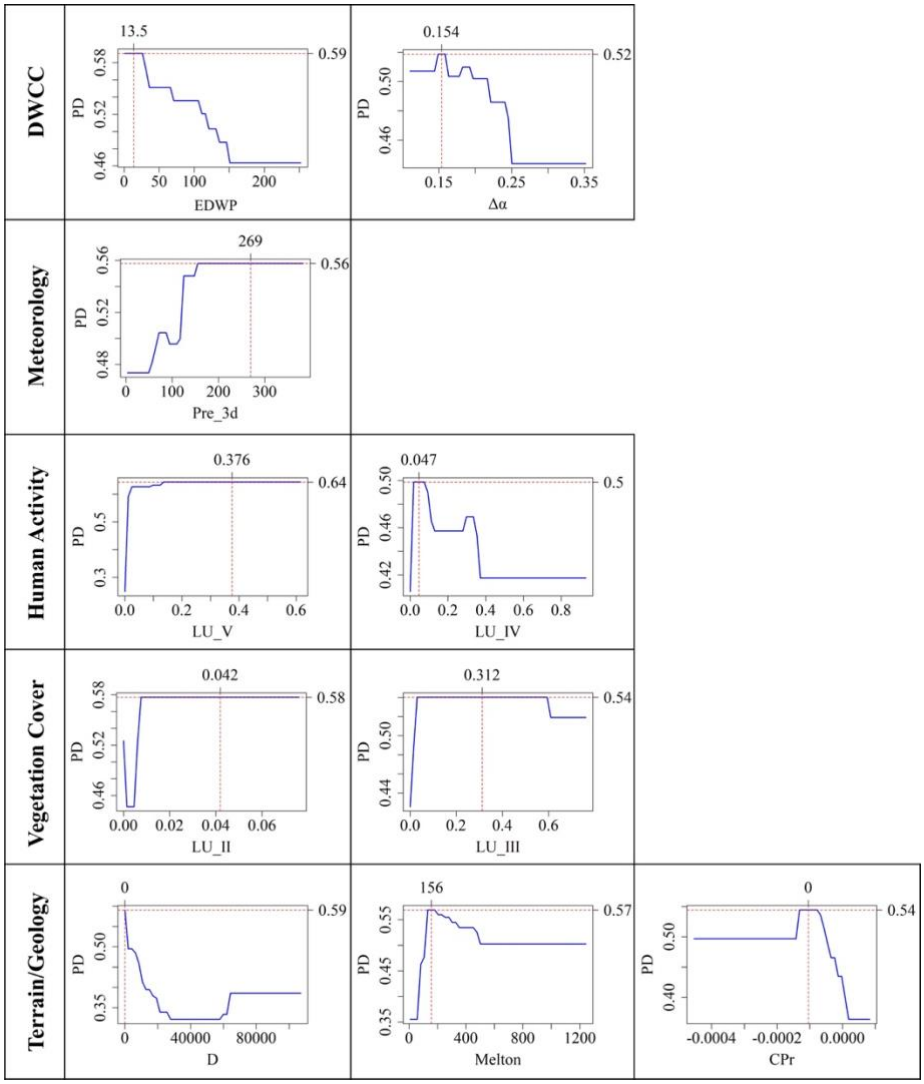

Fig. 6-5. Partial dependence plot for main drivers in Zone III of SMCRS

By comparing the PD plot results for different USC zones within the SMCRS, which include DWCC, meteorological, human activities, vegetation coverage, and topographical and geological assessment factors, the characteristics of how various assessment factors influence debris flow susceptibility in different USC zones were disclosed. The objective is to clarify the characteristics of debris flow susceptibility variations by examining the influence of each assessment factor

across distinct environments, thereby providing an understanding of the assessment factors contributing to debris flow susceptibility in a region characterized by complex climatic and physical geographic conditions.

Based on the assessment factors related to DWCC and meteorology, the results indicate that in Zone I and Zone II, watersheds with a higher probability of extreme drought events, surpassing the probability of extreme precipitation events, are more susceptible to debris flows. This highlights the significant role of extreme drought in the formation and initiation of debris flows. In Zone I, severe extreme precipitation events contribute substantially to debris flow susceptibility, while in Zone II, both high and low probabilities of extreme precipitation events have a notable contribution, suggesting that the triggering of debris flows in Zone I regions is associated with short-duration, high-intensity rainfall, whereas in Zone II regions, the triggers may not be limited to intense rainfall with short duration but could also include prolonged periods of lower intensity rainfall. This inference is supported by PD plots for the maximum daily (3-day) precipitation amount and debris flow susceptibility, where the precipitation thresholds related the most to trigger debris flows in watersheds of Zone I and Zone II are 49.4 mm (1-day) and 87.1 mm (3-day), respectively. Thus, extreme precipitation characteristics triggering debris flows in Zone I are short-duration heavy rainfall, whereas in Zone II, they are longer-duration, more frequent rainfall. Considering the USC of Zone I and Zone II, it can be reasonably

inferred that in areas with more intense geological activity and steeper terrain, due to the relatively lower ability of the surface to intercept water flows, debris flows are more easily triggered by short-duration heavy rains. In contrast, in areas with milder geological activity and flatter terrain, prolonged precipitation is required to achieve saturation of the surface soil, which then triggers debris flows.

The results based on human activity assessment factors demonstrate that human activities significantly influence debris flow susceptibility. Land use types representing human activities, such as built-up land and cropland, show that in Zone I, a larger proportion of cropland correlates with lower debris flow susceptibility. This can be interpreted as most watersheds in Zone I being steep and generally unsuitable for agriculture, while those suitable for agriculture tend to have relatively flatter terrain, thus being less prone to debris flows. However, in both Zone I and Zone II, an increase in the proportion of built-up land is associated with higher debris flow susceptibility. This phenomenon can be understood from two perspectives. First, large-scale construction activities may increase the source materials on slopes, thereby raising the susceptibility to debris flows. Second, historical records of debris flows tend to focus on areas affecting human settlements, including houses, roads, and various infrastructures, leading to a higher incidence of recorded debris flow events in watersheds within built-up land, thus amplifying the perceived contribution of built-up land to debris flow susceptibility.

The results from the assessment factors of vegetation cover indicate that, in both Zone I and Zone II, the influence of shrubland and grassland cover on debris flow susceptibility is essentially consistent. The larger the proportion of shrubland and grassland area, the higher the debris flow susceptibility. This suggests that although vegetation can stabilize the material on slopes (Sujatha et al., 2017), the growth process of vegetation can also generate debris flow materials such as sandy soil, silt, and clay (Fan et al., 2018; Neave et al., 2001). Moreover, the soil water retention capacity of vegetation types such as shrublands and grasslands is relatively weaker compared to woodland (Zhang et al., 2021), making them more prone to debris flows under heavy rainfall conditions. Consequently, watersheds with a larger proportion of shrubland and grassland are at a higher susceptibility to debris flows. In Zone I, where watersheds are relatively steeper, the force of gravity plays a more intense role in the erosion process on slopes. This results in bare/sparse vegetation land that is less capable of accumulating substantial loose materials, thus oppositely reducing the likelihood of large-scale debris flow events.

Results from the assessment of topographic and geologic factors reveal that in both Zone I and Zone II, watersheds with moderate slopes, located at a certain distance from faults and exhibiting slight concave or convex terrain, exhibit a higher susceptibility to debris flows. Moderate slopes in watersheds are more likely to trigger debris flows because excessively steep slopes may not

accumulate sufficient debris flow materials, while too flat slopes may not provide enough potential energy for debris flow movement (Hai et al., 2023). The distance to faults typically indicates more frequent geological activity, which facilitates the formation of the materials needed for debris flows. However, high debris flow susceptibility at certain distances from faults cannot be solely explained by the intensity of geological activity. Although geological activity may be less frequent at these distances, other factors such as increased human activity could contribute to debris flow susceptibility. The slight convex surface along the direction of maximum gradient descent is relatively less stable, with material on convex surfaces being more prone to slippage during heavy rainfall, leading to debris flows. Slight concave surfaces along the direction of maximum gradient descent are also susceptible to debris flows due to their capacity to accumulate and retain more loose materials. When the surface is slightly concave or convex perpendicular to the direction of maximum gradient descent (i.e., horizontal direction), debris flows are likely to occur, but the two conditions affect the debris flow process differently. Horizontal convex surfaces cause debris flows to diverge and form larger-scale debris flow events, while horizontal concave surfaces accelerate the convergence of debris flows to make them more destructive (Achour et al., 2018).

To further elucidate the impact of main drivers on debris flow susceptibility in typical coastal monsoon regions and to clarify the characteristics of debris flow

susceptibility variations, PD plots for debris flow susceptibility assessment factors were constructed also for the HKSAR, as illustrated in Fig. 6-6.

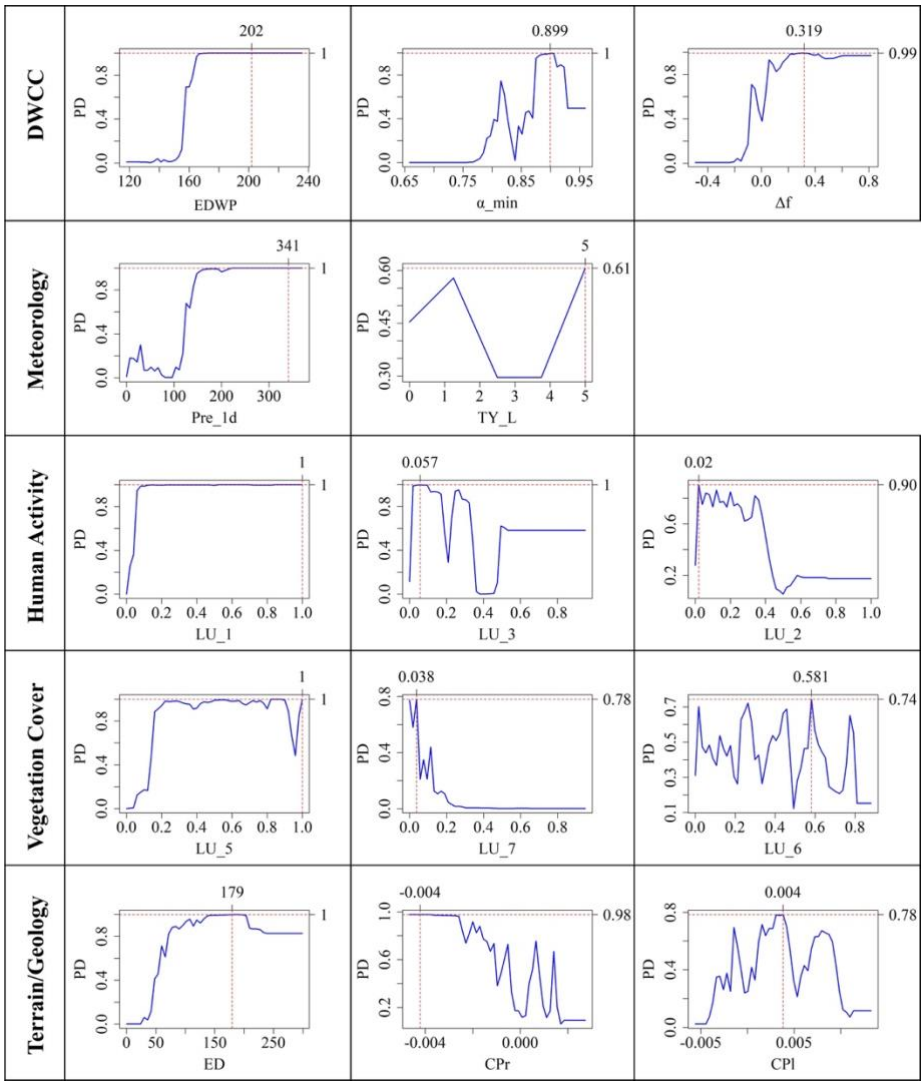

Fig. 6-6. Partial dependence plot for main drivers in the HKSAR

According to the results of PD plots based on DWCC, the susceptibility to debris flows has a strong correlation with both the maximum daily precipitation and the maximum PD value of the DWCC, both exceeding 0.95. This indicates a very strong correlation between debris flow susceptibility and DWCC. Higher PD

values are observed when the EDWP is longer, Δf is slightly greater than 0, and α_{min} is moderate. This suggests that longer dry-wet cycles, a slightly higher probability of extreme precipitation events than extreme drought events, and moderate intensity of extreme precipitation events are associated with increased debris flow susceptibility. The PD plot for DWCC reflects the pattern of how extreme dry-wet conditions affect debris flow susceptibility, indicating that the longer the HKSAR experiences dry-wet cycles and the longer it is subjected to medium-intensity extreme precipitation conditions, the higher the likelihood of triggering debris flow events. This phenomenon implies that the region requires longer dry-wet cycle periods to accumulate sufficient source materials for debris flows, which can then be triggered by extreme precipitation events.

Based on the results of PD plots from the meteorological assessment factors, there is a very strong correlation between debris flow susceptibility and the maximum daily precipitation, with the maximum PD value exceeding 0.95. This suggests that higher maximum daily precipitation is associated with larger PD values, indicating that greater amounts of daily rainfall are more likely to trigger debris flow events. The maximum PD value corresponding to the highest typhoon intensity is only 0.62, and it peaks when the typhoon reaches the highest level of 5, which is when the typhoon is at its strongest, correlating with increased debris flow susceptibility. The PD plots suggest a certain consistency in the impact patterns of the highest level of typhoons and maximum daily precipitation on

debris flow susceptibility. This consistency arises since typhoons carry a significant amount of moisture from the ocean during their formation and landfall. As this moisture encounters the complex terrain of the land, it lifts and cools, leading to intense localized rainfall. The more severe the typhoon, the more moisture it transports from the ocean, resulting in greater precipitation amounts.

According to the results of PD plots for human activity assessment factors, the maximum PD values for the proportion of built-up land, roads/railways, and agricultural land all exceed 0.9, indicating a high degree of correlation between human activities and the susceptibility to debris flows. Specifically, a greater proportion of built-up land is associated with higher debris flow susceptibility, which may be related to the majority of reported debris flow incidents occurring in areas with dense construction. The PD values increase and then decrease with the proportion of roads/railways and agricultural land, suggesting that regions with less development of roads/railways and agricultural land exhibit higher susceptibility to debris flows, which decreases as the developed area increases. This phenomenon can be attributed to the high population density and limited land resources of the HKSAR, which necessitates intensive development of slopes to increase land use efficiency, accompanied by substantial efforts in slope protection and management. The PD plot findings indicate that in the HKSAR, human activities have increased the susceptibility to debris flows, with regions of frequent construction activity being more prone to debris flows compared to those

with more agricultural activity. This is due to agricultural land typically requiring flatter terrain, while construction activities on slopes like hillsides contribute to the accumulation of slope materials, thereby increasing the debris flow susceptibility.

According to the results from PD plots of the vegetation cover assessment factors, the maximum PD values for the proportion of shrubland and woodland area both exceed the level of 0.95. A larger proportion of woodland corresponds to a higher PD value, and the PD value is maximized with a moderate proportion of shrubland, indicating the highest susceptibility to debris flows. Conversely, a smaller proportion of grassland area results in a higher PD value, and thus, greater susceptibility to debris flows. Among the different types of vegetation cover, areas with a larger proportion of woodland have higher susceptibility to debris flows, whereas areas with higher proportions of shrubland and grassland show lower susceptibility. Although woodlands with higher vegetation cover provide greater slope stability and soil water retention compared to shrublands and grasslands, woodlands possess more transportable underlying materials, such as debris, trees, and rocks. Particularly after woodlands are damaged by typhoons, not only do they generate more debris flow material than shrublands and grasslands, but the reduced retention capacity to water flows also leads to a dramatic increase in runoff, which in turn transports the generated material, forming debris flows.

Based on the results from the PD plots for topographic and geological assessment factors, the maximum PD values for susceptibility to debris flows reach 0.95 with maximum elevation difference and profile curvature, indicating an extremely strong correlation between debris flow susceptibility and both elevation difference and profile curvature. The susceptibility to debris flows is highest at a medium elevation difference, specifically an elevation difference of 179 m within a 250 m grid cell, corresponding to an approximate slope angle of 35.6°. This finding is consistent with previous research in the HKSAR, where most debris flows occur on slopes between 30° and 40°. This is due to slopes that are too flat lacking the necessary conditions to convert the potential energy of loose materials into kinetic energy, while slopes that are too steep are mostly composed of rock with no loose material cover, and thus slopes with higher rock strength have a lower likelihood of debris flow occurrence (Fuchu et al., 1999). A profile curvature less than 0 correlates with a higher PD value and increased debris flow susceptibility, suggesting that surfaces convex in the direction of the maximum slope gradient are more prone to debris flow occurrences due to relatively lower slope stability and the ease with which loose materials can slide under heavy rainfall. Plan curvature values slightly greater than or less than 0 also correspond to maximum PD values, indicating high susceptibility to debris flows on surfaces that are slightly convex or concave perpendicular to the direction of the maximum slope gradient. However, when the surface is concave in the horizontal direction, debris flows are likely to accelerate and converge, increasing their destructive

potential, whereas when the surface is convex in the horizontal direction, the debris flow disperses in different directions, potentially forming larger-scale debris flows.

By contrasting the PD plots of the main drivers in debris flow susceptibility assessment models between the SMCRS (focusing on Zone I and Zone II) and the HKSAR, it is possible to elucidate the mechanisms by which various assessment factors affect debris flow susceptibility in typical inland and coastal monsoon areas. This comparative analysis can clarify the characteristics of changes in debris flow susceptibility across different geographic and climatic contexts. Such an approach not only contributes to a deeper understanding of the regional variation in factors influencing debris flow susceptibility but also aids in refining the predictive accuracy of susceptibility models by accounting for the distinct environmental and meteorological conditions inherent to inland versus coastal monsoon regions.

The findings based on the DWCC suggest that in the HKSAR, a longer duration of dry-wet cycles, coupled with a higher probability of extreme precipitation events compared to extreme droughts, is associated with increased susceptibility to debris flows. This relationship is in contrast to that observed in the SMCRS. These results indicate that, unlike typical inland monsoon areas, coastal monsoon regions may require longer dry-wet cycle periods to accumulate the necessary materials for debris flow occurrences due to the relative scarcity of extreme

drought events. Consequently, the occurrence of debris flows in coastal monsoon areas is more dependent on frequent extreme precipitation events. In line with the SMCRS, the severity of extreme precipitation events in the HKSAR also correlates with higher debris flow susceptibility. This highlights that intense rainfall is a significant factor in the increased susceptibility to debris flows in both inland and coastal monsoon typical areas.

Results derived from meteorological assessment factors demonstrate that in the HKSAR, debris flow susceptibility peaks when the maximum daily precipitation exceeds 150 mm. This threshold is significantly higher compared to the maximum rainfall required to trigger debris flows in Zone I of the SMCRS at 49.4 mm over a single day, and Zone II of the SMCRS at 87.1 mm over three days. This disparity suggests that typical coastal monsoon regions, such as the HKSAR, necessitate a higher rainfall threshold for the initiation of debris flows. Additionally, coastal monsoon areas are also influenced by typhoons, with the debris flow susceptibility reaching its peak when typhoon intensity is at its highest, stressing the substantial impact of severe tropical cyclones on the incidence of such geohazards in these regions.

Results based on human activity assessment factors indicate that human activities significantly impact debris flow susceptibility in both the HKSAR and the SMCRS. A higher proportion of built-up land correlates with increased susceptibility to debris flows, while a larger proportion of agricultural land is

associated with lower susceptibility. Additionally, a greater coverage of roads and highways contributes to reduced susceptibility to debris flows. These findings suggest that, in both typical inland and coastal monsoon areas, construction activities generally lead to higher debris flow susceptibility. Specifically, in the HKSAR, the construction of roads and highways, similarly to the siting of agricultural lands, tends to occur in relatively flat terrain areas, thereby decreasing the susceptibility to debris flows.

Based on the assessment factors for vegetation cover, the results reveal that in contrast to the SMCRS, debris flow susceptibility in the HKSAR does not increase with a higher proportion of shrubland and grassland areas but does increase with an increased proportion of woodland areas. This result may be related to the distinct DWCC and typhoon factors prevalent in the HKSAR. Shrublands and grasslands are unable to provide sufficient material for debris flows through frequent dry-wet cycles, whereas woodlands, despite their greater soil and water conservation capabilities, also contain more sources of debris flow source materials. Especially during typhoon landfalls, the transport and accumulation of source materials such as broken branches and rocks contribute to the loose materials required for debris flows. Consequently, in the coastal monsoon typical areas, the influence of typhoons results in higher debris flow susceptibility in woodland areas compared to shrublands and grasslands.

According to the assessment factors of topography and geology, the results show that consistent with the SMCRS, the HKSAR exhibits higher susceptibility to debris flows in areas with moderate slopes. This is due to excessively steep slopes being less capable of accumulating the materials necessary for debris flow occurrences, and in the HKSAR, steeper slopes are usually composed of rocks of greater strength, which limits material accumulation (Fuchu et al., 1999). Conversely, slopes that are too flat cannot provide sufficient potential energy for the transfer of debris flow source materials. The relationship between debris flow susceptibility and profile curvature in the HKSAR mirrors that seen in Zone I of the SMCRS. The highest susceptibility is associated with profile curvatures less than zero, meaning that convex slopes in the direction of maximum gradient descent are more prone to debris flows. The relationship between plan curvature and debris flow susceptibility in the HKSAR is also similar to that in the SMCRS, with higher susceptibility slightly above or below zero, indicating that slopes that are slightly convex or slightly concave perpendicular to the direction of maximum gradient descent are more susceptible to debris flows.

The comparison of the PD plots for the main drivers across inland and coastal monsoon typical regions reveals that the latter is more significantly influenced by extreme precipitation events than the inland monsoon regions. In coastal monsoon areas, typhoons contribute to debris flow susceptibility by damaging vegetation and creating substantial material sources, a process that bears certain

similarities to the influence of earthquakes in inland monsoon regions. Besides, typhoons also intensify extreme precipitation, leading to more severe extreme rainfall events and triggering debris flows.

However, the analysis based on PD plots also has limitations, as using a single factor to explain the influence on debris flow susceptibility is not comprehensive. This is due to the interactions that exist between multiple assessment factors, such as the potential correlation of greater distances to faults with other indicators like human activities. This correlation may arise as the siting of human settlements often considers the impact of geological activities. Such interactions between factors can affect the analysis results of individual factors and the performance of various factors, leading to inconsistencies in the PD results for the same factor across different regions. Therefore, the interpretation of PD plots should be integrated with regional characteristics (e.g., the specific USC of Zone I and Zone II in the SMCRS or the typhoon factors in the HKSAR) for a comprehensive analysis. This integrated approach is necessary for proposing adaptive disaster prevention and mitigation recommendations tailored to the characteristics of the study areas.

6.3 Factors affecting the applications of dry-wet cycle characteristics

By comparing the debris flow susceptibility assessment models in typical inland and coastal mountainous regions from the aspects of the evaluation methods and the differences and similarities in model interpretations, the factors that may influence debris flow responses to climate dry-wet cycles may be identified. These comparisons aim to clarify the applicable conditions for constructing debris flow susceptibility assessment models based on the DWCC.

6.3.1 Impacts of data sources

The representativeness of debris flow records in the SMCRS and the HKSAR may influence the results of how debris flows respond to dry-wet cycles. The SMCRS, characterized by its complex terrain and abundant rainfall during the rainfall season, experiences large-scale and frequent debris flows. However, due to its vast area and uneven population distribution, it is challenging to accurately report all debris flow events, making the determination of positive and negative debris flow samples difficult. In this study, for the SMCRS, selected samples are those that have been identified through geological surveys, news reports, or scientific research, typically involving events that caused casualties or economic losses. In the case of the HKSAR, even though there are 7,091 historical debris flow records identified using UAV imagery, only those that resulted in casualties

or road closures were selected as typical samples. Consequently, the debris flow susceptibility assessment results presented in this study reflect only those events that have impacted human society, termed as disasters, and do not encompass all natural phenomena, which would be considered hazards.

However, the method of selecting debris flow samples in this manner somewhat diminishes the influence of the DWCC on the formation and initiation of debris flows. Both dry-wet cycles and debris flows are natural phenomena, fundamentally independent of human society. Yet, by filtering the debris flow samples, the study focuses solely on disaster events that affect human society, which limits the ability to accurately reveal how debris flows respond to the natural pattern of dry-wet cycles.

6.3.2 Impacts of assessment unit

The total area of the SMCRS and the HKSAR differs significantly, leading to distinct choices in the scale of assessment units for each study area. For the SMCRS, which encompasses 16,195 watersheds, the total area amounts to 266,000 km^2, whereas the land area of the HKSAR is approximately 1,100 km^2, making the SMCRS about 240 times larger than that of the HKSAR. The division of the HKSAR into 20,451 grid cells based on the length of historical debris flow gullies considers two factors. First, the grid cells need to cover the smallest debris

flow assessment unit, which is the debris flow gully. Second, by aligning the number of assessment units in the HKSAR with those in the SMCRS, the study ensures that the ratio of debris flow samples to the number of assessment units is approximately the same for both areas, at 5%. By employing different assessment unit delineation methods for the two study areas, the study maintains the representativeness and consistency in the distribution patterns of debris flow samples within both study areas.

However, due to the relatively small area of the HKSAR and the minimal climatic variability within it, there are only slight differences in the DWCC between positive and negative debris flow samples. This phenomenon is reflected in Fig. 3-3, where the differences in the PDSI time series before debris flow occurrences between positive and negative samples in the HKSAR are not pronounced. The limited spatial variability in meteorological conditions within the HKSAR may also contribute to the observation in Fig. 6-2 that the DWCC have a lesser contribution to the debris flow susceptibility assessment compared to the contributions of human activities.

6.3.3 Impacts of source material generation

Differences exist in the contribution of various assessment factors to the debris flow susceptibility between the SMCRS and the HKSAR. For one thing, during

the construction of the assessment factor system, the SMCRS incorporated the impact of earthquakes, adding an assessment factor for the distance to faults, while the HKSAR considered the impact of typhoons, incorporating assessment factors such as frequency, highest level, and longest duration of typhoons. For another, there are differences in the construction of certain assessment factors, such as the differences in rock types between the SMCRS and the HKSAR. Additionally, the maximum elevation difference is calculated based on watersheds in the SMCRS and on grid cells in the HKSAR. Furthermore, regarding land use types, since the division of watersheds in the SMCRS has taken rivers into account, water bodies are not considered in the land use types.

There are distinct differences in the performance of various assessment factors in debris flow susceptibility assessment within the two study areas. In the SMCRS, seismic factors are a significant assessment factor for debris flow susceptibility. Generally, the closer a watershed is to a fault, the higher the susceptibility to debris flows, due to more frequent geological activities providing a greater amount of source materials for debris flows in areas closer to faults. In contrast, typhoon factors are a dominant factor in the debris flow susceptibility assessment in the HKSAR, although their importance is relatively minor compared to other assessment factors. This may be due to not all debris flows being induced by typhoons, since rainfall-induced debris flows affected by monsoons remain predominant. However, it is undeniable that typhoons are closely associated with

larger-scale debris flow disasters due to the extreme precipitation they bring. The contribution of DWCC to debris flow susceptibility differs between the SMCRS and the HKSAR, with the latter requiring longer dry-wet cycle periods to form debris flows. This may be attributed to the lack of frequent geological activities in the HKSAR that generate source materials, necessitating the compensation of source materials through more frequent human activities or extended dry-wet cycle periods.

6.4 Summary

This chapter interprets the debris flow susceptibility assessment results by quantifying the contributions and characteristics of the main drivers and comparing DWCC applicability in the two study areas.

Based on the proposed model for assessing debris flow susceptibility, the RI of each assessment factor was calculated and ranked to identify the main drivers in the debris flow susceptibility assessment for each study area or zone. A comparison of the performance of assessment factors in the debris flow susceptibility models for two typical areas reveals that DWCC are considered the main drivers in both areas, and they are crucial indicators for assessing susceptibility in regions prone to debris flows, reflecting frequent and severe dry-wet cycles in these areas. By comparing the commonalities and uniqueness of the

main drivers of the debris flow susceptibility assessment models across different study areas or zones, the study reveals the distinctive aspects of factors that affect debris flow susceptibility in regions with different USC or different locations in inland and coastal regions. Based on these commonalities and uniqueness, the study proposes targeted recommendations for debris flow disaster prevention and mitigation. The findings suggest that in areas with frequent earthquakes and complex topography, ecological engineering methods should be prioritized for prevention and control, while in areas affected by typhoons, particularly those with sufficient vegetation cover along the coast, attention should be paid to the potential accumulation of debris flow source materials due to typhoons, which can lead to large-scale debris flows triggered by extreme precipitation also caused by typhoons. It is important to note, however, that typhoons are only related to larger-scale debris flows and do not significantly impact the majority of rainfall-induced debris flows recorded.

To elucidate the mechanisms by which the main drivers of debris flow susceptibility assessment models affect debris flow susceptibility in different study areas or zones, PD plots were constructed to quantitatively disclose the relationship between debris flow susceptibility and each main driver. Beyond DWCC, earthquakes, and typhoons, the impact of other assessment factors on debris flow susceptibility shows no significant difference between the typical inland and coastal monsoon areas. Coastal monsoon areas are subject to more

extreme precipitation events than inland monsoon areas. Similar to the process in inland monsoon areas where earthquakes generate loose materials and accumulate sources for debris flows, typhoons in coastal monsoon areas create a large amount of loose material by destroying vegetation. However, in addition to this, typhoons also contribute to extreme precipitation, leading to more severe extreme precipitation events and thus triggering debris flows.

Comparing the application of DWCC in debris flow susceptibility assessment in two study areas, it has been discovered that focusing exclusively on debris flows that impact human society can to some extent affect the understanding of responsive patterns between debris flow susceptibility and DWCC. Additionally, if the scale of the study area is too small, the insufficient spatial variability of DWCC may influence the identification of debris flow units with high susceptibility. Moreover, the various formation mechanisms of debris flow source materials are a key factor influencing the impact of climate dry-wet cycles on debris flow susceptibility. The fewer ways for generating debris flow materials in the study area, the greater the demands for dry-wet cycles to compensate for source materials, making debris flow susceptibility more closely related to longer dry-wet cycle periods.

Chapter 7 Conclusions and Future Work

7.1 Conclusions

This study utilizes historical debris flow and geo-environment databases from inland and coastal monsoon regions affected by extreme climates to investigate the impact of dry-wet cycles on debris flow susceptibility and apply these patterns in regional assessments. Initially, the study uses the PDSI to characterize long-term dry-wet status and extracts DWCC to describe the historical extreme events in the study areas. Methods are proposed to estimate debris flow ARI, revealing the relationship between dry-wet cycles and debris flow susceptibility. The study constructs and validates a model incorporating DWCC for debris flow susceptibility in both inland and coastal areas, interpreting main drivers and characteristics based on the model structure.

The main conclusions of this study are summarized as follows:

(1) Dry-wet cycles commonly precede debris flow occurrences. Debris flow months show significant extreme precipitations, and extreme drought conditions are consistently observed 6 to 8 years prior, indicating extreme dry-wet events. Differences in dry-wet status between high- and low-susceptibility areas are influenced by climate spatial variability, with no significant differences noted where variability is low. To address this, wavelet and multifractal analyses are proposed, constructing DWCC that include cycle period, severity, and frequency

of extreme dry-wet events. These analyses explore differences in dry-wet cycle patterns among assessment units in regions with low climate variability. Comparative analyses based on DWCC consistently indicate more severe dry-wet cycles in areas susceptible to debris flows in both inland and coastal monsoon regions.

(2) A responsive relationship exists between climate dry-wet cycles and regional debris flow susceptibility. Using typical records from watersheds in the inland monsoon area, two methods are proposed to estimate debris flow recurrence periods, validated through comparison. The recurrence period reflects the spatiotemporal distribution of debris flows, showing a higher correlation with dry-wet cycle periods than with maximum daily precipitation, suggesting that dry-wet cycle characteristics may be more effective than rainfall thresholds in debris flow early warning systems. Susceptibility is characterized by calculating FS from soil samples in typical debris flow gullies, revealing that extreme precipitation significantly reduces FS and increases susceptibility, while extreme drought conditions precede debris flow occurrences. These findings mechanistically validate the responsive relationship between DWCC and debris flow susceptibility. Analyzing the correlation between DWCC and FS quantifies this pattern, indicating that frequent and severe extreme dry-wet events enhance debris flow susceptibility in the context of climate dry-wet cycles.

(3) Regional debris flow susceptibility assessment based on climate dry-wet cycles is effective and stable. The model, incorporating DWCC, empirically verified the responsive pattern between climate dry-wet cycles and debris flow susceptibility, achieving 93.1% accuracy in identifying highly susceptible inland areas and 76.7% in the coastal monsoon region. Monthly assessment results align with the spatiotemporal distribution of debris flows indicated by the recurrence period, validating the effectiveness of using DWCC. Despite some deviations in predicted dry-wet indices, these do not significantly affect the model accuracy in identifying areas with high susceptibility, confirming the stability of using DWCC in debris flow susceptibility assessment. The effectiveness and stability of the DWCC-based debris flow susceptibility assessment model offer new insights for advanced debris flow prediction based on climate dry-wet cycles.

(4) The responsive pattern between climate dry-wet cycles and debris flow susceptibility is influenced by the formation mode of debris flow source materials. DWCC are identified as the main drivers in different areas, with a consistent PD relationship indicating frequent and intense dry-wet cycles in debris flow-prone areas. In typical inland regions like the Sichuan monsoon climate zone, shorter dry-wet cycle periods are enough for debris flow occurrences due to frequent geological activities providing source materials. In typical coastal areas like the Hong Kong Special Administrative Region, while dry-wet cycles contribute to debris flow source materials, frequent construction is the main contributor.

Nevertheless, substantial slope management investments have mitigated the impact of human activities, resulting in longer dry-wet cycle periods required for debris flow occurrences in the susceptible areas.

7.2 Limitations and future work

This study has revealed the responsive relationship and elucidated the responsive mechanism between climate dry-wet cycles and regional debris flow susceptibility, successfully applying this pattern to the debris flow susceptibility assessment. However, limitations at various stages still exist and further research is required.

(1) Representativeness of debris flow records. In this study, only debris flow events impacting human society are selected as samples for both the SMCRS and HKSAR, which may not fully represent the natural phenomenon of the relationship between climate dry-wet cycles and debris flow susceptibility. Complete identification of debris flow events within the study area is quite challenging. Accurate timing of debris flow occurrences is needed to explore DWCC before the events, and debris flows without impact on human society generally lack reporting.

(2) False alarm rate of the debris flow susceptibility assessment model. The model constructed based on DWCC exhibits fewer missed debris flow events. However,

due to incomplete debris flow data, particularly the lack of reports on regional debris flow events without impact on human society, the machine learning model may not fully discriminate between assessment units with and without recorded debris flow events. This leads to the occurrence of false alarms in predicting debris flow events.

(3) Soil experiments during dry-wet cycles. This study calculates FS changes under extreme precipitation through soil experiments and infers historical dry-wet conditions from surface monitoring data. However, it has not yet simulated debris flow susceptibility mechanisms based on soil experiments specifically targeting the dry-wet cycle process.

To address shortcomings (1) and (2), future research should construct a more comprehensive debris flow disaster database. This can be achieved by identifying unreported hazards using interferometric synthetic aperture radar and integrating deep learning for batch identification of debris flow gullies and dynamic database updates. This will provide a more comprehensive understanding of the responsive relationship between climate dry-wet cycles and regional debris flow susceptibility, and reduce the false alarm rate of the susceptibility assessment model. For shortcoming (3), additional soil experiments simulating dry-wet cycles can further reveal how these cycles increase debris flow susceptibility.

References

Achour, Y., Garçia, S., Cavaleiro, V., 2018. GIS-based spatial prediction of debris flows using logistic regression and frequency ratio models for Zêzere River basin and its surrounding area, Northwest Covilhã, Portugal. *Arabian Journal of Geosciences*, 11(18).

Addi, M., Gyasi-Agyei, Y., Obuobie, E., Amekudzi, L.K., 2022. Evaluation of imputation techniques for infilling missing daily rainfall records on river basins in Ghana. *Hydrological Sciences Journal*, 67(4): 613-627.

Afrifa-Yamoah, E., Mueller, U.A., Taylor, S., Fisher, A., 2020. Missing data imputation of high-resolution temporal climate time series data. *Meteorological Applications*, 27(1): e1873.

Allen, R.G., Pereira, L.S., Raes, D., Smith, M., 1998. FAO Irrigation and drainage paper No. 56. *Rome: Food and Agriculture Organization of the United Nations*, 56(97): e156.

Amiri, M., Jensen, R., 2016. Missing data imputation using fuzzy-rough methods. *Neurocomputing*, 205: 152-164.

Anastasiadis, A.D., Magoulas, G.D., Vrahatis, M.N., 2005. New globally convergent training scheme based on the resilient propagation algorithm. *Neurocomputing*, 64: 253-270.

Bai, Q., Li, X., Yan, M., Xu, H., Wu, Y., 2019. Experimental study on the effect of water content on the cohesive force of unsaturated sand soil. *Science Technology and Engineering*(7): 5.

Barman, U. et al., 2020. Comparative assessment of AR, MA and ARMA for the time series forecasting of Assam and Meghalaya rainfall division, 2020 International Conference on Computational Performance Evaluation (ComPE). IEEE, pp. 507-511.

Bohling, G., 2005. Introduction to geostastics and variogram analysis. *Kansas Geological Survey*, 1: 1-20.

Bregoli, F., Medina, V., Chevalier, G., Hürlimann, M., Bateman, A., 2015. Debris-flow susceptibility assessment at regional scale: Validation on an alpine environment. *Landslides*, 12(3): 437-454.

Cao, Y., Sun, Q., Yang, X., Dang, C., Geng, J., 2022. Sandstone weathering under dry–wet cycling in NaCl solution. *Bulletin of Engineering Geology and the Environment*, 81(11): 490.

Carrara, A., Crosta, G., Frattini, P., 2003. Geomorphological and historical data in assessing landslide hazard. *Earth Surface Processes and Landforms: The Journal of the British Geomorphological Research Group*, 28(10): 1125-1142.

Chang, J.M., Lam, Y.F., Lau, S.P., Wong, W., 2021. Development of fine-scale spatiotemporal temperature forecast model with urban climatology and geomorphometry in Hong Kong. *Urban Climate*, 37: 100816.

Chen, C., Chen, T., Yu, F., Yu, W., Tseng, C., 2005a. Rainfall duration and debris-flow initiated studies for real-time monitoring. *Environmental Geology*, 47(5): 715-724.

Chen, D., Gao, G., Xu, C.-Y., Guo, J., Ren, G., 2005b. Comparison of the Thornthwaite method and pan data with the standard Penman-Monteith estimates of reference evapotranspiration in China. *Climate Research*, 28(2): 123-132.

Chen, N., Lu, Y., Zhou, H., Deng, M., Han, D., 2014. Combined impacts of antecedent earthquakes and droughts on disastrous debris flows. *Journal of Mountain Science*, 11(6): 1507-1520.

Chen, N. et al., 2020. Effectiveness analysis of the prediction of regional debris flow susceptibility in post-earthquake and drought site. *Journal of Mountain Science*, 17(2): 329-339.

Chen, X., Li, Y., Cui, P., 2004. An overview of transformation of landslide into debris flow. *Mountain Research*, 22(5): 6.

Cheng, G., 2002. Study on quasi-period of breaking out debris flow under storm. *Journal of Natural Disasters*, 11(4): 6.

Cheng, G., 2004. Risk and size estimation of debris flow caused by storm rainfall in mountain regions. *Science in China E: Technological Sciences*, 46(7): 12.

Cheng, Z., Zhu, P., Gong, Y., 2003. Typical debris flow triggered by ice-lake break. *Mountain Research*, 21(6): 716-720.

Cheung, R.W., 2021. Landslide risk management in Hong Kong. *Landslides*, 18(10): 3457-3473.

Coe, J., Godt, J., Parise, M., Moscariello, A., 2003. Estimating debris-flow probability using fan stratigraphy, historic records, and drainage-basin morphology, Interstate 70 highway corridor, central Colorado, USA, Debris-Flow Hazards Mitigation: Mechanics, Prediction, and Assessment,

edited by: Rickenmann, D. and Cheng, Ch., Proceedings 3rd International DFHM Conference, Davos, Switzerland, pp. 207-217.

Cui, P., Wen, L., Xiang, L., 2011. ENSO Impacts on Debris Flows in Xiaojiang River Basin. *Climate Change Research*, 7(5): 7.

Das, M., Ghosh, S.K., 2018. Data-driven approaches for meteorological time series prediction: A comparative study of the state-of-the-art computational intelligence techniques. *Pattern Recognition Letters*, 105: 155-164.

Dash, R.K., Falae, P.O., Kanungo, D.P., 2022. Debris flow susceptibility zonation using statistical models in parts of Northwest Indian Himalayas-implementation, validation, and comparative evaluation. *Natural Hazards*, 111(2): 2011-2058.

Di, B., Stamatopoulos, C.A., Stamatopoulos, A.C., Liu, E., Balla, L., 2021. Proposal, application and partial validation of a simplified expression evaluating the stability of sandy slopes under rainfall conditions. *Geomorphology*, 395: 107966.

Di, B. et al., 2019. Assessing susceptibility of debris flow in southwest China using gradient boosting machine. *Scientific Reports*, 9(1): 1-12.

Dickey, D.A., Fuller, W.A., 1979. Distribution of the estimators for autoregressive time series with a unit root. *Journal of the American Statistical Association*, 74(366a): 427-431.

Dikshit, A., Pradhan, B., Alamri, A.M., 2021. Pathways and challenges of the application of artificial intelligence to geohazards modelling. *Gondwana Research*, 100: 290-301.

Dowling, C.A., Santi, P.M., 2014. Debris flows and their toll on human life: a global analysis of debris-flow fatalities from 1950 to 2011. *Natural Hazards*, 71(1): 203-227.

Du, J., Hu, M., Zhang, W., 2020. Missing data problem in the monitoring system: A review. *IEEE Sensors Journal*, 20(23): 13984-13998.

Duan, Z., Li, Z.-Y., Wu, Y.-B., Niu, B., Shen, R.-J., 2023. Mechanical and microscopic properties of soil according to the rate of increase in pore water pressure. *Soil and Tillage Research*, 225: 105530.

Efron, B., Tibshirani, R., 1986. Bootstrap methods for standard errors, confidence intervals, and other measures of statistical accuracy. *Statistical Science*, 1(1): 54-77.

Fan, R., Zhang, L.M., Wang, H., Fan, X., 2018. Evolution of debris flow activities in Gaojiagou Ravine during 2008–2016 after the Wenchuan earthquake. *Engineering Geology*, 235: 1-10.

Fan, X. et al., 2019. Two multi-temporal datasets that track the enhanced landsliding after the 2008 Wenchuan earthquake. *Earth System Science Data*, 11(1): 35-55.

Fan, X. et al., 2021. Rapidly evolving controls of landslides after a strong earthquake and implications for hazard assessments. *Geophysical Research Letters*, 48(1): e2020GL090509.

Farhangfar, A., Kurgan, L., Dy, J., 2008. Impact of imputation of missing values on classification error for discrete data. *Pattern Recognition*, 41(12): 3692-3705.

Fielding, E.J., McKenzie, D., 2012. Lithospheric flexure in the Sichuan Basin and Longmen Shan at the eastern edge of Tibet. *Geophysical Research Letters*, 39(9).

Fischer, L. et al., 2012. Debris flow modeling for susceptibility mapping at regional to national scale in Norway, Proceedings of the 11th International and 2nd North American Symposium on Landslides, pp. 3-8.

Friedman, J.H., 2001. Greedy function approximation: a gradient boosting machine. *Annals of Statistics*, 29(5): 1189-1232.

Fuchs, M., Torizin, J., Kühn, F., 2014. The effect of DEM resolution on the computation of the factor of safety using an infinite slope model. *Geomorphology*, 224: 16-26.

Fuchu, D., Lee, C., Sijing, W., 1999. Analysis of rainstorm-induced slide-debris flows on natural terrain of Lantau Island, Hong Kong. *Engineering Geology*, 51(4): 279-290.

Furuichi, T. et al., 2018. Disastrous sediment discharge due to typhoon-induced heavy rainfall over fossil periglacial catchments in western Tokachi, Hokkaido, northern Japan. *Landslides*, 15(8): 1645-1655.

Gan, L. et al., 2018. Performance comparison of different interpolation methods on missing values for time series data - A case study of meteorological and hydrological data in subtropical small watershed. *Chinese Journal of Agrometeorology*, 39(3): 10.

Garankina, E.V. et al., 2019. Magnitude and frequency of debris and slush flows in the Khibiny mountain valleys, Kola Peninsula, NW Russia. *Proceedings of the International Association of Hydrological Sciences*, 381: 37-47.

Germain, D., Gavrilă, I.G., Elizbarashvili, M., Pop, O.T., 2020. Multidisciplinary approach to sediment connectivity between debris-flow channel network and the Dolra River, Mazeri Valley, Southern Caucasus, Georgia. *Geomorphology*, 371: 107455.

Guzzetti, F. et al., 2020. Geographical landslide early warning systems. *Earth-Science Reviews*, 200: 102973.

Hai, L., Lv, Y., Tan, S., Feng, L., 2023. Study on the influences of the fractal dimension of the root system and slope degree on the slope stability. *Scientific Reports*, 13(1): 10282.

Hewelke, E. et al., 2018. Intensity and persistence of soil water repellency in pine forest soil in a temperate continental climate under drought conditions. *Water*, 10(9): 1121.

Hu, G. et al., 2017. Debris flow susceptibility analysis based on the combined impacts of antecedent earthquakes and droughts: a case study for cascade hydropower stations in the upper Yangtze River, China. *Journal of Mountain Science*, 14(9): 1712-1727.

Hu, K., Cui, P., You, Y., Chen, X., 2011. Influence on debris supply on the activity of post-quake debris flows. *The Chinese Journal of Geological Hazard and Control*, 22(1): 6.

Hu, X., Wang, Y., Yang, Y., 2018. Research actuality and evolution mechanism of post-fire debris flow. *Journal of Engineering Geology*, 26(6): 12.

Huang, H., Wang, Y., Li, Y., Zhou, Y., Zeng, Z., 2022. Debris-flow susceptibility assessment in China: a comparison between traditional statistical and machine learning methods. *Remote Sensing*, 14(18): 4475.

Huang, J. et al., 2020. A hybrid machine-learning model to estimate potential debris-flow volumes. *Geomorphology*, 367: 107333.

Hürlimann, M. et al., 2019. Debris-flow monitoring and warning: Review and examples. *Earth-Science Reviews*, 199: 102981.

Ilinca, V., 2021. Using morphometrics to distinguish between debris flow, debris flood and flood (Southern Carpathians, Romania). *Catena*, 197: 104982.

Jakob, M., Bovis, M., Oden, M., 2005. The significance of channel recharge rates for estimating debris flow magnitude and frequency. *Earth Surface Processes and Landforms: The Journal of the British Geomorphological Research Group*, 30(6): 755-766.

Jiang, D., Tian, Z., Lang, X., 2015. Mid-Holocene global monsoon area and precipitation from PMIP simulations. *Climate Dynamics*, 44(9-10): 2493-2512.

Kean, J.W., Staley, D.M., Cannon, S.H., 2011. In situ measurements of post-fire debris flows in southern California: Comparisons of the timing and magnitude of 24 debris-flow events with rainfall and soil moisture conditions. *Journal of Geophysical Research: Earth Surface*, 116(F4).

Keim, M.E., 2008. Building human resilience: the role of public health preparedness and response as an adaptation to climate change. *American Journal of Preventive Medicine*, 35(5): 508-516.

Kjekstad, O., Highland, L., 2009. Economic and social impacts of landslides. Landslides-Disaster Risk Reduction. Springer, Berlin, Heidelberg, 573-587 pp.

Ko, F.W., Lo, F.L., 2016. Rainfall-based landslide susceptibility analysis for natural terrain in Hong Kong-A direct stock-taking approach. *Engineering Geology*, 215: 95-107.

Kobiyama, M., Michel, G.P., Goerl, R.F., 2019. Proposal of debris flow disasters management in Brazil based on historical and legal aspects. *International Journal of Erosion Control Engineering*, 11(3): 85-93.

Kumar, A., Sarkar, R., 2023. Debris Flow Susceptibility Evaluation - A Review. *Iranian Journal of Science and Technology, Transactions of Civil Engineering*, 47(3): 1277-1292.

Lai, W.Y., Kuok, K., 2019. A study on bayesian principal component analysis for addressing missing rainfall data. *Water Resources Management*, 33(8): 2615-2628.

Lee, C., Chen, H., 1997. Landslides in Hong Kong - Causes and prevention. *Acta Geographica Sinica*, 64(S1): 114-121.

Li, M., Tang, C., Chen, M., Shi, Q., 2020. Spatio-temporal evolution characteristics of landslides in debris flow catchment in Beichuan County in the Wenchuan Earthauake zone. *Hydrogeology & Engineering Geology*, 47(3): 9.

Lian, B. et al., 2022. Creep mechanical and microstructural insights into the failure mechanism of loess landslides induced by dry-wet cycles in the Heifangtai platform, China. *Engineering Geology*, 300: 106589.

Lin, C. et al., 2004. Impact of Chi-Chi earthquake on the occurrence of landslides and debris flows: example from the Chenyulan River watershed, Nantou, Taiwan. *Engineering geology*, 71(1-2): 49-61.

Liu, K., Jiang, D., 2015. Analysis of dryness/wetness over China using standardized precipitation evapotranspiration index based on two evapotranspiration algorithms. *Chinese Journal of Atmospheric Sciences*, 39(1): 23-36.

Liu, M. et al., 2020. Effects of loose deposits on debris flow processes in the Aizi Valley, southwest China. *Journal of Mountain Science*, 17(1): 156-172.

Liu, Y., Di, B., Zhan, Y., A.Stamatopoulos, C., 2018. Debris flows susceptibility assessment in Wenchuan earthquake areas based on random forest algorithm model. *Mountain Research*, 36(5): 765-773.

Mika, J., Horvath, S., Makra, L., Dunkel, Z., 2005. The Palmer Drought Severity Index (PDSI) as an indicator of soil moisture. *Physics and Chemistry of the Earth, Parts A/B/C*, 30(1-3): 223-230.

Mizuyama, T., Egashira, S., 2010. Sediment induced disasters in the world and 1999-Debris flow disasters in Venezuela. *Journal of Disaster Research*, 5(3): 229-235.

Mudelsee, M., 2019. Trend analysis of climate time series: A review of methods. *Earth-Science Reviews*, 190: 310-322.

Muntohar, A.S., Liao, H.-J., 2010. Rainfall infiltration: infinite slope model for landslides triggering by rainstorm. *Natural Hazards*, 54: 967-984.

Neave, M., Abrahams, A.D., 2001. Impact of small mammal disturbances on sediment yield from grassland and shrubland ecosystems in the Chihuahuan Desert. *Catena*, 44(4): 285-303.

Ng, C.W.W., Yang, B., Liu, Z., Kwan, J., Chen, L., 2021. Spatiotemporal modelling of rainfall-induced landslides using machine learning. *Landslides*, 18(7): 2499-2514.

Nie, Y., Li, X., Xu, R., 2022. Dynamic hazard assessment of debris flow based on TRIGRS and flow-R coupled models. *Stochastic Environmental Research and Risk Assessment*, 2022(36): 94-114.

Nyman, P., Rutherfurd, I.D., Lane, P., Sheridan, G.J., 2019. Debris flows in southeast Australia linked to drought, wildfire, and the El Niño–Southern Oscillation. *Geology*, 47(5): 491-494.

Ouyang, C., Wang, Z., An, H., Liu, X., Wang, D., 2019. An example of a hazard and risk assessment for debris flows: A case study of Niwan Gully, Wudu, China. *Engineering Geology*, 263: 105351.

Özer, I.E., Rikkert, S.J., van Leijen, F.J., Jonkman, S.N., Hanssen, R.F., 2019. Sub-seasonal levee deformation observed using satellite radar interferometry to enhance flood protection. *Scientific Reports*, 9(1): 1-10.

Palmer, W.C., 1965. Meteorological drought, 30. US Department of Commerce, Weather Bureau.

Pan, H.-L., Jiang, Y.-J., Wang, J., Ou, G.-Q., 2018. Rainfall threshold calculation for debris flow early warning in areas with scarcity of data. *Natural Hazards and Earth System Sciences*, 18(5): 1395-1409.

Park, D.W., Nikhil, N.V., Lee, S.R., 2013. Landslide and debris flow susceptibility zonation using TRIGRS for the 2011 Seoul landslide event. *Natural Hazards and Earth System Sciences*, 13(11): 2833-2849.

Pastorello, R., D'Agostino, V., Hürlimann, M., 2020. Debris flow triggering characterization through a comparative analysis among different mountain catchments. *Catena*, 186: 104348.

Pavlova, I. et al., 2014. Debris flow activity related to recent climate conditions in the French Alps: A regional investigation. *Geomorphology*, 219: 248-259.

Phillips, C., Marden, M., 2005. Reforestation schemes to manage regional landslide risk. *Landslide Hazard and Risk*: 517-547.

Poljansek, K., Marín Ferrer, M., De Groeve, T., Clark, I., 2017. Science for disaster risk management 2017: knowing better and losing less. ETH Zurich.

Qin, S. et al., 2019. Mapping debris flow susceptibility based on watershed unit and grid cell unit: a comparison study. *Geomatics, Natural Hazards and Risk*, 10(1): 1648-1666.

Rajagukguk, R.A., Ramadhan, R.A., Lee, H.-J., 2020. A review on deep learning models for forecasting time series data of solar irradiance and photovoltaic power. *Energies*, 13(24): 6623.

Ratner, B., 2009. The correlation coefficient: Its values range between + 1/− 1, or do they? *Journal of Targeting, Measurement and Analysis for Marketing*, 17(2): 139-142.

Ren, R. et al., 2019. Typhoon triggered operation tunnel debris flow disaster in coastal areas of SE China. *Geomatics, Natural Hazards and Risk*, 10(1): 562-575.

Ripley, B.D., 2002. Modern applied statistics with S. Springer.

Samsudin, R., Shabri, A., Saad, P., 2010. A comparison of time series forecasting using support vector machine and artificial neural network model. *Journal of Applied Sciences*, 10(11): 950-958.

Sauer, T.J., Horton, R., 2005. Soil heat flux. *Micrometeorology in Agricultural Systems*, 47: 131-154.

Scanlon, B.R. et al., 2022. Linkages between GRACE water storage, hydrologic extremes, and climate teleconnections in major African aquifers. *Environmental Research Letters*, 17(1): 014046.

Scordo, F., Perillo, G.M., Cintia Piccolo, M., 2018. Effect of southern climate modes and variations in river discharge on lake surface area in Patagonia. *Inland Waters*, 8(3): 341-355.

Segoni, S., Piciullo, L., Gariano, S.L., 2018. A review of the recent literature on rainfall thresholds for landslide occurrence. *Landslides*, 15(8): 1483-1501.

Sewell, R. et al., 2015. Dating of debris flow fan complexes from Lantau Island, Hong Kong, China: The potential relationship between landslide activity and climate change. *Geomorphology*, 248: 205-227.

Shu, Z., Chan, P.W., Li, Q., He, Y., Yan, B., 2021. Characterization of daily rainfall variability in Hong Kong: A nonlinear dynamic perspective. *International Journal of Climatology*, 41: E2913-E2926.

Staley, D.M. et al., 2016. Prediction of spatially explicit rainfall intensity-duration thresholds for post-fire debris-flow generation in the western United States. *Geomorphology*, 278(1): 149-162.

Stamatopoulos, C.A., 2015. Constitutive and multi-block modeling of landslides on saturated sands along slip surfaces. *Soils and Foundations*, 55(4): 703-719.

Stancanelli, L.M., Peres, D.J., Cancelliere, A., Foti, E., 2017. A combined triggering-propagation modeling approach for the assessment of rainfall induced debris flow susceptibility. *Journal of Hydrology*, 550: 130-143.

Sujatha, E.R., Sridhar, V., 2017. Mapping debris flow susceptibility using analytical network process in Kodaikkanal Hills, Tamil Nadu (India). *Journal of Earth System Science*, 126(8): 1-18.

Sun, J. et al., 2021. Exploring the impact of introducing a physical model into statistical methods on the evaluation of regional scale debris flow susceptibility. *Natural Hazards*, 106: 881-912.

Sung, C.H., Liaw, S.C., 2020. A GIS-based approach for assessing social vulnerability to flood and debris flow hazards. *International Journal of Disaster Risk Reduction*, 46: 101531.

Svoboda, M.D., Fuchs, B.A., 2016. Handbook of drought indicators and indices. World Meteorological Organization Geneva, Switzerland.

Swain, D.L., 2021. A shorter, sharper rainy season amplifies California wildfire risk. *Geophysical Research Letters*, 48(5): e2021GL092843.

Tan, W., Han, Q., 1992. Study on regional critical rainfall indices of debris flow in Sichuan province. *Journal of Catastrophology*, 7(02): 39-44.

Thornthwaite, C.W., 1948. An approach toward a rational classification of climate. *Geographical Review*, 38(1): 55-94.

Tian, S. et al., 2022. Extreme climate and tectonic controls on the generation of a large-scale, low-frequency debris flow. *Catena*, 212: 106086.

Tie, Y., Malik, I., Owczarek, P., 2014. Dendrochronological dating of debris flow historical events in high mountain area - Take Daozao debris flow as an example. *Mountain Research*(2): 7.

Tsai, C.-F., Chang, F.-Y., 2016. Combining instance selection for better missing value imputation. *Journal of Systems and Software*, 122: 63-71.

van der Schrier, G., Jones, P.D., Briffa, K.R., 2011. The sensitivity of the PDSI to the Thornthwaite and Penman-Monteith parameterizations for potential evapotranspiration. *Journal of Geophysical Research: Atmospheres*, 116(D3).

Venter, Z.S., Barton, D.N., Chakraborty, T., Simensen, T., Singh, G., 2022. Global 10 m land use land cover datasets: a comparison of dynamic world, World Cover and Esri Land Cover. *Remote Sensing*, 14(16): 4101.

Vergara Dal Pont, I., Moreiras, S.M., Santibanez Ossa, F., Araneo, D., Ferrando, F., 2020. Debris flows triggered from melt of seasonal snow and ice within the active layer in the semi-arid Andes. *Permafrost and Periglacial Processes*, 31(1): 57-68.

Wang, J., Huang, R., Nie, W., Su, X., 2014. Experimental study of early warning system model of landslide induced by rainfall based on infinite slope method. *Rock and Soil Mechanics*, 35(12): 3503-3510.

Wang, S., Luo, S., 2015. Discussion on the relationship between debris flow and formation lithology. *Urban Geology*(S1): 5.

Wang, W. et al., 2020. Mapping the susceptibility to landslides based on the deep belief network: a case study in Sichuan Province, China. *Natural Hazards*, 103(3): 3239-3261.

Wasantha, P.L., Ranjith, P.G., 2014. Water-weakening behavior of Hawkesbury sandstone in brittle regime. *Engineering Geology*, 178: 91-101.

Wei, F., Hu, K., Lopez, J.L., 2015. Debris flow risk zoning and its application in disaster mitigation. *The Chinese Journal of Geological Hazard and Control*, 2007(01): 23-27.

Wei, J., Dong, G., Zhao, B., 1994. Relationship between activity periods of modern mud-rock flow and storm in the mountain areas of Beijing. *The Chinese Journal of Geological Hazard and Control*(4): 6.

Wei, T., Chen, G., Wu, L., Liu, F., 2022. Rapid reduction in the shear resistance and permeability of the weak layer in the evolution of water-rock weathering. *Engineering Geology*, 299: 106545.

Wells, N., Goddard, S., Hayes, M.J., 2004. A self-calibrating Palmer drought severity index. *Journal of Climate*, 17(12): 2335-2351.

Wieder, W., Boehnert, J., Bonan, G., Langseth, M., 2014. Regridded harmonized world soil database v1.2. *Distributed Active Archive Center for Biogeochemical Nynamics*.

Wu, S. et al., 2022. Classification and detection of dominant factors in geospatial patterns of traditional settlements in China. *Journal of Geographical Sciences*, 32(5): 873-891.

Xiong, K. et al., 2020. Comparison of different machine learning methods for debris flow susceptibility mapping: A case study in the Sichuan Province, China. *Remote Sensing*, 12(2): 295.

Xu, J., Li, Y., Wang, S., Wang, Q., Ding, J., 2020. Shear strength and mesoscopic character of undisturbed loess with sodium sulfate after dry-wet cycling. *Bulletin of Engineering Geology and the Environment*, 79(3): 1523-1541.

Xu, W., Yu, W., Jing, S., Zhang, G., Huang, J., 2013. Debris flow susceptibility assessment by GIS and information value model in a large-scale region, Sichuan Province (China). *Natural Hazards*, 65: 1379-1392.

Xu, X., Chong, W., Li, S., Arabo, A., Xiao, J., 2018. MIAEC: Missing data imputation based on the evidence chain. *IEEE Access*, 6: 12983-12992.

Ye, T., Huang, C., Deng, Z., 2017. Spatial database of 1:2500000 digital geologic map of People's Republic of China. *Geology in China*, 44(S1): 19-24.

Zang, H. et al., 2020. Short-term global horizontal irradiance forecasting based on a hybrid CNN-LSTM model with spatiotemporal correlations. *Renewable Energy*, 160: 26-41.

Zhang, K., Wang, S., Bao, H., Zhao, X., 2019. Characteristics and influencing factors of rainfall-induced landslide and debris flow hazards in Shaanxi Province, China. *Natural Hazards and Earth System Sciences*, 19(1): 93-105.

Zhang, X., Ye, B., Liu, H., Zhao, L., Zhao, H., 2022. Spatial and temporal variation of precipitation in Jiangsu province in recent 58 years based on wavelet power spectrum and Anusplin. *Water Resources and Power*, 40(1): 4.

Zhang, Y., Wang, K., Wang, J., Liu, C., Shangguan, Z., 2021. Changes in soil water holding capacity and water availability following vegetation restoration on the Chinese Loess Plateau. *Scientific Reports*, 11(1): 1-11.

Zheng, Y. et al., 2018. GIS-based mapping of local climate zone in the high-density city of Hong Kong. *Urban Climate*, 24: 419-448.

Zhou, S., Gao, L., Zhang, L.M., 2019. Predicting debris-flow clusters under extreme rainstorms: a case study on Hong Kong Island. *Bulletin of Engineering Geology and the Environment*, 78(8): 5775-5794.

Zhou, Y., Gao, Q., 2017. A dataset of climate extreme indices over the Tibetan Plateau (1960-2012). *China Scientific Data*(2): 9.